UTS UNIVERSITY OF TECHNOLOGY SYDNEY

EMG Control Strategy of a Cable-based Upper Limb Rehabilitation Robot and its Verification

by Yao Huang

Thesis submitted in fulfilment of the requirements for the degree of

Doctor of Philosophy

under the supervision of Steven Su

University of Technology Sydney
Faculty of Engineering and Information Technology

September 2020

CERTIFICATE OF ORIGINAL AUTHORSHIP

I, Yao Huang declare that this thesis, is submitted in fulfilment of the requirements for the award of Doctor of Philosophy, in the School of Biomedical Engineering/Faculty of Engineering and Information Technology at the University of Technology Sydney.

This thesis is wholly my own work unless otherwise referenced or acknowledged. In addition, I certify that all information sources and literature used are indicated in the thesis.

This document has not been submitted for qualifications at any other academic institution.

This research is supported by the Australian Government Research Training Program.

Signature:

Production Note:
Signature removed prior to publication.

Date: 03/09/02020

Acknowledgements

I would like to express my sincere gratitude to my supervisor A/Prof. Steven Su for his continual support, guidance, help, and encouragement during my Ph.D. study. Dr. Su has brought me into the topic of rehabilitation robot control strategies and provided brilliant insights into my research works. It is my honor to have a supervisor who always inspires me to achieve higher targets. His conscientious and meticulous attitude on research has a significant influence on my work.

I am grateful to my co-supervisor, Dr. Trang Nguyen, for her kind support and constructive suggestions on my research. I would also like to thank my external supervisor Prof. Hung Nguyen (Swinburne University of Technology), Prof. Rong Song (Sun Yat-sen University, China), and Dr. Ahmadreza Argha (The University of New South Wales) for their support in providing platform and opportunities and their constructive advice to my research. I would also deeply appreciate Prof. Branko G Celler (The University of New South Wales) and Prof. Andrey V Savkin (The University of New South Wales) for their precious guidance and contribution to my chapters. I would also like to thank Prof. Daniel P. Ferris (University of Florida, USA) and Ms. Kara McArthur for the valuable comments and delicate editing on my publications.

I also wish to express my appreciation to the staff members in the Centre for Health Technologies, School of biomedical engineering, University of Technology Sydney, especially to Prof. Joanne Tipper, Prof. Gyorgy Hutvagner, and Dr. Steve Lin. I have received a unique and memorizable experience to work with these professional and inclusive people.

I am grateful to my colleagues in A/Prof. Steven Su's research group, in particular, Dr. Lin Ye, Dr. Wentian Zhang, Dr. Wenhui Chen, Dr. Hairong Yu, Kairui Guo,

Taopin Liu, Miao Zhang, Yujiao Wu, Linmeng Li, and Li Wang, for their selfless help and technical support. Working together with them brings a lot of happiness and a good memory for me. I would also be grateful to my colleagues in Prof. Rong Song's research group, in particular, Dr. Qianqian Yang, Yuanyu Wu, Ying Chen, Yu Zhuang, Na Tian, Jie Zhou, Xianming Li, Tian Xie, Chenlin Xie, Lefei Zhou, and Qiurong Deng for their great help in our cooperation project. I also sincerely appreciate my friends, Dr. Zhichao Sheng, Dr. Ye Shi, Dr. Haimin Zhang, Zhiyuan Shi, Hanjie Wu, and Dr. Daniel Roxby, for their warm support.

Lastly, my deepest gratitude goes to my family and my boyfriend for their immeasurable support and encouragement throughout my graduate studies.

Abstract

Post-stroke motor recovery highly affected by patients' active participation in rehabilitation. Surface electromyography (EMG) signals are related to a subject's intention. It is also one of the most widely used biosignals in the area of motion intention estimation and rehabilitation robot control. However, due to the complicated relationship between multiple muscles and movements, few studies have applied continuous multiple EMG signals to control rehabilitation robots and provide assistant to users' multi-joint movements in real-time.

In this dissertation, new methods for decoding EMG signals during robot-assisted movements are proposed and applied to manipulate a cable-based rehabilitation robot. Different EMG decoders for continuously estimating voluntary motion intention are developed to fulfil different rehabilitation needs. These decoders are used to establish a human-robot cooperative control scheme for promoting users' active participation in rehabilitation.

Firstly, an EMG decoder is build up with a switching mechanism and submodels for decoding EMG signals to motion need forces during a multi-joint complex task in three-dimensional space. The switching mechanism aims to carve up the task into separate simple subtasks. For each simple subtask, a linear six-input three-output time-invariant submodel is established by the state-space modelling method. The inputs are the processed muscle activations of six arm muscles, and the outputs are motion need forces of users when executing the task with visual feedback. The outputs are used to indicate three motors of the robot. The switching logic of the mechanism is to change the parameters of each submodel by times. However, we observed a 'bump' behaviour of the estimated forces (i.e., discontinuity) when switching parameters of

two submodels. A sudden change in control signals of motors might cause unexpected impacts on patients, so it is unacceptable during rehabilitation.

After that, to improve the smoothness of the estimated forces, we attempted to maintain the continuity of the decoder outputs when switching among submodels. A bumpless switching mechanism is proposed by constructing a generic multirealisation for all submodels. The generic multirealisation has a common output matrix, which helps to continuously predict the outputs. For submodels with the same order, the multirealisation is constructed by finding the common denominator matrix of the subsystems' Matrix Fraction Description (MFD). Furthermore, the best submodel, in terms of goodness of fit, established in each simple subtask, may have a different order. For different-ordered submodels, the generic multirealisation is constructed by finding the common highest-degree-coefficient matrix and expanding the hidden states of submodels. To this end, the bumpless switching mechanism for achieving continuous outputs is achieved.

Finally, to expand the application of a rehabilitation robot, it is vital to use less and accurate EMG decoders for multiple tasks and to reduce the impact of individual differences. A decoder based on a time-variant long short-term memory (LSTM) network is proposed. We attempt to train one LSTM network for each time step, so the decoder is seen as a time-variant system. All parameters of the decoder are trained with error functions of both time step accuracy and task accuracy. This method does not need a secondary feature extraction or preprocessor and can be applied in real-time robot control.

The experiments for examining these decoders included model training, model testing, and online verification to control the robot in real-time. Healthy subjects who participate in the linear system-based EMG decoders and nonlinear system-based EMG decoders were instructed to perform different tasks in three-dimensional space with visual interactions.

Experimental results demonstrated that EMG decoders with the switching mechanisms and linear system-based submodels could effectively recognise arm motion intention and provide appropriate assistance to users. The outputs achieved by the bumpless switching mechanism with submodels are significantly smoother than those

without it. The bumpless switching mechanism can avoid users from the risk of unpredictable loads. These approaches performed well in specific subjects and tasks with no need for an immense database and complicated model parameters.

The results of the time-variant LSTM-based decoders showed that this nonlinear system approach outperforms linear system approaches in both model testing and online verifications. The complicated structure and well-trained parameters ensure that the nonlinear system approach does not need to take account of individual differences when applying in real-time. The findings also suggested that the time-variant LSTM system decoders may be feasible for practical use in both single and multiple complex tasks.

An investigation on the differences in recruited muscle patterns when users perform multi-joint multi-directional arm movements with the robot assistance or naturally without a robot is carried in this dissertation. The results indicated that both the natural and robot-assisted multi-joint movements could be generated by similar sets of synergies of limited dimensionality. This is a supportive finding that the proposed human-robot cooperative control strategy based on a proper EMG decoder may not significantly affect human motion control pattern while supporting users.

Furthermore, the effects of task variety and tracking accuracy by visual feedback on muscle synergies and their activation patterns were explored by statistic analysis. The results showed that, for active rehabilitation applications, if the purpose is to enhance the synergy indication from the neural system, the task completion accuracy should be emphasised. If the purpose is to expand the motion area, the task variety should be diversified. These results supported that different decoders should be used and developed to meet the different assistance requirements of post-stroke patients.

In conclusion, the proposed EMG decoders based on the linear system approach and the nonlinear system approach have a wide range of application in rehabilitation. These approaches showed high potential in controlling robots to support users with safe, smooth, and accurate assistance in rehabilitation.

Publications

The contents of this thesis are based on the following chapters that have been published, accepted, or submitted to peer-reviewed journals and conferences.

Journal Chapters:

1. Yao Huang, Rong Song, Ahmadreza Argha, Andrey V. Savkin, Branko G. Celler, and Steven Su, "Continuous description of human 3D motion intent through switching mechanism," *IEEE Transactions on Neural Systems and Rehabilitation Engineering*, vol. 28, no. 1, pp. 277-286, Jan 2020.

2. Yao Huang, Qianqian Yang, Ying Chen, and Rong Song, "Assessment of motor control during three-dimensional movements tracking with position-varying gravity compensation," *Frontiers in Neuroscience*, vol. 11, no. 253, May 2017.

3. Yao Huang, Rong Song, Ahmadreza Argha, Andrey V. Savkin, Branko G. Celler, and Steven Su, "Human motion intent description based on bumpless switching mechanism for rehabilitation robot," under review at *IEEE Transactions on Neural Systems and Rehabilitation Engineering*.

4. Yao Huang, Rong Song, Ahmadreza Argha, Andrey V. Savkin, Branko G. Celler, and Steven Su, "EMG-based continuous motion intention description by a mixed-order bumpless decoder for rehabilitation robots control," ready to submit.

5. Yao Huang, Rong Song, Ahmadreza Argha, Andrey V. Savkin, Branko G. Celler, and Steven Su, "Continuous estimation of motion intention based on EMG signals using a time-variant long short-term memory network," ready to submit.

6. Yao Huang, Rong Song, Ahmadreza Argha, Andrey V. Savkin, Branko G. Celler, and Steven Su, "The effect of assistance from an EMG-based control robot on upper limb muscle synergies," ready to submit.

Book Chapter:

1. Yao Huang, Steven Su, and Rong Song, "Voluntary intention-driven rehabilitation robots for the upper limb," in *Intelligent Biomechatronics in Neurorehabilitation*, Academic Press, pp. 111-130, 2020.

Conference Chapters:

1. Yao Huang, Rong Song, Wenhui Chen, Hairong Yu, Ahmadreza Argha, Branko G. Celler, and Steven Su, "The effects of different tracking tasks on muscle synergy through visual feedback," in *Proc. 2019 41st Annual International Conference of the IEEE Engineering in Medicine and Biology Society (EMBC)*, pp. 417-420, July 2019.

2. Yao Huang, Ying Chen, Jie Niu, and Rong Song, "EMG-Based control for Three-Dimensional upper limb movement assistance using a cable-based upper limb rehabilitation robot," in *Proc. 2017 International Conference on Intelligent Robotics and Applications*, pp. 273-279, August 2017.

Table of contents

List of figures

List of tables

Chapter 1

Introduction

-

1.1 Problem Statement

Stroke is one of the biggest killers in Australia and worldwide. It is also a leading cause of motor disability. A stroke occurs when a vessel supplying blood to the brain is suddenly blocked (an ischaemic stroke) or ruptures (a haemorrhagic stroke). Both strokes may lead to part of the brain dying, which in turn causes sudden impairment and problems with a variety of bodily functions [8]. In Australia, there were more than 56,000 new and recurrent strokes in 2017. Worse still, this number will more than double by 2050 [9]. The annual financial cost of stroke in Australia in 2012 was around $3 billion [10]. However, the high financial costs caused by stroke do not constitute the biggest impact to society. It is instead the loss of healthy life and the long-term impacts on individuals, families, and society. Furthermore, the health care costs of stroke will inevitably increase owing to the corresponding rise of the aging population worldwide.

Individual impairments caused by stroke mostly involve a combined loss of motor, sensory, and cognitive functions. The loss often leads to weak muscles, reduced movement coordination, and diminished ability in thinking, communicating, decision making, feeling, vision, and hearing. Most survivors after stroke normally suffer from

neurological deficits, which cause muscle weakness and loss of movement ability (i.e. paralysis) in their limbs. Accordingly, their ability to perform daily living activities is restricted. As reported by [10, 11], 65% of survivors suffer a disability that impedes daily living activities, and 30% of survivors are of working age (i.e., under 60).

To help stroke survivors to return back to their normal lives, long-term rehabilitation treatment after initial intervention should be highly encouraged. It is generally accepted that for people with impaired limbs, repeating multiple functional multi-joint exercises is a vital and common form of stroke rehabilitation. Thus, common rehabilitation programs are composed of repetitive, frequent, and intensive movements. These programs mostly aim to reduce permanent damage and enhance adaptation, therefore increasing patients' motion ability for the performance of their daily living activities. It is possible for survivors to partly or fully regain motor functions by undertaking an individual rehabilitation program which starts immediately after their condition is considered stable. Many studies reveal that recovery of motor function is linked to motor learning during repetitive movements, and if the amount of repetitions is large enough, structural neurological changes can be induced [12, 13]. Repetitive movements lead to increases in sensorimotor activity, and this is mainly related to neural plasticity, which is the ability of adjacent areas of the damaged brain to reorganise and compensate for the loss of function. Structural neurological changes may be the ultimate goal to substantially improve patients' motion ability and quality of life in a long-term rehabilitation phase.

In a traditional rehabilitation program, physical therapists treat stroke patients on a one-on-one basis. The most significant shortcoming is that therapists often perform heavy physical labour. The number of patients receiving treatment is also severely limited by the number of therapists. In Australia, the number of registered therapists is far fewer than the number of new strokes each year [14]. On the other hand, when the physical therapist manually assists the patient to perform repetitive movements, the therapist can be prone to fatigue, and this may even cause injury. Thus, the amount and duration of treatment given to patients in a stroke outpatient clinic [15, 16] is far less than the necessary treatment that can induce structural neurological change. This is because therapists are often unable to give patients the time and attention that they require for maximum recovery. Furthermore, through the use of fixed measuring scales,

it may be challenging to quantify accurately the improvement in patients' motion ability after the rehabilitation intervention performed by physical therapists. Therefore, patients' rehabilitation progress and functional evaluation are severely restricted by factors such as the fatigue of physical therapists, time, limited budgets, and insufficient objective rehabilitation assessment progress.

The increasing demand for stroke rehabilitation makes the capacity of the existing health care system increasingly strained. Therefore, both physical therapists and patients require a highly efficient system that can provide patients with sufficient high quality rehabilitation treatment. Based on this demand, researchers have developed many rehabilitation tools and training methods. One of the advanced methods is the development of robots and auxiliary training methods with robotic systems. It is known that robots can be controlled to complete precise actions without experiencing the fatigue associated with humans, and they make fewer mistakes. In the robot-assisted treatments, therapists can focus on designing rehabilitation programs and monitoring treatment progress without having to employ physical effort. Furthermore, the robot can quantitatively evaluate the user's motion ability in real time during the treatments, thereby more accurately and objectively evaluating the rehabilitation effect. In addition, robotic technologies can also enable family or group therapy, e.g., one therapist can serve multiple patients simultaneously [12]. Therefore, robotics has received widespread attention in the field of rehabilitation. In order to match the characteristics of rehabilitation and meet the patients' recovery demands, researchers mainly develop robotics from two main aspects. The first is the design of the robotic structure, and the second is the development of robot control strategies.

In terms of robotic structure, researchers have mainly developed three types of structures, including endpoint-fixation systems (e.g. MIT-Manus [17]), exoskeleton systems (e.g. ARMin [4], Washington Univ.[18]) and cable suspension systems (e.g. Freebal [19]). These structures can be used in different stages of a rehabilitation program, but they have particular advantages and disadvantages.

Serial robots (mainly end-point fixing systems) have simple transmission structures and can be easily controlled, but they frequently have a relatively large mass and volume, which means they are inconvenient for the purposes of transportation. A

major disadvantage is that when these robots provide assistance to the limbs through the means of rigid structures, they can pose risks to patients [20].

Compared with serial robot systems, parallel robot systems with a cable-driven structure can interact with users more compliantly. The cables are connected to an end effector and a fixed frame through connectors. Movements of the end effector are completed by changing the length of the cables while maintaining the cable tension [21]. Parallel robot systems usually have a large working space, which can meet the space requirements of different patients and different movements in rehabilitation. With a cable-driven structure, the transmission structure can be adjusted by changing the cable connection points of the connectors and the end effector and relocating the installation of the connectors on the frame. Different end effectors can also be configured to assist the various movements of different limbs and joints. The different components are highly functional and concentrated, and cables and end effectors are generally lighter. Therefore, this structure can also be modular, and it has good inertial behaviour [20]. It is also very convenient to assemble, disassemble, and transport. In clinical applications, parallel robot systems with a cable-driven structure without rigid links prevent the user's limbs from being completely restrained, which increases the safety of movements. These advantages mean that cable-based parallel robots have the potential to be used as medical/commercial/home rehabilitation treatment systems. However, the obvious disadvantage of the cable-based structure is that it can only provide tensile force but not thrust, so its working space shape may be complicated and irregular [20]. The impact on practical applications of this shortcoming can be avoided by having a good transmission structure design and an accurate workspace analysis.

The different rehabilitation robots mentioned above can be used for several goals, e.g., 1) enhance the motion ability of healthy people, and improve their endurance to learn the characteristics of human sports [22, 23]; 2) assist patients with limb movement disorders in completing rehabilitation training, improving the rehabilitation effect, and recovering motion ability to a healthy level [24, 25]. Although the goals may seem different, the common requirement is that the robot should be capable of obtaining and understanding the users' motion intention and responding appropriately to provide the needed assistance to users in the required amount of time. For this reason, the

development of a robot control scheme that can recognise the users' motion intention and provide the appropriate level of assistance is one of the most important tasks in the field of rehabilitation robots.

A widely studied method for recognising the users' motion intention is based on the estimation of the joint torques/forces required when performing motion [26]. The process of using the recognised motion intent to provide users with assistive forces/torques is a typical control scheme for rehabilitation robots. This scheme can provide users with different levels of assistance and can meet the patients' needs in rehabilitation. The goal of the assistance is usually to relieve the users' burden and improve their motion performance [27].

When it comes to the control schemes, like many robotic systems in other fields, the basic control schemes (based on position, force, and torque signals of limbs during movements)are mostly developed and mature. Furthermore, these control signals are stable and can be collected conveniently. Some robots with control schemes based on these signals have proved to be effective in offering accurate assistance to patients in rehabilitation [28–31]. However, research shows that patients' participation and their own efforts will greatly affect the recovery outcomes [32]. But these signals are not closely related to human effort so they cannot greatly increase the patients' participation.

Due to the increasing demand for patient initiative during the rehabilitation process, biosignals were introduced to control these robotic devices, such as Electroencephalography signals (EEG), Electrooculography signals, Electromyography signals (EMG), and voice signals. These signals are highly correlated with the particular subject's initiative. Among these biosignals, the EMG signal is relatively stable, hardly upset by external factors, and has a high signal-to-noise ratio [33]. The EMG signal is produced by motor neuron impulses which serve to activate muscle fibres during muscle contraction. The surface EMG signal can be collected easily by pasting electrodes on the skin surface. It can be collected continuously in different muscles simultaneously by pasting multiple paired electrodes. It is highly related to muscle force and joint torque [34, 35] and widely used in many devices for detecting user intent [36].

Although EMG signals have been widely accepted for the purposes of controlling devices, they are not easy to implement. This is because the relationship between EMG signals and forces/torques is very complicated. During multijoint movements, if the multiply related muscles contract several times, and the contraction level of each muscle has a different amplitude, the resultant corresponding force is difficult to estimate. EMG signal also involves a variety of nonlinear characteristics under different conditions (i.e. static and dynamic) [27]. The different forms of muscle anatomy, muscle fatigue level, and usage duration/placement of electrodes would all affect the characteristics of EMG signals [37–39]. These changeable characteristics lead to the main drawback of the EMG-based robot control scheme. That is the strict calibration with sophisticated user-dependence and session-dependence, which is required for building a reliable and precise estimation model. The calibration is time-consuming, and it needs to be done both by letting users move limbs with and without the aid of a robot. Thus, multiple EMG signals are still difficult to be applied in robot control in real-time and outside of the laboratory environment.

Existing algorithms for estimating muscle forces and joint torques based on EMG signals can be divided into physiological models [40], black-box systems for estimation [41], and muscle activity pattern classifiers [42]. These methods are all required to reduce the complexity of the calibration process while reducing the time cost of computation. However, many related studies can only achieve discrete estimations on motion intent, such as the prediction of wrist orientation changes and on-off decision [43, 44]. The limited intent recognition used in robot control may cause problems in terms of motion stability and smoothness, and it may severely limit application scopes.

There are also researchers who try to decode the user's motion intention from the EMG signal based on the Hill-based model with nonlinearity. This model has been developed to describe the physiological structure of one muscle [45]. However, it can only be applied when a small number of muscles are recruited for estimation, and it requires muscle and joint motions to have a significant correspondence, such as the close relationship between ankle joint motions and the gastrocnemius and tibial anterior muscles [46]. Furthermore, the Hill-based model needs to be established for each muscle separately, and a large number of unknown parameters need to be determined.

This makes it quite difficult to apply this method in the intention decoding during multi-joint multi-muscle movements.

Recent works propose that muscles can be collectively activated to form muscle synergy that changes over time [47]. These works reveal that when a person performs a movement, several muscles are recruited simultaneously but in patterns. Some studies try to recognise these patterns known as synergies using classification methods, e.g. an extended LDA-based algorithm and an extreme learning machine algorithm [48, 49]. Some studies have shown that the number of muscles can be reduced by representing muscle activations in a low-dimensional space [50]. This is a similar finding to that of muscle synergies because both of them extract the major information included in a variety of muscle activities. These methods may be a robust way for intention decoding, but not all of the information contained in EMG signals is identified. These pattern recognition methods are more commonly used in the control of prosthetic devices, because the residual EMG signals of amputated patients are relatively more complete [51, 52]. However, the muscles and motor control characteristics of stroke patients may change, and their motor control performance mostly consists of muscle weakness and contractures. Therefore, the pattern recognition control method is relatively difficult to employ in stroke rehabilitation.

Overall, although many reported rehabilitation systems are able to assist patients during the execution of upper-extremity rehabilitation, most of the systems based on position/force/torque signals only have a limited connection to human effort. In recent studies, researchers have paid attention to patients' efforts during rehabilitation. This is because the positive outcome of rehabilitation is highly correlated with patients' condition, attention, and effort [32]. Although EMG signals are well-known in terms of being highly correlated with movement intention [35], there are many difficulties with applying EMG as the control signals in real-time for controlling robots for the purposes of supporting users' multi-joint movements. Present EMG-based control strategies of rehabilitation robots are restricted in tasks recruited to limited joints and limited muscle. The changes in EMG characteristics under different conditions also need to be solved. A rehabilitation robot based on EMG control strategies should be able to support patients with dyskinesia who have different assistance requirements in a variety of multi-joint tasks.

1.2 Motivation and Aims

Motivated by the importance of human effort in rehabilitation and the limitations in present EMG-based robot control strategies, this dissertation focuses on how to continuously provide proper assistance to users based on EMG signals during robot-assisted multi-joint tasks. A newly proposed strategy should be able to deal with problems related to changeable EMG characteristics and computation time delays. It should also be capable of being employed by different users with the same or a variety of assistance requirements. In the dissertation, the platform named the cable-based robot is a cable-based parallel structure for passive/active rehabilitation of the wrist, elbow, and shoulder.

The research in this project has the following aims/outcomes:

- Develop a novel control strategy that is capable of continuously engaging users to maximise their chances of achieving optimal motor recovery.
- The methodology for controlling the cable-based robot will be based on EMG signals from a variety of upper limb muscles.
- Muscle activities during different multi-joint movements can be used to estimate a user's motion needed forces.
- The motion needed forces can be decoded continuously from different users' EMG signals in real-time robot controlling as the control signals.
- Through the means of a large number of experiments, a robotic platform based on the proposed strategy will effectively assist users and enhance their motion ability.
- Examin the effects of the robot assistance on users motor control by analysing the coordination or synergies of multiple muscles.

1.3 Dissertation Contribution

This dissertation presents EMG decoder approaches based on the linear system method and nonlinear system method, which can satisfy different requirements in rehabilitation. These approaches show high potential in decoding motion intent and controlling robots to support participants with safe, smooth, and accurate assistance when they engage in repetitive exercise.

The primary contribution of this dissertation has six aspects, as listed below:

1. This dissertation firstly proposed and applied an EMG-based control strategy together with a decoder model for decoding EMG signals into motion needed forces. The EMG-based control strategy is a human-robot cooperation control scheme with visual interaction. The decoder model is composed of a switching mechanism and multiple submodels. All submodels are built by a linear modelling method, i.e., the state-space model. The decoder is used to reveal the continuous relationship between the multiple muscle activities and motion needed force. This state-space decoder model with a switching mechanism and submodels has the proven capability of accurately estimating the motion needed forces during users' voluntary multi-joint movements in real-time. This method can significantly improve decoding performance in multidirectional upper arm movements rather than other linear system methods. With this EMG-based control strategy, the robot can provide appropriate assistance to users by revealing their voluntary residual motor efforts.

2. This dissertation creatively proposes a bumpless switching mechanism for switching among the same-order submodels. This mechanism is designed to improve an unexpected 'bump' behaviour (i.e., the discontinuity) of decoder outputs and states during the switching between two submodels. This mechanism, together with the same-order submodels, is successfully applied in the EMG-based control strategy of rehabilitation robots. The outputs of the decoder achieved with the bumpless switching mechanism are significantly smoother than those achieved without this mechanism. The mechanism can prevent users from the potential risk of unpredictable output bumps and thereby protect them.

3. Based on the bumpless switching mechanism, a general bumpless switching mechanism is proposed for the first time in the area of robot control. This mechanism is developed to diminish the bumps of decoder outputs during switching among submodels with different orders. This mechanism is capable of selecting the best submodel for every subtask. It can improve the decoder model estimation accuracy, smoothness, and completeness when it is applied to robot-assisted multi-joint tasks. The mechanism allows a random selection of submodel orders and enlarges the application area of the proposed decoder model.

4. A novel time-variant Long Short-Term Memory (LSTM) method is firstly proposed to deal with the changeable characteristics of different users in EMG-based robot control. Unlike the traditional LSTM network, this method requires no secondary feature extraction or preprocessors. This method solves the model switching issues for the intention estimation during multiple tasks. Unlike most of the previous EMG decoder models, the proposed time-variant LSTM method significantly outperforms those decoders in subject-independence. This method can improve the modelling efficiency for patients who have similar motor abilities and similar rehabilitation aims. Its potential in multiple tasks indicates that it may be suitable for the post-stage patients who have regained most of their motion function and need to enlarge their motion area by random tasks.

5. This dissertation investigates the differences in recruited muscle patterns when users perform multi-joint arm movements with the aid of a robot or naturally without a robot. The possibility of describing multiple muscle activities during a tracking task by a linear combination of sets of muscle synergies is examined. The results indicate that both the natural and robot-assisted multi-joint movements can be generated by similar sets of synergies of limited dimensionality. The linear combination of synergies may thus be used in understanding the effect of the EMG-based control method and designing strategies for restoring functions.

6. This dissertation also investigates the recruited muscle patterns of three multi-directional tracking tasks with visual feedback interaction. The effects of task variety and tracking accuracy by visual feedback on muscle synergies and their activation patterns are explored. The task variety would affect the recruited

synergies, and both the task variety and the visual feedback would affect the duration and magnitude of the primary synergies. This investigation revealed that for active rehabilitation if the purpose is to enhance the synergy indication from the neural system, the task completion accuracy should be emphasised, but if the purpose is to expand the motion area, the task variety should be diversified. These results also support our other contributions that different decoders should be used and developed to meet the different assistance requirements of post-stroke patients.

The outcome of this dissertation is a natural integration for human-robot cooperation by using surface EMG signals for continuously, accurately and stably revealing the voluntary motor intention of users. Overall, this dissertation offers reasonable choices in a human-robot cooperation EMG-based robot control strategy with different EMG decoder models. The EMG-based control strategy shows high potential to control a cable-based robot to assist stroke patients who have the residual motor ability and different assistance requirements during rehabilitation.

1.4 Dissertation Outline

The outline of the dissertation is as follows:

Chapter 1

This chapter gives an introduction to the problem statement, motivation, and aims of the dissertation and provides an introduction to the contribution and outlines of the dissertation.

Chapter 2

This chapter firstly gives a brief introduction to the physiological structure of human upper limbs and a basic outline of rehabilitation. Then it introduces a literature review of related research topics to give a clear understanding of the rehabilitation robot and associated control strategies, especially those of EMG-based control schemes. Finally, the cable-based parallel rehabilitation robot used in this dissertation is introduced.

Chapter 3

This chapter describes the details of a state space modelling method that manipulates cable-based rehabilitation robots to assist multi-joint body motions. This uses an EMG decoder for continuous estimation of voluntary motion intention to establish a cooperative human-robot interface for promoting participation in rehabilitation exercises. In particular, for multi-joint complex tasks in three-dimensional space, a switching mechanism has been developed which can carve up tasks into separate simple motions. For each simple motion, a linear multi-inputs multi-outputs time-invariant model is established respectively. The experiments for examining the decoder model and EMG-based controller include model training, testing, and online verification application phases.

The work in this chapter has been published in:

- Yao Huang, Rong Song, Ahmadreza Argha, Andrey V. Savkin, Branko G. Celler, and Steven Su, "Continuous description of human 3D motion intent through switching mechanism," *IEEE Transactions on Neural Systems and Rehabilitation Engineering*, vol. 28, no. 1, pp. 277-286, Jan 2020.
- Yao Huang, Steven Su, and Rong Song, "Voluntary intention-driven rehabilitation robots for the upper limb," in *Intelligent Biomechatronics in Neurorehabilitation*, Academic Press, pp. 111-130, 2020.
- Yao Huang, Ying Chen, Jie Niu, and Rong Song, "EMG-Based control for Three-Dimensional upper limb movement assistance using a cable-based upper limb rehabilitation robot," in *Proc. 2017 International Conference on Intelligent Robotics and Applications*, pp. 273-279, August 2017.

Chapter 4

This chapter describes the details of a bumpless switching mechanism together with the same ordered submodels. The switching mechanism in Chapter 3 can accurately decode EMG signals but it was observed that a 'bump' behaviour of decoder output (i.e., the discontinuity) occurred during the switching between two subtasks. The bumps of outputs might cause unexpected impacts on the affected limb and thus potentially injure patients. To prevent this undesirable transient behaviour, we attempt to maintain

the continuity of the outputs during the switching between multiple EMG-decoder submodels for subtasks. A bumpless switching mechanism is proposed and applied in the control strategy of rehabilitation robots. Numerical simulation and real-time experiments are used to investigate decoder performance. The work in this chapter has been published in:

- Yao Huang, Rong Song, Ahmadreza Argha, Andrey V. Savkin, Branko G. Celler, and Steven Su, "Human motion intent description based on bumpless switching mechanism for rehabilitation robot," under review at *IEEE Transactions on Neural Systems and Rehabilitation Engineering*.

Chapter 5

This chapter describes the details of a general bumpless switching mechanism together with the different-ordered submodels and the effects on the model performance of initial hidden states of submodels. A common-order process is proposed and applied to realise a bumpless switching mechanism among different ordered models. The performance of this mechanism is verified by recruiting five healthy subjects to complete a square shape tracking task together with the robot in three-dimensional space. The effects of initial states are verified by experiments among four different kinds of initial states with the same models. The work in this chapter has been published in:

- Yao Huang, Rong Song, Ahmadreza Argha, Andrey V. Savkin, Branko G. Celler, and Steven Su, "EMG-based continuous motion intention description by a mixed-order bumpless decoder for rehabilitation robots control," ready to submit.

Chapter 6

This chapter describes in detail a method based on a LSTM network and a time-variant system which is thought to achieve better performance in EMG-based robot control. Unlike traditional methods, no secondary feature extraction or preprocessors are needed, and there is the potential in one model to solve the model switching issues for the estimation during multiple complex tasks. Subjects were instructed to produce three multidirectional tasks in three-dimensional space without and with robot assistance. The relationship between muscle activations from EMG signals and motion forces of arm movements are mapped by training two LSTM models based on the data of each

task and based on the data of all three tasks without labels. Furthermore, two methods based on Linear Time-Invariant (LTI) systems, which are a switched state space model and a PCA-based state space model, are also trained as comparisons. The work in this chapter has been published in:

- Yao Huang, Rong Song, Ahmadreza Argha, Andrey V. Savkin, Branko G. Celler, and Steven Su, "Continuous estimation of motion intention based on EMG signals using a time-variant long short-term memory network," ready to submit.

Chapter 7

This chapter investigates the possibility of describing a tracking task finished by healthy participants with assistance from a Myoelectric controlled rehabilitation robot by a linear combination of sets of muscle synergies. Thus, the differences are examined in the neural control mechanisms by comparing the extracted main muscle synergies from the task performed without and with robot assistance. The task required participants to track moving markers in a multi-joint square shape in a horizontal plane in 3-dimensional space. The tracking task was accurately described by a linear combination of a variety of synergies extracted from the multi-joint task of each participant, both with and without robot assistance. The synergies were compared between the two conditions. The work in this chapter has been published in:

- Yao Huang, Rong Song, Ahmadreza Argha, Andrey V. Savkin, Branko G. Celler, and Steven Su, "The effect of assistance from an EMG-based control robot on upper limb muscle synergies," ready to submit.
- Yao Huang, Ying Chen, Jie Niu, and Rong Song, "EMG-Based control for Three-Dimensional upper limb movement assistance using a cable-based upper limb rehabilitation robot," in *Proc. 2017 International Conference on Intelligent Robotics and Applications*, pp. 273-279, August 2017.

Chapter 8

This chapter analyses task effects and tracking accuracy on muscle patterns. Muscle synergies and their activation patterns are identified and extracted from the EMG signals during three multidirectional tracking tasks with visual feedback interaction. A

standard method used in this chapter is the Basic Non-negative Matrix Factorisation (BNMF) with initial estimation. By recruiting a modular organisation of muscle with relative activities, the arm motion can be indicated by the neural system and generated for performing a variety of motor tasks. The effects of task variety and tracking accuracy by visual feedback on muscle synergies and their activation patterns are explored by statistical analysis.

The work in this chapter has been published in:

- Yao Huang, Rong Song, Wenhui Chen, Hairong Yu, Ahmadreza Argha, Branko G. Celler, and Steven Su, "The effects of different tracking tasks on muscle synergy through visual feedback," in *Proc. 2019 41st Annual International Conference of the IEEE Engineering in Medicine and Biology Society (EMBC)*, pp. 417-420, July 2019.

Chapter 9

This chapter summarises the works of this PhD dissertation and presents the future research developments

Chapter 2

Backgrounds and Literature Review

In this chapter, we first briefly describe rehabilitation robots. Then, the rehabilitation control strategies for solving the problems in this dissertation is introduced.

2.1 Physiological Structure of Human Upper Limb

2.1.1 Upper Limb Structure

The basic structure of human upper limbs is composed of shoulders, upper arms, forearms, and hands. The bones that connect the main structures of the upper limbs include the scapula, humerus, radius, ulna, and wrist bones. The main muscles of the upper limbs include the deltoid muscles on the shoulders, the biceps and triceps on the upper arms, and the brachioradialis on the forearms. The main joints of the upper limb are the shoulder joint, elbow joint, and wrist joint. The basic structure of the upper limb is shown in Fig.2.1.

Considering that this topic is mainly aimed at the situation where the shoulder and elbow joints coordinate to drive the upper arm forearm movement, the following describes the Degree of Freedom (DoF) of the relevant structure: 1) The shoulder joint has three DoFs including abduction/adduction, internal rotation/external rotation,

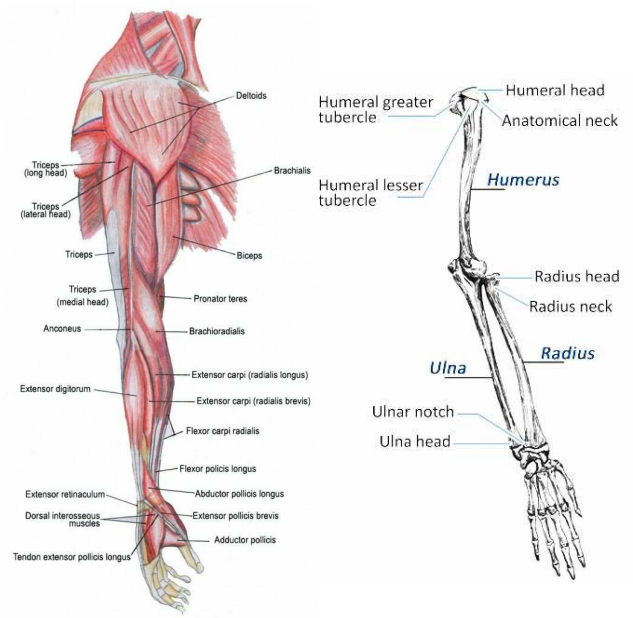

Fig. 2.1 Arm muscles and bones (http://healinghealthyholistic.com/category/anatomy-physiology/).

and flexion/extension; 2) The upper arm is fully constrained, with zero DoF; 3) The elbow joint has only one DoF in flexion/extension; 4) The forearm has only one DoF of rotation in/out.

2.1.2 Main Muscles Responsible for Upper Limb Movements

When the upper limbs complete different movements, different muscles are involved. This topic considers movements with comprehensive multiple DoFs. Therefore, first, some major muscles involved in the thesis are introduced.

Brachioradialis (BR) is innervated by the radial nerve, posterior fascicle nerve, superior trunk nerve, and C5 and C6 nerve roots. The physiological position starts from the upper two-thirds of the lateral supracondylar ridge of the humerus and ends on the lateral surface of the base of the radial styloid process. It is the first muscle on the outside of the biceps tendon. This muscle is the only major elbow flexor muscle

that is not innervated by the musculocutaneous nerve. It can be activated by flexing the forearm in a neutral position.

Biceps brachii (BIC) is innervated by the musculocutaneous nerve, lateral tract nerve, superior trunk nerve, and C5 and C6 nerve roots. It is mainly divided into lateral head and medial head. Its physiological position mainly starts from the coracoid process of the scapula and the scapular glenoid nodule and ends at the back of the radial tuberosity. This muscle can be activated by flexing and supinating the forearm at the elbow joint.

Triceps brachii (TRI) is innervated by radial nerve, posterior fascicle nerve, superior trunk nerve, middle trunk nerve, inferior trunk nerve, and C6, C7, C8 nerve roots. It is mainly divided into lateral head, long head, and medial head. Its physiological position mainly starts from the back of the humeral shaft and under the glenoid of the scapula and ends at the back of the olecranon process. This muscle can be activated by using the elbow joint to extend the forearm.

Deltoid is innervated by axillary nerve, posterior fascicle nerve, superior trunk nerve, and C5C6 nerve root. It is mainly divided into the front part (Anterior Deltoid, DA), the middle part (Middle Deltoid, DM), and the rear part (Posterior Deltoid, DP). The physiological positions of the three parts start respectively from the upper front edge of the outer clavicle, the upper outer edge of the acromion, and the lower edge of the scapular spine, and all end at the humeral deltoid tuberosity. DA can be activated by flexing and internally rotating the upper arm. DM can be activated by the upper arm abduction. DP can be activated by extending and externally rotating the upper arm to the back.

Then, the range of motion of each DoF and the mainly involved muscles are introduced and summarised in Table 2.1.

Table 2.1 Degree of freedom of the upper limbs, mainly related muscles and their range of motion.

Structure	DoF	Mainly related muscle	Range of motion
Shoulder	Flexion	Coracobrachialis, Anterior deltoid, Clavicle of pectoralis major, Short head of biceps	70°-90°
	Extension	Latissimus dorsi, Posterior deltoid, Long head of triceps	40°-45°
	Adduction	Pectoralis major, Latissimus dorsi, Subscapularis	20°-40°
	Abduction	Middle Deltoid, Supraspinatus, Long head of biceps	80°-90°
	Pronation	Latissimus dorsi, Pectoralis major, Subscapularis, Anterior deltoid	70°-90°
	Extorsion	Infraspinatus, Teres minor	40°-50°
Elbow	Flexion	Brachialis, Biceps, Brachioradialis	130°-150°
	Extension	Triceps	0°-10°
Forearm	Pronation	Pronator teres, Pronator quadratus	80°-90°
	Extorsion	Supinator, Biceps, Brachioradialis	80°-90°

2.2 Basic Knowledge of Rehabilitation

2.2.1 Rehabilitation Tasks

The design of upper limb rehabilitation exercises should conform to the actual operating space of the human body, so the size of the human limbs must be used as a reference basis. Two dimensions of limbs' motion are considered simultaneously: one is the size of the human body structure in a static state, and the other is the motion area. In this dissertation, the arm motion is focused. The static size is mainly the length of the upper arm and forearm when at rest. The motion area of the upper limb is mainly the range of motion of the upper arm, forearm, and hand. For all recruited subjects, we measured and recorded their height, weight, and the length of the upper arm, forearm, and hand. Combined with the size relationship between the limbs of the typical size of the human body [53], the upper limb movement reachable space of all subjects can be calculated. All tasks in this dissertation are designed within the intersection of all subjects' reachable space.

The existing rehabilitation theory divides rehabilitation exercises into the following four categories according to the degree of active participation of patients in the process of completing rehabilitation auxiliary exercises [54]: 1) Passive mode [55]: During the training process, the patient does not actively participate at all, and the training is completed with human/machine assistance; 2) Active-assisted mode [55]: During the training process, the patient has a certain degree of active participation together with the assistance from therapists/machines;3) Active mode: During the training process, the patient actively controls the limbs to complete the training without human/machine assistance; 4) Active-constrained mode [56]: During the training process, the patient completes the training while overcoming additional resistance.

Different exercise modes have different requirements for patients' muscle strength and motion control ability. Among the modes mentioned above, the requirements for the motion control ability of patients from weak to strong are the passive mode, the active-assisted mode, the active mode, and the active-constrained mode. The modern rehabilitation treatment process may include the above four modes. The therapist designs a suitable rehabilitation treatment plan for a patient based on his/her actual physiological condition after a stroke, combined with different modes. The optimal expected result of the treatment plan is that the treatment plan can effectively enhance muscle strength and restore motion control ability. In order to achieve different rehabilitation training modes, many researchers have carried out research on the control strategies of rehabilitation robots.

Based on different structures and different control strategies of rehabilitation robots, therapeutic programs can be classified into a passive range of motion, an active range of motion, an active-assisted range of motion, and an active-constrained range of motion [54]. All the programs are widely accepted and applied in clinical post-stroke rehabilitation. The basic challenge of designing a robot-assisted rehabilitation treatment is to execute predesigned tasks and provide assistance or resistance under different requirements [57]. Depending on the actual motion ability of post-stroke patients, the treatments should improve their motion ability and activity functions. For example, the passive range of motion mode is to move the upper limbs of post-stroke patients independently by a well-controlled robot [54]. Gravity compensation is a typical active-assisted range of motion therapy programs [58] that can improve the participation of

robot-assisted rehabilitation training. Gravity compensation is a typical active-assisted range of motion therapy programs that can increase the arm motion area and improve the participation of robot-aided rehabilitation training [59, 58]. An EMG driven system can finish both typical active range of motion therapy programs [60] while a most active-constrained range of motion therapy programs can be realised by robots based on position control[61].

2.2.2 Control Strategy Requirements

Motion ability conditions of different patients

Mainly consider the patient's muscle strength level. Patients with hemiplegia are often divided into the following three levels [62]: 1) Paresis score>3: patients' muscle strength is weaker than healthy people, and patients can still complete most of the daily exercises; 2) Paresis score=2/3: patients' muscle strength is weaker than those patients in 1), and patients can complete some activities with assistance; 3) Paresis score<2: patients' muscle strength is weaker than all other patients, and patients cannot move their limbs independently.

Safety during training

The patient's limb movements may not be easily controlled. Therefore, it is easy to suffer from secondary injuries during training. In rehabilitation training, the absolute safety of the patient's limbs is the most basic requirement. The safety of patients needs to be guaranteed from various aspects such as training strategy, robot platform safety, and strict supervision by therapists.

Effectiveness of training and robot assistance strategy

The designed rehabilitation robot-assisted training strategy should be able to assist patients in completing a variety of tasks effectively. It should also be able to promote the progress of their rehabilitation and achieve the purpose of helping them recover their athletic ability. In the robot-assisted training, combining the observation of therapists, the patient's perception of changes in motion ability, and the objective data measured by the robot sensor system, a data basis can be obtained to analyse and reveal the effectiveness of the training strategy.

Diversity of training tasks

In robot-assisted rehabilitation training, it is necessary to provide as many optional training strategies and tasks as possible. This can introduce a variety of methods to restore motor function for different patients, and their different rehabilitation needs [63, 64].

2.3 Literature Review

2.3.1 Rehabilitation Robots

A serial robot means that the transmission chain of the robot consists of a set of rigid connecting rods. The rigid rods are connected in pairs by rotatable or movable joints. The rods can be driven by moving the connected joints. A serial robot is a traditional form of the robotic system. This kind of robot has the advantages of simple configuration and low construction cost.

One of the most famous and successful rehabilitation robots in the rehabilitation area is the MIT-Manus [65]. It is a two-link serial robot with two DoFs and can interact with a user's arm in a workspace in the horizontal plane [1]. Fig. 2.2 is a side view showing the MIT-Manus robot and how a patient visualises the exercise and move his/her hand. A splint is used to secure the user's forearm to the end-effector of the robot. A torque sensor is used to detect the user's arm motion torque. A virtual interface is designed to offer different training scenarios to users. Clinical tests for proving the effectiveness of the robot-assisted rehabilitation have been performed by MIT-Manus. However, due to the structure limitation, not all arm movements required in a typical rehabilitation therapy can be performed by the robot, especially those multi-directional movements in 3D space. Therefore, many other approaches have been proposed to overcome this limitation.

A spatial workspace can be obtained by combining various serial robots with multiple DoFs. Assisted Rehabilitation and Measurement (ARM) Guide is a typical sample and also is a singly-actuated robot. The ARM Guide robot and how a user moves her arm with visual interactions are shown in Fig.2.3. It consists of a specially

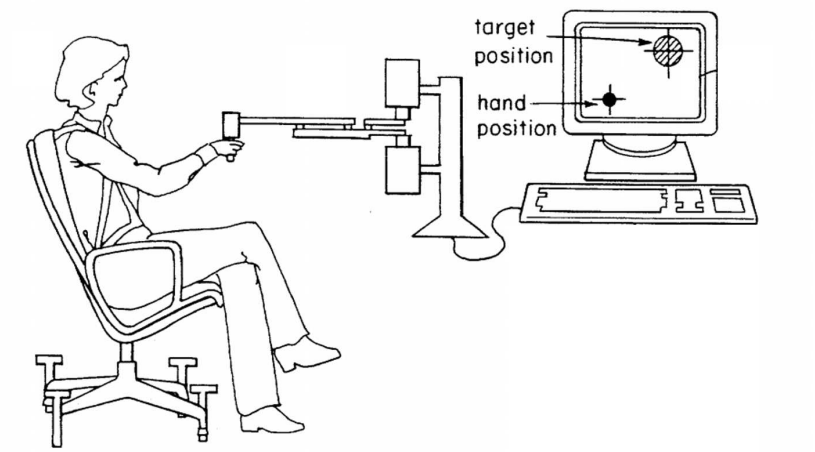

Fig. 2.2 The MIT-MANUS [1].

designed splint that can slide along an orientated linear constraint [2]. When using the ARM Guide to support a user, the user's forearm and hand are attached to the splint which is driven through a chain by a motor. Extra balancing masses are compulsory to balance the heavyweight of the frame. With the masses, the splint could remain in any specific position, and the linear restraint could be placed with any pitch angle. Although the ARM Guide allows wider movements in space, the heavy frame may affect the user's motion quality with robot-assisted assistance.

Fig. 2.3 The ARM Guide [2].

The Mirror-Image Motion Enabler (MIME) system uses a Puma robot with six DoFs to interact with the user's arm and support their arm motion with four modes [55]. The MIME robotic system is shown in Fig.2.4. Three modes are unilateral with

passive assistance, and one mode is bilateral with active-assisted assistance. With the passive mode, the robot directly assists the arm in moving along preprogrammed trajectories without user's own willing of position, and orientation changes [66]. With the active-assisted mode, the robot assists the affected arm of a patient along the desired trajectories under the guidance of the healthy side and his/her initiative effort. This system has been used in stroke patients rehabilitation therapy and compared with traditional rehabilitation therapy. In clinical trials, the results of this robot-assisted therapy showed a more significant increase in strength and reach extent than the traditional therapy [56].

Fig. 2.4 The MIME robotic system [3].

ARMin is a semi-exoskeleton robot with haptic display and has four active and two passive DoFs [4]. The robot structure is perfectly fitting human arms, and support arms in 3D space shown in Fig2.5. With the signal collection in position, force, and torques during a user's arm motion, the robot can support the user in human-cooperative therapy for arms as the user's needs. The main drawback of this multi-DoFs semi-exoskeleton robot is the difficulties of the robot transmission structure design and analysis and the complexity of setting different users' arms inside the robot.

These serial structure robots mostly have dense mass and a high number of mechanical components, which makes them can not be transported or relocated easily. Their main parts are mostly stiff structures and rigid links that potentially cause safety risks when any one part of hardware or software occurs a fault [67]. Other shortcomings are also prominent, including insufficient load-bearing capacity, low structural rigidi-

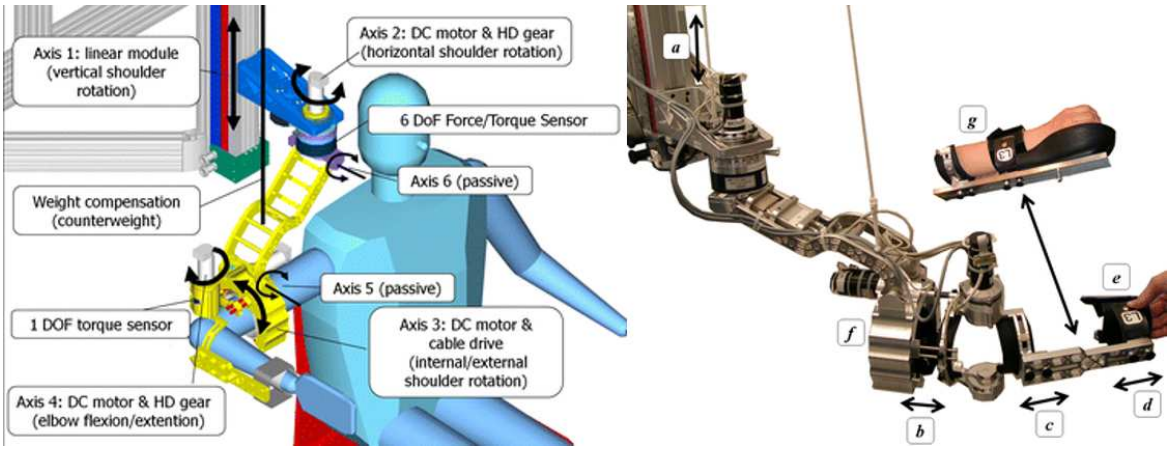

Fig. 2.5 The ARMin and six adaptation choices (a-f) for different arm sizes [4].

ty, unsuitable for high-speed movements, and large cumulative control errors during movements.

A parallel structured robot means that the transmission chain of the robot is connected by a series of connecting rods. There is an interaction force between all connecting rods so that they can support and restrain each other. This parallel structure has the advantages of strong carrying capacity, high structural rigidity, small cumulative control error during movements, and high control accuracy. However, the rigid rods may also cause problems related to the heavyweight structure.

With the improvement of the requirements for control accuracy and user safety in the field of rehabilitation robot, parallel structured robots driven by cables are introduced to overcome the disadvantages of stiff structures and serious structures by interacting with users more compliantly [20]. Compared with the rigid transmission chain, transmission chain structure based on cables has various advantages, including strong reconfigurability, relatively low energy consumption, ample motion space, lightweight, low inertia, and fast operation speed. The structure of cable-driven robots is mostly light and portable that bare no rigid collisions would happen between robots and users. The good reconfigurability and ample motion space can meet the requirements of different rehabilitation training modes. The cable-driven structure provides comfort, safety, and multi-motion options for both patients and therapists in clinical trials based on its flexibility and adjustability. These users' arm motion has been proved can be supported in a 3D space utilising various cable-driven parallel robot systems.

The GENTLE/s project combines a parallel cable-driven robotic system, haptic, and virtual reality technologies to develop new and motivating therapies for neuro and physical rehabilitation [68]. During robot-assisted movements, the user's arm is constrained in an elbow orthosis which is suspended to the frame Fig.2.6. The effects of arm gravity can be eliminated for achieving the active-assisted mode. GENTLE/s is dedicated to helping increase sensory input, relearning brain stimulation, and achieving the goals of improving arm motor independence and coordination [69].

Fig. 2.6 The prototype of GENTLE/S [4].

Multi-Axis Cartesian-based Arm Rehabilitation Machine (MACARM) is a cable-driven robot developed for the upper limb rehabilitation proposed by Mayhew D. et al. [70] A cubic frame is designed to configure motors and connectors that connect to cables and an end-effector Fig.2.7. The end-effector locates in the spatial centre of the frame and has six DoFs. The forces during end-effector movements are recorded by a 6-DoF load cell. The path repeatability of MACARM has been demonstrated favourable for robotic rehabilitation [5].

Marisa Robot (MariBot) [7] is a 5-DoF upper arm rehabilitation robot based on a 3-Dof prototype Neurorehabilitation Robot (NeReBot) [6]. The robot shown in Fig.2.8 is a combination of a 2-DoF plane serial manipulator and a 3-DoF parallel cable-driven structure. The serial manipulator is designed for locating the cable-driven structure to the aim positions on the horizontal plane. The robot provides assistance to a user by pulling the cables connected with a splint. The user's forearm is constrained by the splint and always moves together with the splint. During assisted movements, a

Fig. 2.7 The MACARM cable-driven robot [5].

graphical interface is introduced to catch the user's attention on movement performance. The clinical tests for the robot revealed an increase in motor recovery and positive functional outcomes [71].

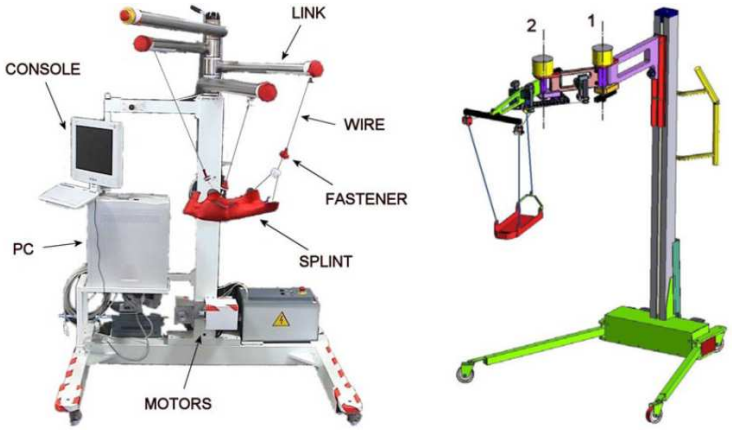

Fig. 2.8 The NeReBot and MariBot [6, 7].

Since the end-effector of these cable-based robots mostly runs under low-speed and cables' configurations may increase interference, the workspace volume of a parallel cable-driven robot may be constrained [72]. At the same time, the control of parallel structured cable-driven robots is more complicated than serial structured robots. To solve the problems, the frame structure and cables' configurations of this kind of robot should be designed appropriately, and the accessible tasks for users should be

well-preprogrammed. Based on the analysis and clinical effects of the above-mentioned rehabilitation robots, a parallel cable-driven structured rehabilitation robot is a good choice that can take into account the rehabilitation training function while satisfying the safety and comfort of the patient.

2.3.2 Control Strategies

The major aim of the robot-assisted rehabilitation is to restore neuroplasticity through a variety of training modes and to improve user's initiative motor function. Therefore, the robot control strategy that controls how a robot physically interacts with users is one of the most important core problems in rehabilitation robot design. For many years, people have tried to reveal the nature and laws of human's motion from a variety of signals generated during human's initiative movements and then used to predict motion intentions. These signals include kinematic and dynamic signals such as position, force, torque, and also various bio-signals [73].

Due to the increasing demand for the patient initiative during the rehabilitation process, biosignals which are closely related to the human effort is highly focused. Bio-signals are regarded as direct information that is related to human movements. It is fully accepted that the correlation between EMG signals of specific muscle and various movements are undeniable. With the noninvasiveness and relative robustness in the EMG collection, the EMG signal has been proved effectively applied in the field of prostheses, exoskeleton, stroke rehabilitation, and robot control. EMG-based control strategies have become a popular and practical hotspot in the rehabilitation robot field [43, 74–77]. Compared with the physical sensor-based robot control strategy, the biosensor-based robot control strategy for rehabilitation can more naturally trigger movements by human intention motion.

EMG signals are capable of reflecting muscle activities and status, which is required for robot-assisted rehabilitation therapy. In the early stages of rehabilitation of clinical trials, muscle activities of post-stroke patients have most possibly stayed at a low activation level, and their muscle strength is mostly weak. Based on the EMG signals in this stage, the training mode and task difficulty should be easy to encourage patients' initiative and control robots easily. In the later stages of rehabilitation, patients' muscle

activities are always higher after a period of training, and they have stronger muscles. In this stage, the training mode and task difficulty should be changed to adapt to patients' motion ability better. Recent work by Colombo et al. has described a robot that can match the abilities of each patient in different stages by task difficulty levels [78]. This work has proved to bring positive effects on patients' motor recovery. [66].

To better explore patients' motor function and assist patients, recent studies have attempted to develop neural networks that map EMG signals to muscle strength and apply them in robot-assisted rehabilitation. Specifically, EMG decoders are mostly used to estimate motion intention from EMG signals [79, 80] and are highly concerned with control strategy and motor function evaluation research. There are two main design schemes for them: pattern recognition and direct control [81].

The pattern recognition scheme in myoelectric control is more likely to extract and classify basic patterns that happen during motion. Phinyomark et al. [82] analyzes time and frequency domain features and found four groups of features that are mainly useful for EMG-based motion pattern recognition. Antuvan et al. [49] applied an extreme learning machine together with using synergy feature for online myoelectric control. The method shows the robustness of online decoding of upper-limb motions and motor intentions. However, despite its reliability in results, the outputs of the scheme are predefined motion classes, the number of patterns that can be chosen is limited [83]. The requirements of the coordination of multiple physiological degrees of freedom across multiple joints and the continuity among different classes are intractable issues that needed to be addressed [84]. In the field of rehabilitation robot control, simultaneous and continuous control of multiple DoFs is necessary.

For a direct control scheme, the main aim is to estimate forces or torques in time series for simultaneously controlling robotics or prostheses directly from EMG signals or their characteristics. Based on muscle's physiology characteristics, a nonlinear Hill-based muscle model is derived for continuously predicting the limb moment from the muscle activities and joint kinematics [85]. However, due to the vast parameters needed for each muscle and nonlinearity of the model equations, the hill-based model is rarely applied in control involving multiple joints and muscles.

By applying binary or multiclass classification algorithms, the robot can be controlled in discrete mode. Dipietro et al. map the EMG signals into the binary output for determining the onset and end of the movement [44]. Ding et al. represent the relationship between the EMG patterns and predefined static postures or movements by the Artificial Neural Network algorithm [86]. For *continuously* controlling a single joint robot to assist participants, apart from the Hil-based model [85], a linearly proportional EMG control strategy is proposed [60]. Based on the theory of muscle synergy [47] and movement primitives [87], Artemiadis et al. [50] proposed a state-space model with reduced dimensionality for continuously mapping the EMG signals to multi-joint movements.

However, the performance of these models is mostly task-dependent and participant-dependent, which settles a big challenge in modelling accuracy with reduced model dimensionality. Moreover, although the linear system modelling methods are easier to be realised and only required individual data for training parameters, the nonlinearity of EMG signals is not fully considered, and more movements related to various DoFs are needed to be represented.

With the development of nonlinear system methods and deep learning methods in biological signals, lots of strategies that can solve many complex problems have been proposed. The non-stationarity of EMG signals across sessions and achieve much better performance are reported by using a decoder model based on kernel ridge regression [88], and a three domains fuzzy wavelet neural network algorithm [89]. In the research of Kiguchi et al. [79], a neuro-fuzzy matrix is used to establish the relationship between EMG signals and joint torque. Choi et al. have established an artificial neural network [90] to estimate the pinch force from several segments of EMG signals. Zhang et al. have proposed a nonlinear force prediction model through the BP neural network [80]. Moreover, some studies also combined different deep learning methods such as convolutional neural network, Recurrent Neural Network (RNN), and LSTM to obtain a much general and robust algorithm with even better performance in decoding EMG signals [83, 91]. Machine learning methods with enormous data support have shown great power for myoelectric control while some variabilities such as fatigue, and physiological factors of EMG signals still need more investigation [92].

Generally, deep learning methods try to extract features on multiple levels of representation and learn very complex functions with the composition of several layers. An advantage also shows in the learning procedure where layer features can be learned without human designing [93], and also no physiological significance needs to be related. It is much easier to be applied in real and commercial rather than traditional linear system methods which require dedicated design based on biomedical experts. Although most of the mentioned research has demonstrated impressive power in force estimation, and controlling prostheses and rehabilitation robots, the complexity and its requirements in data size, and time cost training procession are key points in results.

Compared with other methods, one outperformed virtue of EMG control is that a user can use his/her muscles to control the robot more naturally. However, the muscle activation level is also affected by the electrode's position, skin impedance and time difference. For different individuals and individuals at different collection times, the muscle activation level is not exactly the same. Therefore, few studies only introduce multi-channel EMG signals as the control source to complete the entire cycle of robot-assisted rehabilitation no matter with linear or nonlinear system-based approaches.

To further increase the patient's initiative to participate in rehabilitation, robot control strategies that provide assistance based on the patient's status and needs are needed. In other words, the robot system needs to adaptively examine the patient's movement ability and provide appropriate assistance when needed. Krebs et al. has proposed a 'performance-based' progressive control strategy with its core part as 'assist-as-needed' mode [28]. This method encourages patients to involve in rehabilitation therapy and maximise recovery extent actively. Today, the positive outcomes achieved by actively participate in robot-assisted rehabilitation have made the 'assist-as-needed' mode become one of the most recognised paradigms [73].

2.4 A Cable-based Rehabilitation Robot

2.4.1 Basic Structure and Components

A parallel structured cable-driven upper limb rehabilitation robot (denoted as a cable-based rehabilitation robot) recruited in this dissertation is shown in Fig.2.9 and Fig.2.10 and designed by Yang et al. [94]. The basic structure of the robot includes a cubic frame, a motor unit (DM1B-045G, Yokogawa, Japan) with servo drivers (UB1DG3, Yokogawa, Japan), three cables connected to the motors, pulleys, and connectors, and a selectable end-effector. The cubic frame is made of aluminium profiles and is mainly used to fix the motors and connectors. The motor unit includes three motors with stands and transmission components. The transmission components include a rod responsible for winding cables and controlling the cable's length when the motor rotates, and a coupling accountable for connecting the motor shaft and the rod. The cables are made of steel wire. One end of a cable is fixed on the rod, and the other end is fixed on the end-effector. The cable passes through several fixed pulleys to change the direction reflecting the force/torque from the motor to the end-effector. The connectors and pulley are used to configure the workspace by connecting to cables. The end-effector can be chosen as a splint or a glove according to training modes. The end-effector links the three cables on a specific connection point. The DoF of the end-effector is restricted at three by avoiding rotations in any dimensions. The position of the end-effector in 3D space can be changed by pulling or loosening cables controlled by three motors. A PXI integrated controller contained a high-precision motion control card (4-axis, PXI-7340, National Instruments) is connected with the motors and drivers for directly controlling motors. The rehabilitation robot adopts PC to set control commands of the PXI controller to make it possible to realise more complex control for application in rehabilitation.

The rehabilitation robot platform provides two sets of safety protection measures. One is to set a safety threshold before transmitting instructions between the controller and the driver. If the control signal exceeds the setting, the drive signal will be limited under the safety threshold. To this end, the range of forces was limited to $[-100N, 100N]$. Specifically, if the forces were out of the range, the forces were set to

Fig. 2.9 A photograph of the cable-based rehabilitation robot.

$-30N$ (if less than $-100N$) or $30N$ (if more than $100N$). Second, the robot has an external safety switch and pressing the button can terminate motors instantly. When a user is using the robot, the safety switch is held by the unused hand. When the user notices any potential risks, he/she can protect himself/herself immediately.

2.4.1.1 Kinematics Signal Acquisition System

The robot uses the OptiTrack motion capture system with four cameras (OptiTrack, NaturalPoint, USA) to capture joints' position changes during arm motion. The cameras (shown in Fig.2.11 (a)) emit infrared light and collect the reflected light from markers covered by reflective material. By integrating the data from more than three cameras, the markers' location in the 3D space can be obtained accurately. The precision of this system is 0.1 to 1mm. In the cable-based robot, the four cameras and related components of the kinematics signal acquisition system are installed vertically on the cubic frame, as shown in Fig.2.11 (b). The acquisition range covers the workspace of the robot. Since this dissertation aims to investigate robot-assisted rehabilitation for the whole upper limb, the kinematics of three joints of the arm, i.e., the should, the

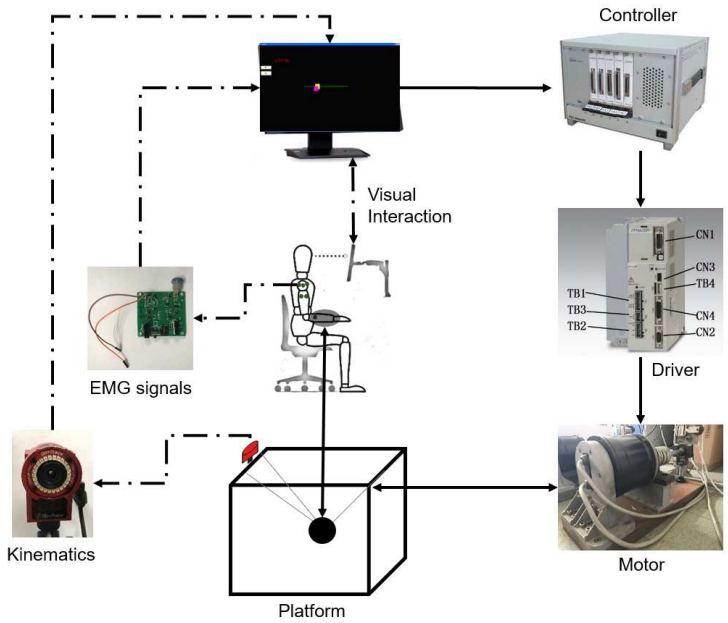

Fig. 2.10 Architecture of the cable-based rehabilitation robot.

elbow, and the wrist are all needed to be analysed. Three markers are placed on the outer side skin surface of the three joints centre for collecting these joints' kinematics signals. The sampling rate is set to 100 Hz, and the original data is filtered using a second-order Butterworth filter with a cutoff frequency of 6 Hz.

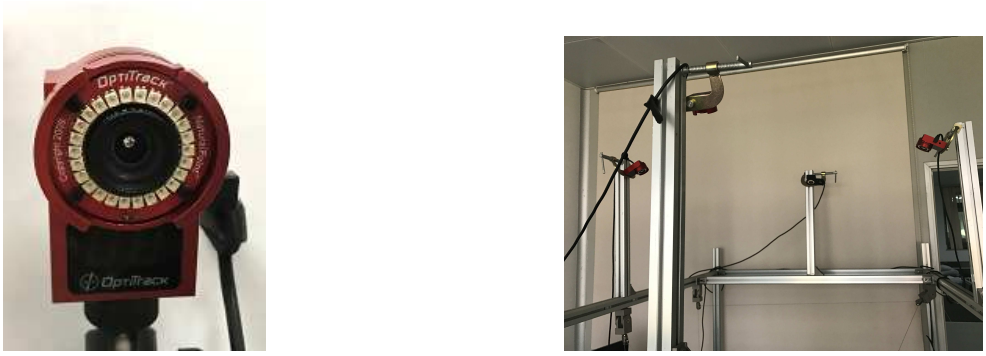

(a) (b)

Fig. 2.11 The Optitrack motion capture system. (a) Cameras. (b) Installation location on the frame.

2.4.1.2 Surface EMG Signal Acquisition System

The surface EMG signal refers to the weak physiological electrical signal generated by muscle fibres when a muscle contract. It can be collected non-invasively by pasting paired-electrodes on the surface of the skin. The EMG signal is a physiological signal that can reflect the physical condition of the limbs and the intention of motion changes, and it is closely related to the characteristics of muscle and joint movement. It is widely used in many research fields, especially in the field of rehabilitation [95]. By analysing the EMG signal, the intactness of the muscle can be investigated [96], and the change of joint position can be inferred to predict movement intention. The robot uses a self-made multi-channel surface EMG signal acquisition system, as shown in Fig.2.12, to realise the acquisition, amplification, and filtering of EMG signals. The surface EMG signal acquisition system involves six pairs of electrodes, six single-channel EMG acquisition circuit boards with the amplifier (gain of 5000) and the physical low-pass filter, and one 16-bit analog-to-digital data acquisition card (PXI-6229, National Instruments, USA). The acquisition system records the EMG signals of six superficial muscles for upper limb movements. The six muscles are BIC, TRI, DA, DM, DP and BR. The EMG signals are all recorded at a frequency of 1000 Hz. Then they are band-filtered by a 4th-order Butterworth filter with a frequency band of $10 - 400$ Hz.

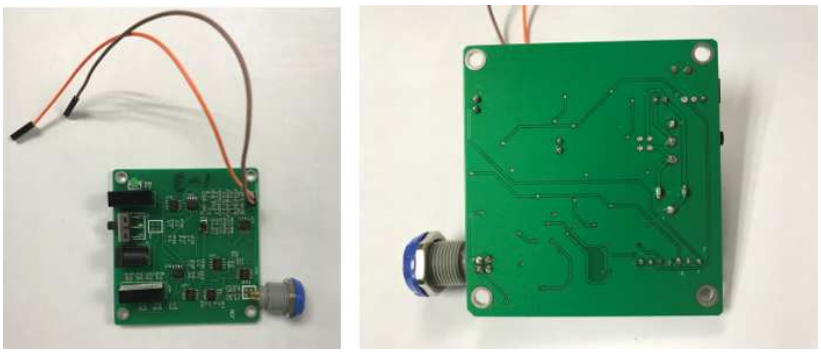

Fig. 2.12 Surface EMG signal acquisition card.

For synchronisation between the muscle activations and the motion required forces in some chapters, the muscle activations were decimated into a new serial with the frequency of 100 Hz.

2.4.2 Robotic Dynamic Analysis

The dynamic model of a robot is the relationship model between the kinematics characters and the dynamic characters. It is also an essential part of the research on robot control. The precision of the dynamic model will directly affect the control accuracy of the robot. In this parallel cable-driven rehabilitation robot, the cable stiffness is not taken into consideration and is assumed to be infinite. During the end-effector's movement, it is assumed that the end-effector always moves within the workspace in a fully constrained state, and all cables connected to the end-effector are tight. Under these mentioned conditions, the dynamic model can be analysed similarly to a traditional parallel structured robot. The analysis is thoroughly investigated by Yang et al. [94] when applying the robot in a passive rehabilitation mode. In this part, only significant characteristics of the robot dynamic model are introduced. First, the static model of the end effector is introduced. Then the dynamic model considering the system speed and acceleration is introduced. The dynamic model includes the dynamic model of the end-effector's, the winding rod's (the motor-cable connection) and the entire robot system's dynamic model.

2.4.2.1 Robot Statics Model

The statics model of the robot refers to the assumption that the end-effector is in a static state and, the end-effector is subjected to other external forces besides the cable tension. The model can be used to calculate the length and change of the three cables based on the spatial positions of the end-effector and those connectors on the frame. It can always solve the cable tension matrix when knowing the external force matrix and position matrix received by the end-effector. According to the principle of static balance, the vector sum of the end-effector's external moments is equal to the vector sum of the tension of the three cables. The formula is as follows:

$$X_{di} = \sqrt{(p_{ix} - x_i)^2 + p_{iy} - y_i)^2 + p_{iz} - z_i)^2} \tag{2.1}$$

where p_{ix}, p_{iy}, and p_{iz} represent the 3D coordinates of the i-th connector. x_i, y_i, and z_i represent the 3D coordinates of the end-effector.

When the robot is applied to robot-assisted rehabilitation, the moving speed of the end-effector together with the user's arm, is always low. Therefore, the static force model is capable of investigating the robot's dynamic characteristics, as shown in Fig.2.13. The cable tension can be modelled and calculated based on the static model with the assumption that all cables maintain tension. The equation of the static model is expressed as follows:

$$T = J^{-1}F \tag{2.2}$$

where $T = [t_1, t_2, t_3]^T$ is the cable tension matrix, and $J = [u_1, u_2, u_3]$ is the unit vector matrix of the mechanism and $F = [f_x; f_y; f_z]^T$ is the forces matrix along three dimensions.

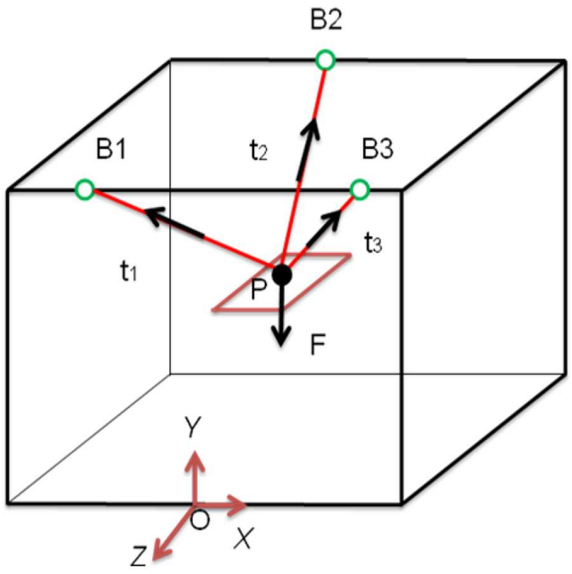

Fig. 2.13 The static force model of the cable-based robot. Points B_{1-3} are the positions of the connectors. Point P is the connection points between cables and the end-effector.

According to the cable tensions and the total mass of the end-effector and the arm, the needed acceleration of the three cables for changing the position of the end-effector can be calculated as follows:

$$\Delta X'' = (T_a - T)/m \tag{2.3}$$

where $T_a = [t_{a1}; t_{a2}; t_{a3}]$ is the actual tension matrix that measured by the force sensors, and m is the total mass of the end-effector and the user's arm, and $\Delta X'' = [\Delta x_1''; \Delta x_2''; \Delta x_3'']$ denotes the cables' accelerations matrix.

2.4.2.2 Robot Dynamic Model

When the end effector assists the subject in completing arm movements, the end effector and the subject's upper limb can be approximately equivalent to the whole. It is not necessary to consider the rotation and interaction between the two. At this time, the end effector is under the control of motors, and its kinematics needs to be considered. During the movement, the force analysis of the end-effector can be regarded as a mass point. The force balance equation of the end-effector is as follows:

$$\sum_{i=1}^{3} t_i + f_q + mG - m\dot{v} = 0 \tag{2.4}$$

where f_q is the external force (without gravity) applied on the end-effector, and m is the total mass of the end-effector and the user's arm, and $G = [0, g, 0]^T$ is the acceleration vector of gravity, and v is the velocity of the end-effector.

The winding rod is a component that connects and fixes a motor and a cable. Each cable is tightly wound on the winding rod and kept tangent to the rod. The dynamic equation of the winding rod is:

$$J_r\ddot{\beta} + C\dot{\beta} + rT = \tau \tag{2.5}$$

where J_r is the moment of inertia of the rod, and β is the rotation angle of the rod, and C is the damping coefficient of the rod, and r is the radius of the rod, and T is the cable tension, and τ is the torque produced by the motor. The winding scheme of the three cables is the same, and three motors of the same type are connected, and the moment of inertia and damping coefficient of each rope winding rod is the same.

Combining Eq.2.1, Eq.2.4 and Eq.2.5, the dynamic model of the robotic system is:

$$J\frac{J_r}{r}\tau - JJ_r\ddot{\beta} - JJ_rC\dot{\beta} = f_q + mG - m\dot{v} \tag{2.6}$$

Chapter 3

Continuous Description of Human Motion Intent through a Switching Mechanism

3.1 Introduction

To regain lost motor functions, rehabilitation training with sufficient intensity and voluntary participation of post-stroke patients is essential for brain reorganisation [97]. Due to the superiority of robotic system in terms of efficiency, precision, and controllability, a range of robots have been developed for post-stroke rehabilitation on the recovery of motor capacity [98, 12]. As a kind of parallel robot, cable-based robots show great advantages with respect to high accuracy and low inertia during continuous rehabilitation training and can provide proper assistance for upper limb rehabilitation and daily activity training while guaranteeing the safety of patients[99, 100].

The key characteristic of the robots used in different modes and phases of rehabilitation in neuro-rehabilitation is whether the robot with control strategies can provide appropriate assistance and reliable assessments for participants. The assistive mode as the most developed control algorithms is to help participants move the affected limbs in the desired therapy patterns[101]. Participants' voluntary involvement is proved to be essential for provoking the motor plasticity [97] and inducing the brain plasticity

[102]. For patients in the early stages of poststroke rehabilitation, the control strategies for providing passive assistance are applied. For example, an advanced proportional and differential controller [61] and a sliding mode controller [103] have been used to accurately control a rehabilitation robot to passively assist the patient to move to the desired end position. To increase and maintain the participants' efforts, by increasing the compliance of passive controllers, the rehabilitation robot is expected to provide only *partial* assistance. To this end, the control techniques such as the impedance control and admittance control that can implement a law for compromising between training quality and robotic compliance are developed [104].

With the high requirements of the participants' voluntary involvement during rehabilitation, the EMG signals which are highly related to the muscular forces and joint torque are valued [105, 106]. Furthermore, another reason for the popularity of EMG based control strategy is that the traditional electromechanical force/torque based control often involves electromechanical delay. For EMG based control, a nonlinear hill-based muscle model is derived for continuously predicting the limb moment from the muscle activities and joint kinematics [85]. However, due to the vast parameters needed for each muscle and nonlinearity of the model equations, the hill-based model is rarely applied in control involving multiple joints and muscles. An alternative approach is to train a decoder between the EMG signals and motor control variables by simply considering the relationship between them as a *black* box.

By applying binary or multiclass classification algorithms, the robot can be controlled in discrete mode. Dipietro et al. map the EMG signals into the binary output for determining the onset and end of the movement [44]. Ding et al. represent the relationship between the EMG patterns and predefined static postures or movements by the Artificial Neural Network algorithm [86]. For *continuously* controlling a single joint robot to assist participants, apart from the Hill model based approach [85], a linearly proportional EMG control strategy is proposed [60]. Based on the theory of muscle synergy [47] and movement primitives [87], Artemiadis et al. [50] proposed a state-space model with reduced dimensionality for continuously mapping the EMG signals to multi-joint movements. However, the performance of these models is mostly task-dependent and participant-dependent, which settles a big challenge in modelling accuracy with reduced model dimensionality.

Several research groups have developed switch schemes for decoding EMG signals to accomplish different tasks. Nizamis et al. [107] have developed an EMG-based control interface to detect the participant movement intention with an interface switching between two horizontal and one vertical tracing tasks. This switch regime for these tasks is based on the simple EMG-based proportional (direct) control and the counts of the wrist extensor contraction. Artemiadis et al. [108] have a switching decoding scheme where the switching variable was described by the participant to perform force tasks in ten different points in the 3D arm workspace. This switch regime can assist a participant to finish different reaching movement, but these movements are not continuously executed between every two movements. Artemiadis et al. [109] also put up a switching regime decoding model between multi-channel EMG signals and joint angles of arm movements in 3D space. They set up a discrete switching variable which controlled through a Bayesian classifier for choosing different decoding models for different movements.

Motivated by the switch model based approaches [109, 108, 107], in this chapter, an EMG decoder is developed using switched linear system models to continuously estimate participants' voluntary motion during multi-joint arm movements. Different from switching control based approach [107], the developed EMG decoder served as a human-robot interface rather than a controller. Although the functionality of the developed EMG decoder is similar to the one developed by Artemiadis et al. [109], the modelling strategy adopted in this chapter is quite different. In [109], the model dimensionality reduction is applied for models of every task and the dimensions of all these models are reduced into two for both inputs and outputs. As discussed earlier, since the dimensionality-reduction might cause the loss of limb dynamics and detailed information included in the EMG signals, its applicability to the problem of cable rehabilitation robot used for multi-joint motion in 3D space needs to be further investigated. Moreover, these models are mostly task-dependent and participant-dependent approaches, limiting their application.

In this chapter, a switched system model is established to continuously decode EMG signals during a multi-directional arm tracking task for the application of controlling a cable-based rehabilitation robot in active assistive mode. The EMG signals of six muscles are processed into muscle activations as the model input, while the voluntary

forces of participants are processed as the model output. By dividing the complex task into several simple subtasks, we individually identify a model for each subtask with appropriate dimensionality. Three single-models with different orders for the whole complex task are also trained for comparison purposes. The efficiency and the feasibility of the switching mechanism have been demonstrated in both numerical analysis and experimental verification in terms of model fitness, tracking accuracy and muscle activations for human-robot cooperative manipulation.

It is well known that the human brain is a complex nonlinear time-varying system. Description of the motor intent, under a very specific condition, is feasible but very difficult. The research work in this chapter demonstrates the effectiveness of using a switching mechanism to describe brain motion intent; just as the spline interpolation can be applied to approximate the static nonlinear functions, the dynamic switched system model can effectively approximate the time-variant nonlinear dynamical system.

The rest of this chapter is organised as follows. The proposed system architecture and experiments are analysed and reported in Section 3.2, while Section 3.3 gives the results and Section 3.4 discusses and concludes this chapter.

3.2 Method

The cable-based upper limb rehabilitation robotic system as shown in Fig.3.1(a) is used to provide assistance to participants. The details of the robot are described in Section.2.4.

3.2.1 EMG-based Human-robot Cooperation Controller

The human-robot cooperation controller based on an EMG decoder (Fig.3.2 (a)) is used for controlling the robot. The EMG decoder (Fig.3.2 (b)) is trained to estimate the EMG-driven forces along the cables from muscle activations. The muscle activations are obtained by basic EMG processing and EMG-activation model based on a previous research [60]. The arm and robot dynamic models are built for reckoning the voluntary forces driven by muscle's EMG from the kinetics of arm together with the splint on the

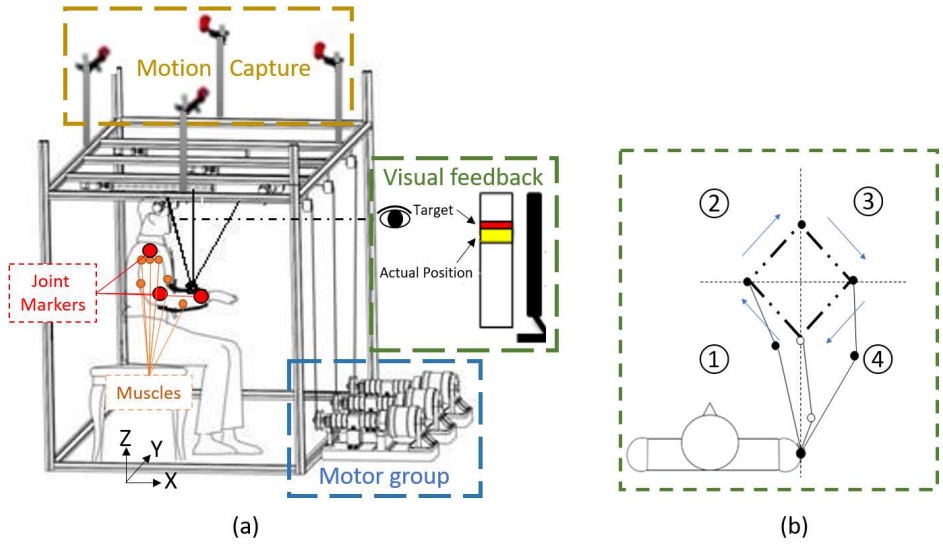

Fig. 3.1 A cable-based upper limb rehabilitation robotic system and a multi-directional arm tracking task including four rectilinear movements: (a) The platform. (b) Task trajectory and direction.

basis of arm and robot structure. The EMG-driven forces can be further transferred into a motor torque for driving the motor group.

3.2.1.1 EMG-activation Model

The EMG to muscle activation model is built for calculating the muscle activated levels from the amplified EMG signals measured by the EMG acquisition system. First, the amplified EMG signals are full-wave rectified by a 4-th order Butterworth low-pass filter to obtain the envelope of amplified EMG signals [50]. Then, the envelop magnitude of each muscle is normalised to the values of its Maximum Voluntary Isometric Contraction (MVC) [110].

The neural activations $n(t)$ are then obtained from the normalised envelope $e(t)$ of EMG signals in real-time by a second-order discrete-time linear model [111]:

$$n(t) = \alpha e(t-d) - \beta_1 n(t-1) - \beta_2 n(t-2), \tag{3.1}$$

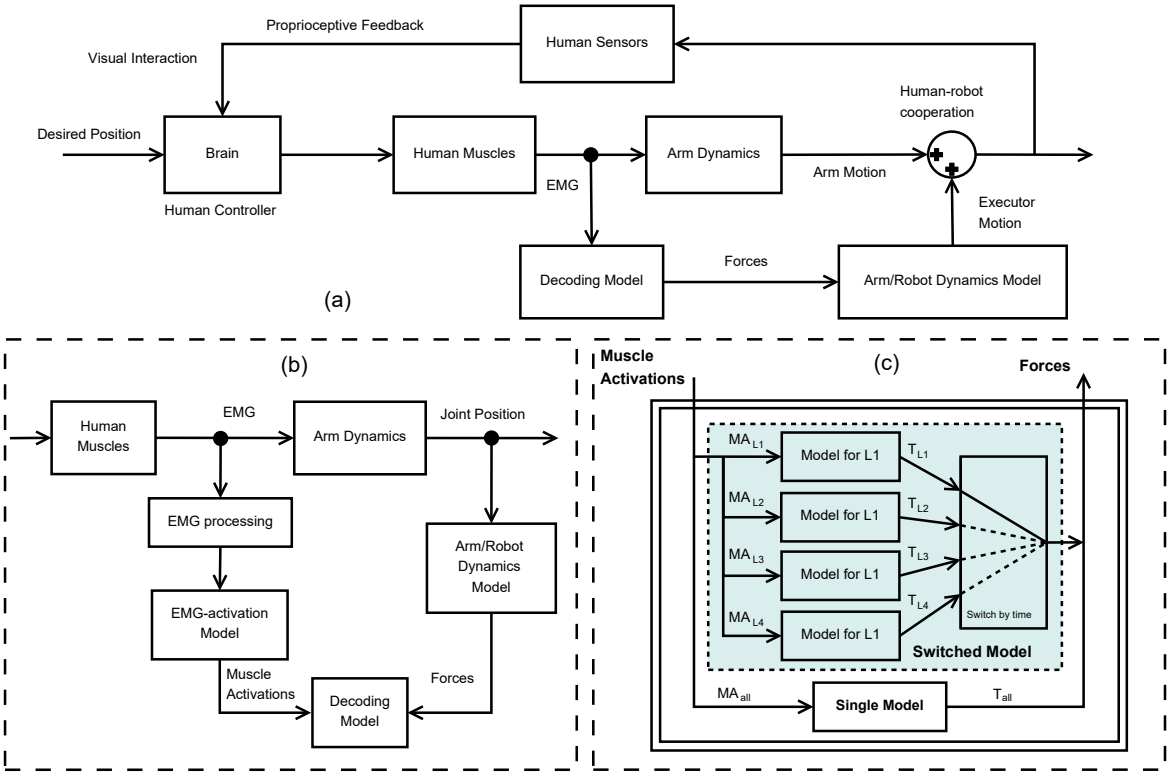

Fig. 3.2 The detailed architecture of the proposed EMG-based human-robot cooperation controller, the EMG decoder, and real-time decoding mechanism with the single-model and the switched system model. (a) Interfaces with a trained EMG decoder. The EMG-driven forces mapped from the EMG by the decoder is used as an interface to assist participants together with their voluntary motion intention. (b) Training Decoder Model. The decoder is trained to map the relationship between muscle activations from EMG signals and voluntary forces driven by muscles from arm dynamics. After being trained, the decoder is used to estimate the EMG-driven forces and are realised by the robot in real-time. (c) Two trained decoding models in the real-time control scheme: the switched system model and the single model.

where $\alpha = 1+\beta_1+\beta_2$ is the gain coefficient, $\beta_1 = c_1+c_2$ and $\beta_2 = c_1c_2$ are the recursive coefficients, c_1, c_2 are adjustable parameters for each muscle based on previous studies [111] and d is the electromechanical delay, which is set as 80 ms in this study.

The muscle activations are then obtained by the coupled relationship between it and the neural activations. The relationship can be presented by first-order dynamics [112] and by a non-linear function at low levels of force [113]. A one-parameter segmented transformation model from the neural activation $n(t)$ to the muscle activation $u(t)$ is proposed by Manal and Buchanan:

$$u(t) = \begin{cases} \alpha^{ma} \ln(\beta^{ma} n(t) + 1), & 0 \leq n(t) < n_0 \\ mn(t) + c, & n_0 \leq n(t) \leq 1 \end{cases} \tag{3.2}$$

where the values of n_0, α^{ma}, β^{ma}, m and c depend only on the shape factor of each muscle [113].

In order to match the frequency of muscle activations and the EMG-driven forces, the muscle activations are further decimated into 100 Hz.

3.2.1.2 Arm and Robot Dynamics Analysis

The dynamic model is used to calculate the EMG-driven forces on the wrist during the human-robot cooperation movements of the arm and splint. The wrist is the contact point between the robot and arm. During the modelling phase, the assistance from the robot is *unavailable*. Therefore, the forces driven by EMG on the wrist consist of the motion-driven forces and the forces for resisting the effects of arm and splint gravities. During the verifying phase, the cables will drive the arm and the splint moving together for executing the task. The forces provided by the motor along the cables are estimated from the EMG decoder model based on the real-time EMG. The kinetics of the robot is applied for calculating the forces along the cables and further the driven torques of the motor group as described in [94].

3.2.1.3 EMG Decoder

A number of algorithms have previously been applied to decode human motion from EMG [114]. However, in most of these works, decoding is resolved using classification techniques, rather than a continuous description of the kinematics. As discussed in the introduction section, in our case, the goal is to develop an EMG decoder to continuously represent the voluntary motion forces using the measured muscle activation in real time.

The EMG decoder developed here is based on the identification of state-space model. There needs a process of model training phase to identify the parameters of the state-space model. Comparing with the approaches using the discrete-time model [114], the linear six-input three-output continuous time-invariant model Eq.3.3 is applied to map the relationship between the muscle activations and the voluntary motion forces. Although the data collection is discrete, here we use a continuous model, which might capture the key characteristics as the actual system is continuous:

$$T_i : \begin{cases} \dot{x}_i = A_i x_i + B_i u(t) \\ y(t) = C_i x_i + D_i u(t) \end{cases} \tag{3.3}$$

where $i \in \{1, 2, 3, 4\}$, $x_i \in \mathbb{R}^k$ is the state vector and k is the order of the i-th model, which can be pre-determined. In this study, k is selected between 3 and 10 depending on different scenarios. $u(t) \in \mathbb{R}^6$ is the input vector of six muscle activations, $y(t) \in \mathbb{R}^3$ is the force vector representing the model output. The matrices $A_i \in \mathbb{R}^{k \times k}$, $B_i \in \mathbb{R}^{k \times 6}$, and $C_i \in \mathbb{R}^{3 \times k}$ are the systematic matrix, input/control matrix, and output matrix, respectively. The matrix $D_i \in \mathbb{R}^{3 \times 6}$ is the direct transfer matrix from the input $u(t)$ to output $y(t)$ and is set as a zero matrix in this dissertation.

The state space model for a given task T_i can be established by identifying the matrices $\{A_i, B_i, C_i\}$ and the initial state x_{0_i} using a model training dataset. These parameters are identified in the continuous time domain using one of the subspace model identification methods, the canonical variate analysis [115]. As the underlying system is stable, the stability of the model is added as a compulsory condition during model identification. In this chapter, in order to reduce transient behaviour due to

switching, the initial value x_{0_i} for each subsystem T_i is adjusted within the range identified in the training phase. This adjustment can reduce the discontinuity of the output during switching so as to improve the transient switching dynamics.

3.2.1.4 A Switching Mechanism for Complex Tasks

To explore the best EMG decoder model during complex tasks, a switching mechanism for carving up the task into several simple subtasks and individually identifying a subsystem model for each subtask is set up as shown in Fig.3.2 (c). The principle of the switching mechanism is to establish subsystem models for every subtask with appropriate dimensionality and construct a switched linear system model for the whole complex task to achieve high accuracy by switching among the subsystem models.

In this study, the complex task is the tracking of a square shape preset trajectory in a horizontal plane (Fig.3.1(b)). This task contains four rectilinear movements (i.e. the four subtasks) with different directions in 3D space. The length of each rectilinear movement is $\sqrt{0.02}m$. Each rectilinear movement can be easily realised by setting the changes of X and Y axes both as $0.1m$ in the developed trajectory setting module. Based on this task, the realisation of the switching mechanism can be described as follows: 1) Divide the whole task into four subtasks; 2) Train a decoder model for each subtask, and achieve four LTI multivariable models $\{A_i, B_i, C_i\}$ with x_{0_i} $(i \in 1, 2, 3, 4)$; 3) Switch the model according to the predefined subtasks.

To simplify the notations, in the following discussions, we use the prefix 'S' to represent the case of a single model and 'MM' to the case the system switching among Multiple Models for a complex task. Based on the switching mechanism, a switched linear system model is trained. In this study, the MM is the integration of four best subsystem models for the four subtasks. For the subtasks, all subsystem models, whose orders could be between three to six (total four different options), are trained. The best subsystem model of each subtask is defined as the model whose average fitting errors of the three model outputs are the smallest among all four models with different orders. The order of each best subsystem model for each participant could be different. After selecting the best model for every subtask, the MM can be grouped and realised.

For comparisons, three single-models with different orders are also trained for the whole square shape task without considering the complexity of the task. For these single-models, their orders are chosen as three (S3), six (S6) and ten (S10) (please see Appendix A for details).

3.2.2 Participants and Experimental Protocol

Seven healthy participants (aged 25.3 ± 0.7 yrs) were recruited. All participants signed the written informed consent forms. This study was approved by the Human Ethics Committee of the first affiliated Hospital of Sun Yat-Sen University ([2013]C-096).

Based on biomechanics literature [116], the surface EMG signals of six muscles (BIC, TRI, DA, DM, DP, and BR), which are mainly responsible for analysing the upper limb motions, were recorded by the EMG acquisition system. Two paired surface EMG electrodes were placed on the specified surface skin of participants. The reference electrodes were placed on the skin of the elbow or wrist bones area. To capture the kinematics characteristics of upper limb, three infrared-reflection markers were attached to the skin surface of the centre of shoulder, elbow, and wrist. The EMG signals and joint position signals were recorded simultaneously.

The efficiency of the proposed switching scheme was verified using both numerical analysis and real-time experiments with seven participants. Numerical analysis (mainly modelling) consists of the EMG decoder model *training* phase and model *testing* phase.

The datasets for the training phase and the testing phase were collected based on a procedure described as follows. Each participant was asked to track a moving cursor shown on the screen using his/her arm for 20 seconds in total without robot's assistance. The robot provided zero assistance to the subjects, as the force feedback loop was open. The trajectory of the moving cursor is the preset square shape trajectory in the horizontal plane. The cursor moved for 5 seconds during each rectilinear movement. Each participant was asked to track the cursor which repeatedly moved along the square shape trajectory three times as 3 trials in one record. All participants were required to finish three records, resulting in a total of 9 trials whose data were collected

for training and testing phases. Two records (i.e. 6 trials) were randomly selected for the training phase and one record (i.e. 3 trials) was for the testing phase. The data for *model training* was processed to train both the multi-model and three single-models.

In the testing phase, the EMG signals were also processed as the input, and the trained models were used to estimate the outputs. The estimated outputs were compared to the targeted output to assess the accuracy of the models. As noted earlier, during testing stage, the muscle activities did not response to the tracking error through human visual feedback.

In the experimental verification stage, the participants were instructed to place their forearms in the splint. All four models were applied in the EMG-based controller to realise the human-robot cooperation movements. Therefore, the robot provided assistance based on EMG signals as the force feedback loop was closed. During this phase, each participant was asked to track the cursor once in one record, indicating one trial in a record. All participants were required to finish three records (i.e. 3 trials) with *robot assistance* estimated by every model together with their muscle contributions. The performance of different models can be assessed in a real-time feedback loop. In this loop, the human 3D motion intent, estimated using the identified models, was reflected in the human visual feedback in real time to reduce the tracking error as indicated on the computer screen.

3.2.3 Evaluation Parameters and Statistical Analysis

To evaluate the performance of different models, the model $fitness$, the trajectory tracking error, and the muscle activations were calculated, analysed and compared.

3.2.3.1 Model Fitness

Based on the EMG decoder models, the target outputs from the joint positions and estimated outputs from the models with the same inputs can be calculated.

The Model Fitting Error (MFE) was defined as the gap between the target outputs and estimated outputs. To evaluate the model accuracy, the Root Mean Square (RMS)

value of MFE was calculated as follows:

$$MFE_{RMS} = \sqrt{\frac{1}{N}\sum_{i=1}^{N}(\Delta F(i))^2} \tag{3.4}$$

where $\Delta F(i)$ is the absolute value of MFE in each output at i-th sampling instant and N is the number of samples.

Furthermore, the Pearson Correlation Coefficient (PCC) between the targeted and estimated outputs was also calculated according to [117].

3.2.3.2 Trajectory Tracking Accuracy

The gap between the desired preset trajectory of the task and the actual trajectories completed by participants was defined as the tracking error (TE). The RMS values of TE were calculated to evaluate the trajectory tracking accuracy in X axis as follows:

$$TE_{RMS} = \sqrt{\frac{1}{N}\sum_{i=1}^{N}(\Delta x(i))^2} \tag{3.5}$$

where $\Delta x(i)$ is the trajectory tracking error in X axis at the i-th sample. The TE_{RMS} of the other axes was calculated similarly. To further explore the effectiveness of the switching mechanism, when the human-robot assistance was available, the TE_{RMS}s in X and Y axes were calculated and compared separately.

3.2.3.3 Muscle Activation

The Mean value of Muscle Activations (MMA) of the six selected muscles during every task execution was used to evaluate the effects on muscular effort by the EMG decoder models.

3.2.3.4 Statistical Analysis

To analyse the influence of model order in model fitting accuracy, the difference of the MFE and PCC was evaluated using Kruskal-Wallis nonparametric test with pairwise

multiple comparisons. To visually show the performance differences among different models in three phases, the mean and standard deviation (SD) values of these evaluation parameters were calculated for all seven subjects.

To analyse whether the robot's participation affects the human motion intention, the difference of TE between the training and verifying phases was evaluated by one-way analysis of variance statistical method and the MME was evaluated by Kruskal-Wallis nonparametric test. The significance level of all statistical tests was 0.05. In the verifying phase, only the model that can support all participants to complete the task was compared. Statistical work was performed using SPSS 19.0 (SPSS Inc., USA).

It should be pointed that some of the participants could not complete the whole task when the single models S6 and S10 were used. Therefore, to analyse the effects of the switching mechanism during experimental verification, only the single model S3 and switched model MM were evaluated by the paired test in terms of the tracking error and muscle activations.

3.3 Result

3.3.1 Model Fitness

First, the estimation of the EMG-driven forces by using various EMG decoder models were presented in Fig.3.3. The data shown in this figure was captured and estimated from one subject as a sample.

The bold solid back lines and the thick grey lines illustrate the target outputs calculated by the dynamic model, while the green thin lines (single-models: S3, S6 and S10) and light orange solid line (switched model: MM) show the the EMG-driven forces estimated by the four different EMG decoder models. In the training and testing phases, all estimated outputs had similar trends with the target outputs during a 20-second trial, and the values were close. During the verifying phase of this sample, the outputs estimated by S6 and S10 went far away from the target, therefore these outputs are not included in this figure. Among all seven participants, the S6 of four participants and the S10 of six participants out of seven participants were not able to

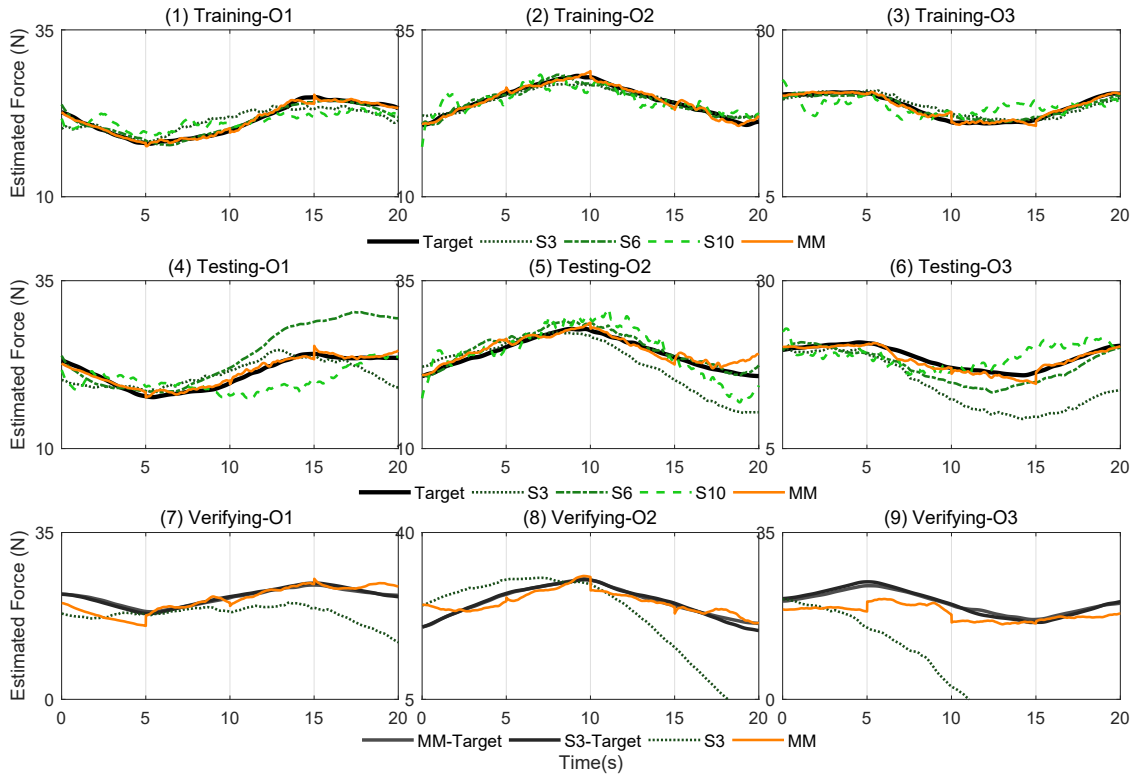

Fig. 3.3 The three outputs of the multi-model (MM) and three single-models (S3, S6, S10) during the training ((1)-(3)), testing ((4)-(6)) and verifying phases ((7)-(9)). The thick black lines in ((1)-(6)) indicate the target outputs from the dynamic model during the training and testing phases. The thick black lines and the thick grey lines in ((7)-(9)) indicate the two target outputs of two experiments during the verifying phase. The light orange solid lines in ((1)-(9)) denote the outputs of MM. The dark green dotted lines in ((1)-(9)) denote the outputs of S3. The medium green dash-dotted lines in ((1)-(6)) denote the outputs of S6. The light green dashed lines denote in ((1)-(6)) the outputs of S10.

help the participants complete the verifying experiments with those outputs out of the range of motor limits. Therefore, there were three subjects who could complete the task with S6 and only one subject who could finish the task with S10.

The RMS values of MFE and the mean values of PCC were compared for each output among different models as shown in Fig.3.4 and Table.3.1. In the training phase, the MFE and PCC of all three single-models, were significantly worse than those of the switched model except one output of S6. Moreover, the MFE and PCC of S6 in two outputs were significantly better than those of S10. In the testing phase, the MFE and PCC of all three single-models were found significantly worse than the switched model while no significant difference was found among single-models. In the verifying phase, the MFE values significantly increased with the increment the order of single-models. Based on the significance test, the performance of MM was significantly better than the S3 except for one output. Also, it is quite clear that the performance of S6/S10 is not as good as the switched model. It should be noted not all the subjects could finish the task with the two single models S6 and S10, as reported in Table.3.1.

3.3.2 Tracking Accuracy

The preset trajectory of the task and actual trajectories by a participant conducting the task in training and verifying phases with different models are shown in Fig.3.5. Notice that, as shown in these trajectories, this participant could not finish the task with the S6 model and S10 model (their trajectories stop at the red circle points in Fig.3.5).

Fig.3.6 presents the mean RMS values of the TEs in X and Y axes during participants tracking the whole task. The values of S6 and S10 (in dashed edges) show great SD because some participants could not finish the tasks. The TE values in X-axis of MM is significantly lower than the values of S3 ($p < 0.05$).

3.3.3 Muscle Activation

The MMAs of the six muscles are displayed in Fig.3.7. All muscle activations decreased when participants tracked the task with assistance from the robot. The activation of

Table 3.1 The comparison between the RMS MFE and PCC values of three single-models and the switched system model during training, testing and verifying phases.

Phase	Output	**MFE (Mean±SD) (N)**				Significance
		S3	S6	S10	MM	
Training	O1	1.01±0.72	0.74±0.32	1.11±0.53	0.41±0.30	a,b,c
	O2	1.19±0.85	0.70±0.41	1.30±0.60	0.43±0.28	a,c,d
	O3	0.85±0.65	0.62±0.14	1.02±0.50	0.33±0.17	a,b,c,d
Testing	O1	1.71±0.97	2.28±0.89	2.40±0.64	0.83±0.26	a,b,c
	O2	1.91±1.26	2.52±1.23	2.46±1.05	0.96±0.45	a,b,c
	O3	1.65±0.96	2.00±0.67	2.10±0.69	0.69±0.20	a,b,c
Verifying	O1	4.02±2.74	(NF) 4.88±3.26	(NF) 8.80±0.36	3.59±1.72	
	O2	4.71±2.25	(NF) 3.77±1.65	(NF) 4.43±0.28	3.23±1.90	a
	O3	4.93±3.61	(NF) 3.94±1.60	(NF) 9.01±0.13	2.71±1.32	a
Phase	Output	**PCC (Mean±SD)**				Significance
		S3	S6	S10	MM	
Training	O1	0.81±0.33	0.95±0.06	0.86±0.12	0.98±0.02	a,b,c
	O2	0.80±0.32	0.94±0.09	0.83±0.16	0.98±0.02	a,c,d
	O3	0.82±0.27	0.96±0.02	0.79±0.21	0.98±0.02	a,b,c,d
Testing	O1	0.76±0.26	0.78±0.28	0.56±0.41	0.96±0.02	a,b,c
	O2	0.68±0.48	0.75±0.18	0.56±0.43	0.93±0.08	a,b,c
	O3	0.76±0.27	0.77±0.21	0.73±0.15	0.96±0.03	a,b,c
Verifying	O1	0.17±0.59	(NF) 0.03±0.62	(NF) 0.01±0.02	0.49±0.51	a
	O2	0.23±0.48	(NF) 0.19±0.46	(NF) -0.17±0.05	0.62±0.20	a
	O3	0.17±0.43	(NF) 0.02±0.65	(NF) 0.13±0.04	0.70±0.12	a

Note: Significant differences between these models are represented by the following alphabets. a: 'S3-MM', b: 'S6-MM', c: 'S10-MM', d: 'S6-S10'. NF: Not all participants have completed the tasks. For those models which cannot support all subjects to complete the task, the mean and SD values of MFE and PCC are only calculated from those subjects who successfully completed the task.

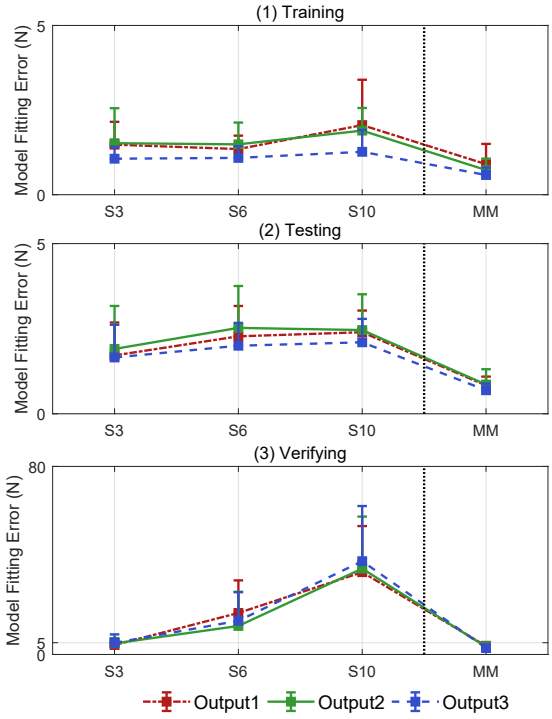

Fig. 3.4 The mean RMS model fitting error values among all participants in training, testing and verifying phases.

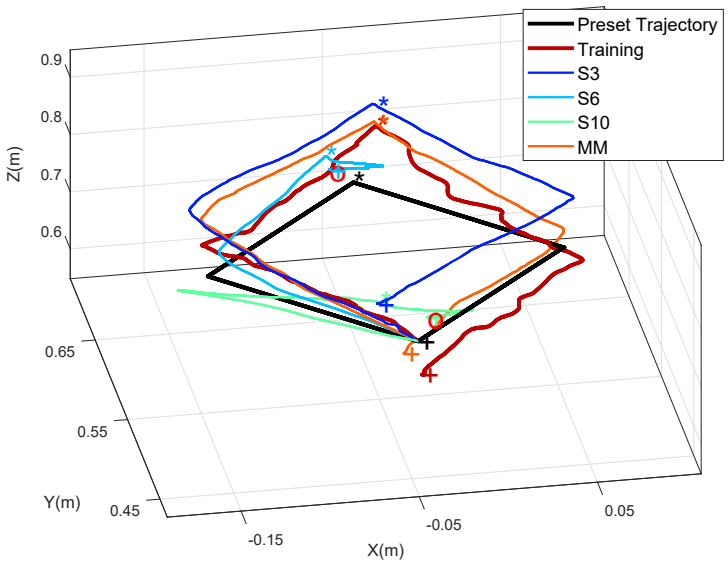

Fig. 3.5 The trajectories of the training and verifying phases. The two red circles 'O' show the end position of the unfinished trajectories. The plus markers '+' show the end position of the finished trajectories. The star markers '∗' show the half position of the trajectories.

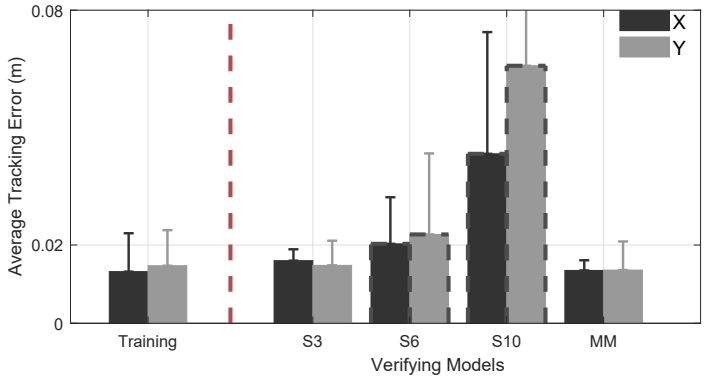

Fig. 3.6 The mean RMS tracking error values in X and Y axes during the training and verifying phases with different models. The dashed edge indicated tasks were not totally finished by all participants.

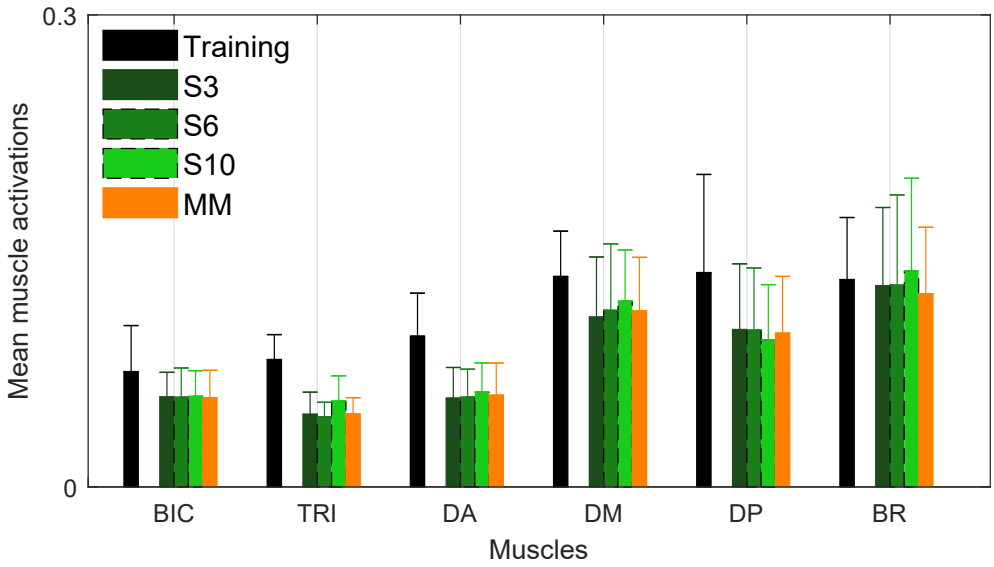

Fig. 3.7 The mean muscle activations of six muscles during the training and verifying phases with different models. The dashed edge indicated tasks were not totally finished by all participants.

TRI and DA during the verifying phase significantly decreased in comparison with the training phase. No significant difference was found between S3 and MM during the real-time verifying phase.

3.4 Discussion

In this chapter, an EMG decoder has been constructed using the state space model without dimensionality-reduction [50] to estimate the forces using the EMG signals of the six arm muscles that contribute primarily and can reveal voluntary intention.

Furthermore, a switching mechanism has been applied for complex motion tracking by integrating simple motion models. The results indicated that the proposed switching mechanism can well estimate the forces when performing complex tasks. It is demonstrated that the proposed approach can be applied in a cable-based rehabilitation robot.

3.4.1 The Novelty of the EMG Decoder without Dimensionality Reduction in Myoelectrical Control

Most EMG decoders for myoelectrical control strategies during human-robot cooperation are either represented in a discrete mode or restricted in one-dimensional space/single joint. Although the Hill-based model [110] is built and frequently used for continuously decoding arm motion from EMG signals[45], the nonlinearity of the decoder model and vast parameters of each muscle needed to be measured make the analysis rather difficult for multiple muscles and joints cooperation movements. The linear state-space model is reported to be able to continuously decode upper limb motion from EMG signals for controlling an anthropomorphic robot in the 3D space by Artemiadis et al. [50], while an extra dimensionality-reduction technique is needed before modelling. The dimension of the inputs and outputs for their model are nine and four before a dimensionality-reduction, respectively. After using PCA to reduce the dimension of both inputs and outputs, the dimensions are reduced to two. The dimensionality-reduction can reduce the difficulty of the modelling, but it might cause the loss of limb dynamics and detailed information included in EMG signals. Moreover, by tuning the parameters of the state-space model, the participant-specific relationship between inputs and outputs can be clearly identified without dimensionality-reduction. A vital part of the modelling scheme is the initial value of the state x, which highly affects the accuracy of the model. However, neither the dimension nor the values of x was fully considered in previous researches.

In this study, the linear state-space model without dimensionality reduction has been developed for decoding EMG signals and further applied to control a cable-based rehabilitation robot in real-time. By training multiple-input (six muscle activations) and multiple-output (three forces) models without reductions, the EMG-driven forces of the upper limb during rehabilitation tasks in 3D space can be estimated and applied to assist the participants based on their voluntary efforts. The results of MFE and PCC analysis in training phases showed that the tracking error of the single-model S6 is the smallest among the three single models. However, the results in testing phase showed that the performance of the lowest order model S3 is the best among all three single-models and is close to the training phase. It indicated that the model with lower

order is more robust than the higher order models and it is in-line with the previous research [50].

However, non single-models can maintain its performance in real-time verification. The difference between the testing and verifying phases is whether the human visual feedback system participates in the control loop of the human brain cooperative motion. In other words, different with testing phase, the $verifying$ phase is the assessment of the model performance in the *closed loop* manner. Due to the robustness of the closed loop control system, the stability can be maintained and the performance degradation is acceptable when the modelling error is small (in the case of MM) or not big (in the case of S3). However, if the modelling error is big, out of the tolerance of the participants, then the closed loop will become unstable, which is the cases of S6 and S10, i.e., for S6 and S10, some participants could not complete the whole tracking task. This indicates the closed loop performance of different models is also related to the motion adaptability of participants. As the motion adaptability of a stroke patient is often much lower than healthy participants, the EMG decoding model needs to be more accurate even for the testing phase. Therefore, the proposed switched model is the most suitable candidature for the active rehabilitation of post-stroke patients.

3.4.2 Superiority of the Switching Mechanism for Modelling the Human-related System

The proposed switching mechanism aims to address current issues of active rehabilitation, and achieved good performance in terms of model accuracy, the required training data size, and the individualisation of models.

By considering the initial state of each subsystem model, the best model is trained for each subtask, and the switching system model exhibits excellent performance in both the test and verifying phases. Therefore, the switching mechanism has high robustness and can decode EMG signals to assist participants during human-robot cooperation movements. This mechanism is able to improve model accuracy and replace the extra dimensionality-reduction technique without losing information.

The switching mechanism for carving up the complex task into simple subtasks and then training for each subtask is similar to the brain's muscle control strategy, i.e., by incorporating different muscle synergies to complete a complex movement. During the real-time robot-assisted control strategy based on physiology signals, due to the involvement of human subjects, both the experimental time and its data size are often limited. During the training phase of the single-models (i.e., without switching), the complex task needs to be finished perfectly by the participants; otherwise the stimulation would not be enough to identify the model parameters. These requirements certainly increase the difficulty in completing the task and further reduce the universality of the model.

On the other hand, to train the model, in each individual subtask, the best model can be quickly trained with limited data. Even if the participant does not complete the entire task but completes two or three subtasks, data can still be used to train the models for these particular subtasks. Therefore, the switching mechanism is more suitable for the modelling of human involved processes, in which, due to safety reasons, the volume of the data is often limited.

During the experiments, when the high order single models were utilised, an unusual situation was observed that those participants who easily feel tired (with the oral report), can often only complete the first two or three subtasks. The reason is that the high order single models (S6 and S10) have bigger modelling errors (see Table.3.1). This requests the participant spending more energy to counteract the error; then in the late stage, the participants often become tired and the muscle fatigue contaminates the normal EMG signals [118]. It thus appears that the switching mechanism can improve modelling accuracy and support the participants to complete complex tasks without muscle fatigue.

3.4.3 Movement Performance of EMG-based Human-robot Cooperation and its Clinical Significance

Overall, although both S3 and MM have training and testing errors, the healthy participants could all complete the tasks with similar tracking accuracy during verifying

phase, demonstrating the motion adaptability of healthy people. The improvement of tracking accuracy with the switching mechanism especially the significance in X-axis indicated the superiority of the switched model in motion control accuracy. It also indicates that for experimental verification, the arm movement performance is less affected when using appropriate EMG decoder models. However, since there exist bump transfers between the switching of two subsystems, a further conjecture to be verified is, the bump change can be decreased by tuning initial states of the models, and the participants' movement performance and control efficiency can be improved.

Under the organisation of motor control by the human brain, healthy participants naturally have the ability to adaptively track an intuitional task without [119] or with appropriate assistance. However, when considering the unfinished movements with the two models: S6 and S10, the 'assistance' from the robot biassed the motion intention, which prevents the human limb to complete complex tasks.

The decreased muscle activations of the six muscles match well with the previous studies [27, 120, 121]. This can be explained as healthy participants can voluntarily adjust their muscle activation and force when external assistance are provided [122]. Therefore, compared with the movement during the training phase, the physical effort of the six muscles are reduced when the participants are performing the same movement with the assistance from the cable-based robot.

The effectiveness of continuous assistance provided by myoelectrical controlled rehabilitation robot is confirmed for the elbow and wrist joint rehabilitation of patients after stroke [123, 60]. The newly proposed EMG decoder model with switching mechanism can be generalised to other multi-joint rehabilitation robots for patients who suffer from neurological diseases, such as stroke, cerebral palsy and so on. As the next step, we aim to apply the proposed method to young patients (20-30 yrs) who had a stroke in the previous year and perform high scores in basic motion ability assessments after passive rehabilitation. In addition, these patients should be able to sit on a chair for at least 30 minutes and hold their affected arms for at least 1 minute.

3.4.4 Summary of Contribution

The major contribution of this study is the proposed new switching based approach for continuously decoding motion intention from multiple EMG signals and further actively supporting the subject's movement by taking human participation into account. By introducing the switching mechanism, an EMG decoder model has been built up with multiple EMG signals and multiple robot control signals for a single but complicated task.

The philosophy behind this is to separate the complex motion task into multiple simple subtasks so that each subtask is simple enough to be modeled by a simple linear state-space model. Then, through the help of the switching mechanism, the complex rehabilitation movement can be implemented. Although we separated the complex task into multiple simple subtasks, we still treated the overall task as a whole task and tried to minimise the transient response during switching (i.e., minimised the jerk during switching).

Theoretically, due to the involvement of human Central Nervous System (CNS), decoding a complex task by using a single model is quite complex. Also, due to the complexity of the multiple-input and multiple-output relationship recorded in our study, the decoder model needs to be a high dimensional nonlinear dynamic model and may be time-variant. An alternative solution is to separate the whole complex tracking task into subtasks and build simple models for subtasks. This is similar to spline interpolation, in which a complex input-output relationship is approximated by a set of piecewise polynomial functions.

Furthermore, motivated by the continuity/smoothness requirement at the knots of the spline interpolation, we considered the problem of reducing discontinuity during switching. To the best of the authors' knowledge, no report exists in the literature which considers the continuity of output during switching for the decoding of human motion intention.

3.5 Conclusion

This study investigated the active robot rehabilitation by using multiple-channel EMG signals. EMG decoders based on LTI state space models, without necessarily having dimension-reduction, were proposed. By introducing a switching mechanism, this approach carves up the complex tracking task into simple subtasks. Then, a switching system model composed of four subsystems were trained. This chapter found that the low-order simple models of the EMG decoder based on the switching mechanism are able to cope with the variation of the underlying system while reducing the complexity of the model, and improve the accuracy during model testing and real-time experimental verification. Overall, the decoder with the switching mechanism can predict the voluntary motion intention with high accuracy from multiple-channel EMG signals and help the participants to finish the human-robot cooperation movement with lower muscle efforts and higher task completion rate.

Chapter 4

Human Motion Intent Description Based on Bumpless Switching Mechanism for Rehabilitation Robot

4.1 Introduction

In the advanced rehabilitation theory, it is generally accepted that users' involvement is essential in both the therapy procedures and the development of rehabilitation technics [124], especially in rehabilitation robotics [125]. Compared with physical sensor-based robot control strategies, strategies using bio-sensors, such as EEG, EMG and Electroneurography, for rehabilitation, allow robotic movements to be triggered more naturally and simultaneously based on human motion. Among different bio-signals, the surface EMG signal has attracted much attention, because it is closely related to patients' muscle activities, and can be collected easily with noninvasive sensors.

On the other hand, for rehabilitation, upper limb motor re-learning and recovery levels are required to be improved with proper intensive physiotherapy. For patients with partial motor capacity, it is essential to estimate patients' motion intention for

further assistance. Therefore, some studies have proposed methods to detect the motion intention by estimating limb motion in both static [30] and dynamic manners [126].

Although a few studies were able to consecutively map the human's intention from EMG to limb motion in a natural neuromuscular control strategy, it is difficult to identify a consistent pattern regarding motor control strategies for different subjects. This is due to the susceptible nature of the EMG signal during dynamic motion. Zhang et al. have proposed an adaptive estimation method to train a model for accurately mapping two-paired muscle activations and elbow motion for covering subject-specific problems [127]. However, the performance of this method is mostly limited to one or two joints' motion and thus modelling accuracy and keeping signal integrity remained as big challenges.

A state-space model together with Principal Component Analysis (PCA) for reducing dimensionality, has been proposed by Panagiotis et al. for mapping the relationship between EMG signals and multi-joint movements [50]. The method together with a switching variable is further used as a switching regime to control a robot arm in random patterns [109]. Both methods work well in a robot arm's trajectory control. However, the dimension reduction comes at the expense of discarding some useful information included in EMG signals. Hence a thorough dynamics describing the relationship between EMG signals and multi-joint movements may not be well captured when applying these methods in human-robot cooperation movements [50].

To further develop a method for consecutively estimating multi-joint motion intention for the control of cable rehabilitation robot, a modelling method without dimension reduction has been proposed for mapping the relationship of six muscle activities and whole arm motion [128]. The method showed good estimation accuracy and was able to support subjects naturally and actively for simple linear tracking tasks. To further improve the performance when applying the method in complex tasks, a switching mechanism [129] has recently been proposed based on the method in [128]. This switching mechanism could improve accuracy, but a problem was identified when it was applied in real-time experiments. That is, when switching between submodels for subtasks, the estimated outputs abruptly change due to large variations in model parameters. Although the overall estimation accuracy of the proposed switching mech-

anism in [129] is high, and the output bumps only show a marginal influence over the majority of healthy subjects' experiments, the impact of the bump is non-negligible for some healthy subjects and is unacceptable for dyskinesia patients.

More specifically, the bump in model outputs in real-time might cause unexpected forces in the affected limb and might be a cause of injury for patients. Furthermore, with an unexpected disturbance, the short term response of participants functionally destabilises posture, and the further compensation of body displacement is generally achieved as a long term response [130]. The affected stability after disturbance cannot recover easily for dyskinesia patients. Although there are some studies about switching methods for different tasks, most of them focus on judging the switching logic for different tasks, [44, 86]. The continuity of estimated outputs when switching between different tasks is rarely discussed. As it is essential to continuously estimate multi-joint motion intention from EMG signals during task switching, we explore a state-shared bumpless transfer for model switching to improve transient performance during switching.

The devised state-shared bumpless transfer is motivated by Multiple Models Adaptive Control (MMAC) [131]. For the MMAC application, only one controller is applied to generate a control signal at any time instant. The idea of this transfer method is to implement a group of different controllers by a single controller with adjustable parameters rather than implementing each controller as an individual system. With the state of the single controller shared by a group of controllers, this implementation is termed as a 'state-shared' multirealisation. This multirealisation technique is first introduced by Morse [132], who employed an adaptive control algorithm that consists of a group of linear Single-Input Single-Output (SISO) controller models and a high-level switching logic for supervising.

For the multirealisation of a family of linear Multiple-Input Multiple-Output (MIMO) systems, the authors of [133, 134] developed a minimal order multirealisation method. As the EMG decoder in this study is a MIMO (six-input three-output) system, we follow the method introduced in [133, 134] to construct an EMG decoder with multiple subsystems.

4.2 Models for Construction of EMG Decoder

The goal of this chapter is to develop an EMG decoder, which uses muscle activations to continuously represent the motion required forces in real-time while retaining all muscle activity information.

In our previous work [129], a switching mechanism with a group of models for a complex arm motion was developed and evaluated, as shown in Fig.4.1(b). A total of four linear state-space models as subsystem models with six-input and three-output were built up for a square shape tracking task. By directly switching among the four subsystem models, the EMG decoder with the switching mechanism can accurately estimate the motion required forces. When comparing to a single model decoder (shown in Fig.4.1(a)), no matter how complex the single LTI model is, i.e. the order of the model is high enough, the EMG decoder with the switching mechanism shows better performance in both simulation and experiment phases [129]. However, a 'bump' behaviour of the outputs which might affect the consecutiveness of the outputs and system state was observed.

As mentioned earlier, the 'bump' in output appears because the subsystem models switch. An effective way for improving the transient response of SISO systems proposed by Morse [132] comes from constructing a stably based state-shared multirealisation. In this study, as the system is a multivariable system, motivated by the elimination of 'bump' outputs, we attempt to solve a general realisation (presented as the 'multirealisation' [133, 134]) for any MIMO subsystems (see Fig.4.1(c)).

Consider the state-space model for one subsystem (denoted as a submodel) as shown in Eq.3.3. The state-space submodels for a given task are built up by identifying the original realisation $\{A_i, B_i, C_i\}$ and the initial values of state vector x_{0_i}. Both $\{A_i, B_i, C_i\}$ and x_{0_i} are identified by the canonical variate analysis in the continuous-time domain [135]. As the whole underlying system should be stable, the stability of each submodel is a necessary condition during the model identification.

For a multirealisation, in general, the order of submodel k_i can be different based on each model's performance. However, in this chapter, we assume that all the submodels

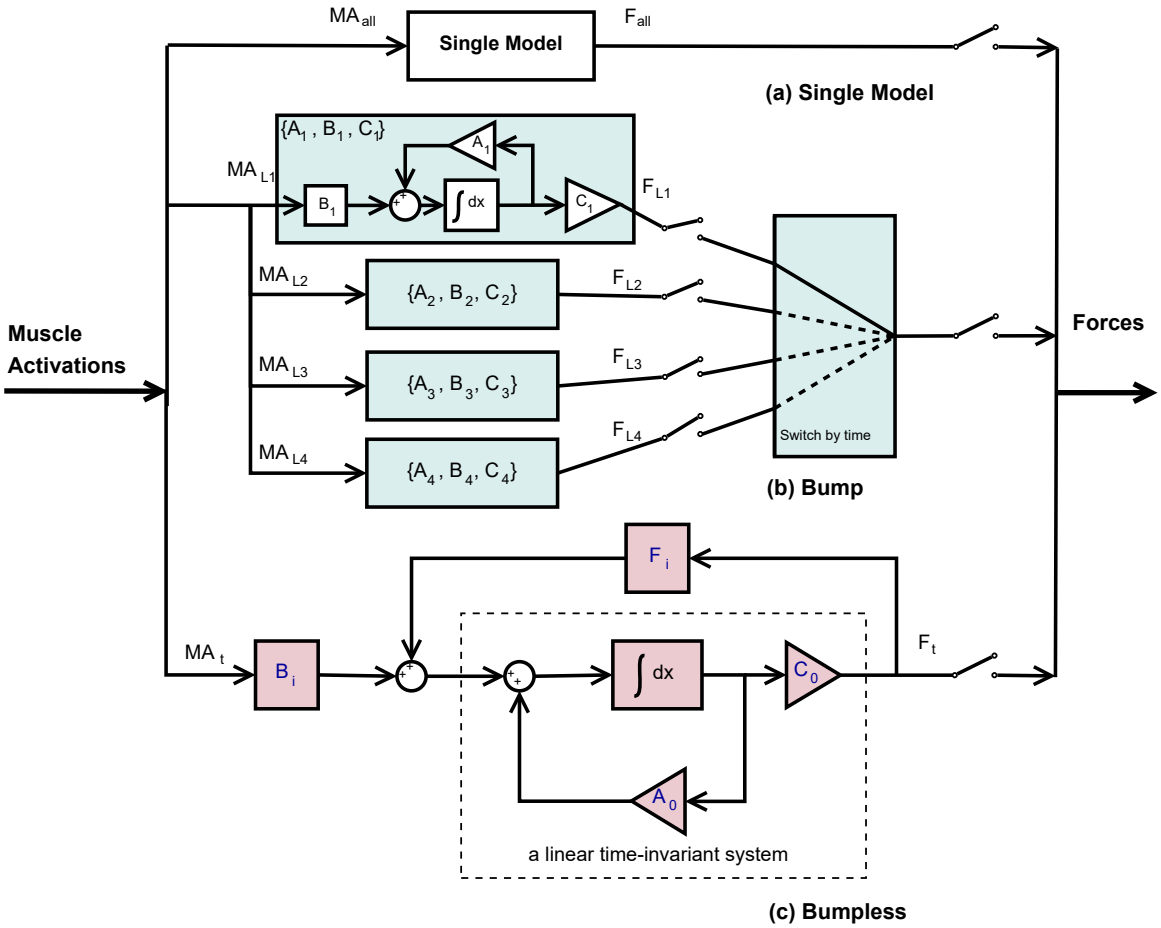

Fig. 4.1 The three kinds of EMG decoder models. (a) Single model. (b) Bump switching mechanism with the realisations $\{A_i, B_i, C_i\}$ for four subsystem models. (c) Bumpless switching mechanism with the multirealisation $\{A_0 + F_i C_0, B_i, C_0\}$ for subsystem models. The realisations $\{A_i, B_i, C_i\}, i \in (2, 3, 4)$ in (b) are all realised the same as $\{A_1, B_1, C_1\}$.

are of the third order, i.e. $k_i = 3$ for all $i = 1, ..., 4$. The reason for this assumption is as follows.

In our earlier study [129], the performance of a single third-order linear system model is better than those of single high order models. As the switching mechanism with multiple models is more complex and has more capacity to capture system dynamics than a single model, to select each subsystem model order as third should be higher enough to accommodate the complexity of this rehabilitation task.

4.3 Multirealisation

In this study, we establish four submodels to describe four simple linear tracking subtasks, and each subtask model is trained using the input and output data from each subject. The transfer function matrix $H_i(s)$ of each subsystem can be calculated by its realisation $\{A_i, B_i, C_i\}$ as follows:

$$H_i(s) = C_i(sI - A_i)^{-1}B_i. \tag{4.1}$$

The transfer function matrix $H_i(s)$ ($i \in \{1, 2, 3, 4\}$) can be expressed by Matrix Fraction Description (MFD) [136]. The specific steps of using MFD to find a multirealisation of the four submodels $H_i(s)$ will be described later.

As explained earlier, for the multirealisation, instead of implementing the subsystems by the individual realisation $\{A_i, B_i, C_i\}$, we find a generic realisation form $\{A_0 + F_iC_0, B_i, C_0\}$. As shown in Fig.4.1(c), by merely adjusting F_i and B_i, the 'bumpless' switching among subsystems can be realised. The serially switching between these multiple controllers can keep both the outputs and states being continuous. Furthermore, a stable LTI system is shared by the four subsystems.

In the following steps, we will show how to find the generic multirealisation form $\{A_0 + F_iC_0, B_i, C_0\}$ to implement the bumpless switching mechanism.

4.3.1 Irreducible Right Matrix Fraction Description

In the first step for finding the multirealisation, we recall the properties of the Right Matrix Fraction Description (RMFD). The multirealisation procedure listed in [133] did not provide an algorithm to calculate RMFD numerically. In this study, we introduce a practical algorithm step by step.

According to Kailath's [136], the RMFD of transfer function which is not unique can be written as

$$H_i(s) = N_i(s)D_i^{-1}(s), \tag{4.2}$$

and it is possible to construct a controllable state-space realisation for each subsystem $\{A_i, B_i, C_i\}$ whose dimension k_i is the degree of RMFD (i.e., the order of the determinant of $D_i(s)$). To minimise the dimension of the controllable state-space realisation for each system, it is essential to pursue the irreducible RMFD (i.e., the minimal RMFD, minRMFD), for which $N_i(s)$ and $D_i(s)$ are right coprime.

The minimum realisation of a single linear transfer function matrix $H_i(s)$ based on MFD description has been well investigated in [136] [137]. The key procedure is to find the minRMFD for $H_i(s)$.

A practical numerical method for finding the minRMFD is the Sylvester matrix based approach as follows [138]:

1) Find a left MFD $H(s)_{p\times q} = D_L^{-1}(s)N_L(s)$ for the given transfer function matrix, where p and q are the numbers of input and output variables. It should be noted that as we do not require $D_L(s)$ and $N_L(s)$ are left coprime, thus finding such a left MFD is an easy task.

2) Find two polynomial coprime matrices $D(s)_{q\times q}$ and $N(s)_{p\times q}$ such that

$$[N_L(s) \quad -D_L(s)] \begin{bmatrix} D(s) \\ N(s) \end{bmatrix} = 0. \tag{4.3}$$

An efficient solution for Step 2) is based on the Sylvester matrices approach [138] for computing a minimal polynomial basis for the right null space of $[N_L(s) \quad -D_L(s)]$ [139] as follows:

(a) An appropriate Sylvester resultant matrix S is constructed by finding the coefficient matrices of $N_L(s)D(s)$ and $D_L(s)N(s)$ of corresponding power;

(b) A search algorithm for exploring the properties of S is used for finding the first q primary dependent columns of S (S_q);

(c) The linear combinations of the preceding linearly independent columns are found with the S_q;

(d) The coefficients of linear dependence are used to form $D(s)$ and $N(s)$.

By using an orthogonalisation process on S [140] in (b), it is possible to determine whether the innovation introduced by a particular column is zero. Hence, it can be determined whether this particular column is linearly dependent on the preceding columns.

During the orthogonalisation process, if S is a high dimension matrix with huge or tiny elements that may happen in a real system, it is necessary to pre-adjust those elements to a proper numerical level before the orthogonalisation process. Also, a robust procedure is introduced in [138] based on the singular value decomposition. There are also other methods for calculating the minRMFD. For the Sylvester matrix-based approach, a Matlab code for low dimension systems has been provided by Ahmadreza Saadatkhah [141].

4.3.2 Multirealisation of Linear Subsystems with the Same Order

A polynomial matrix $D(s)$ [136, 133, 134] can be written as $D(s) = D^{hc}S(s) + D_{lc}(s)$, where $S(s) \triangleq diag\{s^{k_1}, s^{k_2}, ..., s^{k_m}\}$ is the highest (column) degree matrix with k_i being the highest degree of the i-th column of $D(s)$, and D^{hc} is the highest degree-coefficient matrix of $D(s)$, which is constructed from the coefficients of the highest degree polynomials in the columns of $D(s)$, and $D_{lc}(s)$ is the remaining part of the $D(s)$.

The operator ($\mathcal{D}_{hc}\{\cdot\}$) is defined as $\mathcal{D}_{hc}(D(s)) = D^{hc}S(s)$.

Assume the minRMFD of a transfer function $H_i(s) = N_i(s)D_i^{-1}(s) = \bar{N}_i(s)\bar{D}_i^{-1}(s)$ can be found with $\bar{D}_i(s)$ in column reduced form. To simplify the discussion, we can assume that the matrix $\bar{D}_i(s)$ is a Popov form matrix [136].

With the minRMFDs ($\bar{D}_i(s)$ and $\bar{N}_i(s)$) of all subsystems found, a generic minimal multirelisation of the set of subsystems $H_i(s)$ can be achieved by the following procedure [133].

4.3.2.1 Reform the minRMFD

To derive conditions for the multirealisation of multivariable systems, we first reform the $\bar{D}_i(s)$ into $\tilde{D}_i(s)$ with requirements that the elements of $S(s)$ exist on the diagonal in degree reducing, and the D_i^{hc} of the $\tilde{D}_i(s)$ are normalised to I, which can be implemented by elementary transformation with consideration of every element of each $\bar{D}_i(s)$. The transfer function, therefore, is transformed into:

$$H_i(s) = \bar{N}_i(s)X_i[\bar{D}_i(s)X_i]^{-1} = \tilde{N}_i(s)\tilde{D}_i^{-1}(s) \tag{4.4}$$

where X_i is a real matrix for i-th subsystem to reform the minRMFD.

4.3.2.2 Uniform the Common Highest-degree-coefficient Matrix

As described by the previous research [133], a stably based generic minimal multirealisation can be found with a generic minimal common denominator $D_{ms}(s)$, for which $\mathcal{D}_{hc}\{D_{ms}(s)\} = D_m(s)$ has the following form:

$$D_m(s) = [d_{pq}(s)] \tag{4.5}$$

and

$$d_{ij}(s) = \begin{cases} 0, & if \quad p \neq q \\ s^{k_{maxp}}, & if \quad p = q \end{cases} \tag{4.6}$$

where $k_{maxp} = max\{k_p^1, k_p^2, k_p^3, k_p^4\}$ is the highest degree of the p-th column among all $\tilde{D}_i(s)$ ($i \in \{1, 2, 3, 4\}$).

In this step, we try to find out the common D_m^{hc} for four subsystems.

4.3.2.3 Construct a Common RMFD

After finding the generic minimal common denominator $\mathcal{D}_{hc}\{D_{ms}(s)\} = D_m(s)$, for each submodel, it is always possible to transfer $\tilde{D}_i(s)$ by right multiply a matrix $\tilde{X}_i(s)$ such that

$$\mathcal{D}_{hc}\{Dm_i(s)\} = \mathcal{D}_{hc}\{\tilde{D}_i(s)\tilde{X}_i(s)\} = D_m(s).$$

Thus, the $Dm_i(s)$ and $Nm_i(s)$ of i-th system can be constructed by right multiplying the matrix as follow:

$$H_i(s) = \tilde{N}_i(s)\tilde{X}_i(s)[\tilde{D}_i(s)\tilde{X}_i(s)]^{-1} = Nm_i(s)Dm_i^{-1}(s). \tag{4.7}$$

After we constructed the new RMFDs for subsystems, it is ready to multi-realise all the submodels.

4.3.2.4 Construct a Generic Multirealisation

Based on the previous research [133], to implement the multirealisation form as depicted in Fig.4.1.(c), we need to construct $Nm_i(s)$ and $Dm_i(s)$ for the transpose form of $H_i(s)$, i.e.,

$$H_i^T(s) = Nm_i(s) \cdot Dm_i^{-1}(s).$$

Then, construct a stable polynomial matrix $D_{ms}(s)$ such that $\mathcal{D}_{hc}\{D_{ms}(s)\} = D_m(s)$. By using the method in [136] (pp. 403-407), a controller form realisation $\{A_{c0}, B_{c0}, C_{ci}\}$ of $Nm_i(s)D_{ms}^{-1}(s)$ can be found with the pair $\{A_{c0}, B_{c0}\}$ controllable and A_{c0} stable and $C_{ci} = Nm_{ilc}$. Let $K_i = D_{mlc} - Dm_{ilc}$. Then, a generic minimal multirealisation for the set of subsystems $H_i^T(s)$ $(i \in \{1, 2, 3, 4\})$ is $\{A_{c0} + B_{co}K_i, B_{co}, C_{ci}\}$.

Then, the multirealisation form depicted in Fig.4.1.(c) for the original submodels $H_i(s) = (H_i^T(s))^T$ can be obtained as $\{A_0 + F_iC_0, B_i, C_0\}$ by letting $A_0 = A_{c0}^T$, $B_i = C_{ci}^T$, $C_0 = B_{c0}^T$, $F_i = K_i^T$ where only the F_i and B_i are needed to be adjusted during switching. As A_0 and C_0 are constant during switching, the stable LTI system with the switching mechanism can ensure bumpless outputs in real-time (i.e., the outputs keep continuous under the switching of F_i and B_i).

4.4 Experimental Design

The cable-based upper limb rehabilitation robotic system (described in Section.2.4) was used to provide assistance to participants. A scenario of the experiment is shown in Fig.4.2.

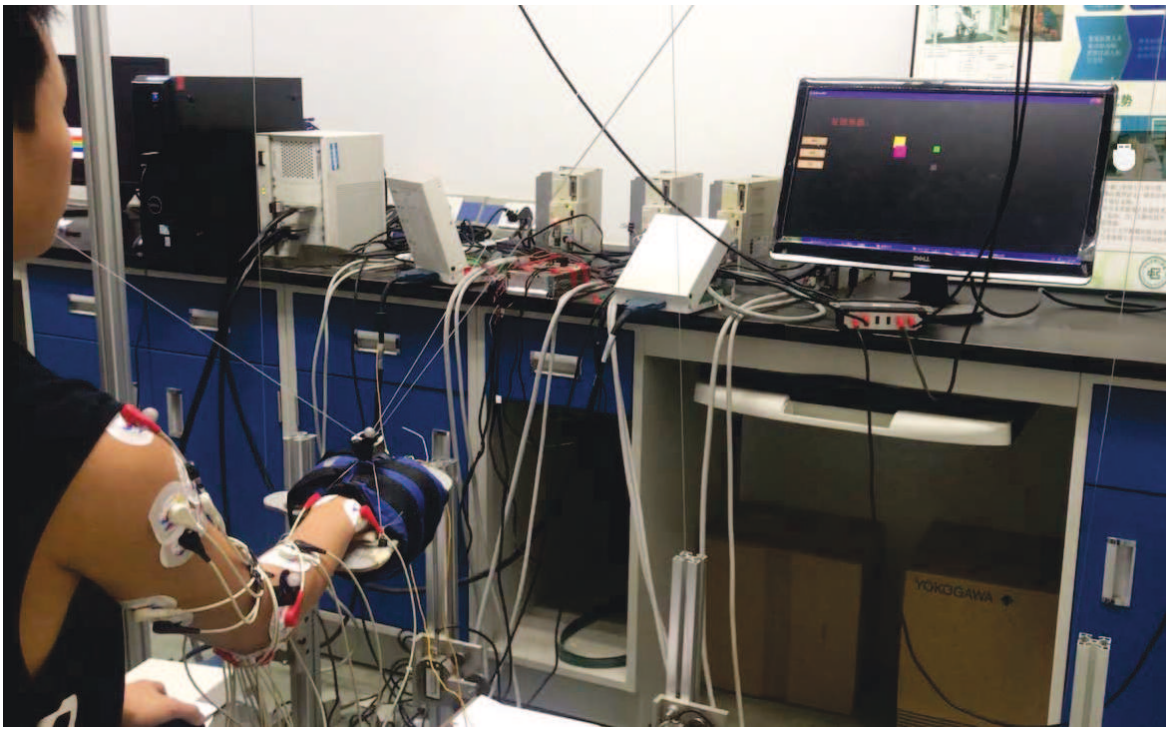

Fig. 4.2 An experimental scenario.

Specifically, the arm motion in 3D space and EMG signals of six arm muscles were captured. The EMG signals were processed into six muscle activations as inputs of the EMG decoder. The arm motion was analysed, and the required forces of arm motion were used as the decoder outputs. The required forces of arm motion along the cables were computed from the human-robot dynamics model [94] to reflect real-time human motion intention. The required forces of arm motion were further processed to calculate the driven torques of the three motors. The EMG envelopes were full-wave rectified from EMG signals and normalised by the MVC values [110]. The muscle activations were further calculated from the EMG envelopes [50] by a neural-muscle activation model [111–113]. For synchronisation between the muscle activations and

the motion required forces, the muscle activations were decimated into a new serial with the frequency of 100 Hz.

4.4.1 EMG-based Human-robot Cooperation Controller

For the purpose of controlling the robotic system, a human-robot cooperation controller based on the EMG decoder was applied. In this controller, the human brain first reacted to the position gap between the human-robot executor and the target position and stimulated the related muscles. By capturing the muscle EMG signals, the built-in EMG decoder estimated the required forces of arm motion.

The forces were then processed according to the human-robot dynamics model and the motor dynamics model of the robot system, and were transmitted along the cable. The force applied along the cable was used to support the human-robot actuator to aid cooperative human-robot movement.

To train the EMG decoder, the six muscle activations were selected as its inputs, and the required forces of arm motion were selected as its outputs. For a complex tracking task designed for robot-assisted rehabilitation, a switching mechanism for carving up the task into a group of subtasks was proposed earlier[129]. A group of submodels were trained for these subtasks. Each submodel was treated as an individual subsystem. The switch mechanism was realised by the introduced multirealisation technique (i.e., the bumpless switching mechanism). The identified submodels with the bumpless switching mechanism could be applied to estimate the motion required forces from muscle activations in both simulation and real-time.

4.4.2 Participants

This study included seven healthy women and men aged 25.3 $\pm$ 0.7 yrs who signed informed consent forms. This study was approved by the Human Ethics Committee of the first affiliated Hospital of Sun Yat-Sen University ([2013]C-096).

The muscle activities of the BIC, TRI, DA, DM, DP, and BR were recorded. These muscles were mainly responsible for analysing the upper limb motion based

on biomechanics [116]. Pairs of two surface EMG electrodes were placed at the skin surface corresponding to the six muscles of each participant. The reference electrodes were placed at the skin surface corresponding to the carpal, elbow and acromion bones. Three infrared-reflection markers of the motion system were placed at the skin surface corresponding to the centre of wrist, elbow and shoulder.

4.4.3 Experimental Protocol

The effectiveness of the EMG decoder with bumpless switching mechanism was verified through the numerical analysis of the participants and the real-time experiments of the participants and the robot system.

The numerical analysis included *training* and *testing* phases. The experiments as the $verifying$ phase were for validating the performance of the EMG-based controller in real-time human-robot cooperation tasks.

During the tracking task of participants, the EMG signals and joints positions in 3D space were collected. The details of the tracking task for the model training and the testing phases are as follows:
1) A target cursor moves on the screen according to a preset square shape trajectory in the horizontal plane for 20 seconds once triggered;
2) A wrist cursor representing the actual position of the participant's wrist locates on the screen and is controlled by participants;
3) As one trial, participants control the wrist cursor to track the target cursor for 20s until the target stops;
4) Each participant needs to finish nine trials where six of them are randomly chosen for the training phase, and the other three are for the testing phase.
It should be noted that both the target cursor and the wrist cursor were shown on the screen with three dimensions.

The data of *model training* phase was used to train a decoder by a single state-space model with the order as three denoted previously as S3 (see Fig.4.1 (a)), four submodels without the 'bumpless' switching mechanism (denoted as the nonbumpless decoder, NBL) (see Fig.4.1 (b)) and four submodels with the 'bumpless' switching

mechanism (denoted as the bumpless decoder, BL) (see Fig.4.1 (c)). The orders of all models were selected as third (as discussed in Section 4.2.B).

In the model testing phase, the three trained decoders (i.e. S3, NBL, and BL) and the processed inputs of this phase were applied to estimate outputs. The related target outputs were also processed based on joints motion. The difference between the estimated outputs from different decoders and the target outputs were explored to evaluate the performance. As noted earlier, the testing in this phase was under the *open loop* condition, because the muscle activities as inputs did not respond to the tracking error through human visual feedback.

In the experimental verifying phase, each participant would cooperate with the robotic system to finish three trials of the same tracking task. The muscle activities and joints positions in 3D space were also recorded. The real-time EMG signals were processed and applied together with the three decoders, respectively. During the cooperation movements, the participant's brain would respond to the visual feedback and control muscles to produce arm movements together with the assistance from the robotic system. Participants were able to mobilise their arms and proactively track the target with fewer errors in real-time. Therefore, the performance of the three decoders was evaluated under *closed loop* configuration with real-time feedback. In this loop, the estimated forces of the required arm motion not only supported participant's movements but also their impact on movements could be perceived by the brain and the visual system through the visual interactions.

4.4.4 Evaluation Parameters

The performances of three decoders (S3, NBL, and BL) were evaluated by the following indicators: six muscle activations during the task, model fitness difference between target outputs and estimated outputs, and smoothness of three outputs.

4.4.4.1 Muscle Activation

The MMA during a trial, which reflects the average muscular efforts, were calculated in all six muscles (i.e., BIC, TRI, DA, DM, DP, and BR). Since the muscle activations

of the training and testing phases are all collected in open-loop, the MMA values of these two phases were analysed together as a group (*modelling* in Fig.4.3).

4.4.4.2 Model Fitness and Output Smoothness

The difference between the target outputs and the estimated outputs from different decoders were used to evaluate the performance in decoding EMG signals.

The MFE, which was the absolute difference between the target and estimated outputs, was calculated to evaluate the accuracy. For the purpose of assessing the overall accuracy, the RMS value of the whole trial MFE was calculated as Eq.3.4.

The PCC, which shows the relationship between the targeted and estimated outputs, was calculated to evaluate whether the trend of the estimated motion intention was consistent with the actual intention [117].

Model fitness is used to describe the overall accuracy of the model estimation, which considers a balance between absolute and relative differences. A good model fitness performance relates to a low MFE and a high PCC.

To quantify the smoothness of the outputs, Normalised Jerk Score (NJS) of the outputs during the testing and real-time experimental verification, was calculated [142] as follows:

$$NJS = \sqrt{\frac{1}{2}\frac{T^5}{D^2}\int jerk^2 dt} \tag{4.8}$$

where t refers to the actual time, $jerk$ is the third-order derivative of outputs with respect to time t, T and D refer to the duration time and amplitude respectively, which were applied to normalise the jerk and to eliminate the influence of time and amplitude. The Relative NJS (RNJS) of the outputs estimated by different EMG decoders were calculated for comparing with target outputs as follows:

$$RNJS = \frac{NJS_{est}}{NJS_{tar}} \tag{4.9}$$

where the NJS_{est} is from the decoder estimated output and NJS_{tar} is from the target outputs.

4.4.4.3 Statistical Analysis

All significance tests of the above indicators among decoders and phases were analysed by the Kruskal-Wallis nonparametric test with pairwise multiple comparisons at a conventional significance level of 0.05. All tests were performed by SPSS 19.0 (SPSS Inc., USA).

4.5 Results and Discussion

4.5.1 Difference and Consistency in Muscle Activation Levels

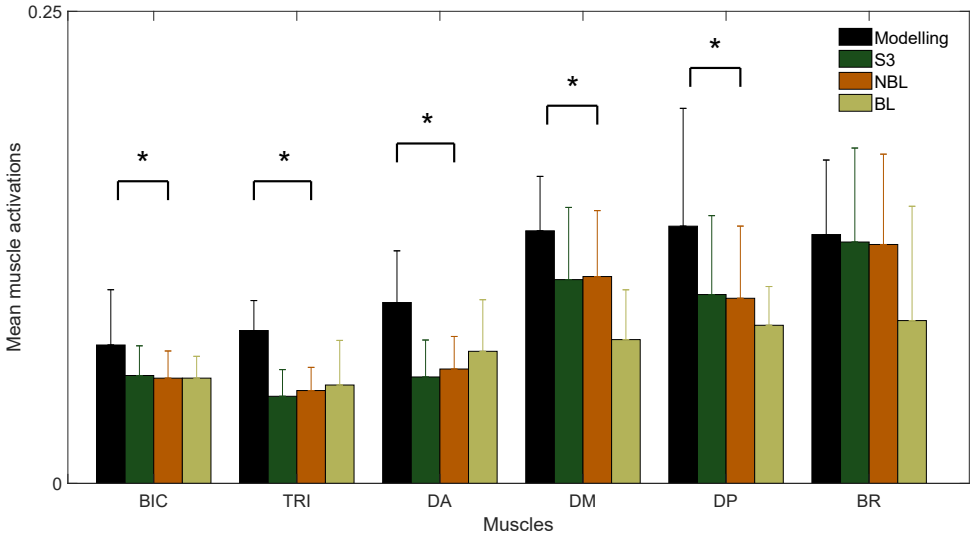

Fig. 4.3 The mean muscle activations of six muscles (BIC, TRI, DA, DM, DP, and BR) during the training and testing phases (modelling) and verifying phases with different decoders (S3, NBL, and BL).

The results of the MMA in different phases and with different decoders were shown in Fig.4.3. When comparing the MMA values of the modelling group with that of the verifying phase, there exist significant differences in most muscles (BIC, TRI, DA, DM, and DP). The decreased overall muscle activation performance is acceptable and predictable. As reported in a previous study [143], the support of the robotic platform would reduce the muscle burden from the arm gravity. When comparing MMA in

the verifying phase, the performances of each muscle in different decoders were quite similar to each other. No significant difference was found among different decoders. This agrees with the fact that the healthy subjects could naturally control their arm and finish the task no matter which model was applied unless the assistance is out of control. Muscle activation nature of how a subject controls the arms in tracking the same task is always similar and should never be different. Otherwise, it means the subject is not healthy, or there is a resistance applied to the subject that obstacles the subject's natural arm control.

Over the whole task, the arm movements of all participants were slow stretching and retracting movements. The activities of all six muscles illustrated low amplitudes but producing multiple neural bursts [144] with the response after each switching operation. This may be related to the task design, in which the trajectory varies sharply at the vertex of the quadrilateral, and the task direction in one of the dimensions changes reversely. As described in [145], when the subject controls the arm to follow the target's rapid changes, the muscle contraction amplitude and the degree of co-contraction may change.

4.5.2 Comparision of the Estimation from Different Decoders

The MFE, PCC, and RNJS results are shown in Table.4.1. The target outputs and the estimated outputs of the three models in the training and testing phases are shown in Fig.4.4. Furthermore, the target outputs and the estimated outputs of the three decoders in the verifying phase are shown in Fig.4.5. The results of the RNJS during both testing and verifying phases were shown in Fig.4.6 and Fig.4.7.

In the testing phase, both NBL and BL had significantly lower MFE and higher PCC than S3. In the verifying phase, NBL showed the best model fitness performance, while BL showed great but slightly worse model fitness performance. Moreover, no significant difference between NBL and BL was found. The model fitness performances of S3 in both phases was the worst. In terms of RNJS of both phases, it is evident that the differences between S3 and NBL and those between BL and NBL are both significant, with RNJS of NBL being the highest among three decoders.

In terms of MFE and PCC, NBL could estimate the outputs more accurately than BL. However, there are significant differences between NBL and BL, in terms of output smoothness, for both testing and verifying phases. It was also observed that in the testing phase the 'bump' behaviour in outputs of NBL is not always sharp (i.e., the amplitude changes within a small range), but in the experimental verifying phase, more sharp changes occurred.

The 'bump' in NBL model was mainly caused by the 'direct' changes in submodel parameters (i.e., C_i and x_{0i}, see Fig.4.1(b)) during the switching between different motion phases. Although the 'bump' was not so sharp in some cases, its overall impacts on output smoothness were significant. Since movement smoothness is regarded as an important indicator of post-stroke motor impairment [146] and the decoder performance for patients may decrease with decreasing movement smoothness [147], the application of NBL would have high limitation in stroke recovery assessment. In contrast, although S3 can estimate outputs smoothly, its model fitness in both phases is not as good as other published decoders [147–149]. In clinical rehabilitation, patients with dyskinesia naturally expect assistance that is more in line with their motion intention. The more accurate a decoder model is, the more potential it may show good performance in practical applications.

During rehabilitation, it is often required to provide $assist-as-needed$ supports to the users. To this end, the EMG signal has been widely applied for the estimation of human motion intent. However, for complex upper limb movements, muscle activities are mostly nonlinearly involved in human motion intent; they are so complex that it often cannot be correlated to force magnitude or direction even for pre-processed EMG signals. A conclusion in line with this is that EMG decoder models for specific objects/tasks on a specific hand of specific subjects may offer better accuracy than a generic model [150]. The EMG decoder modelling approaches proposed in this chapter are targeted to investigate the probable relationship between the arm movement and muscle activations during different parts of a complex tracking task.

Based on the obtained results, the inaccurate estimation of S3 and discontinuity outputs of NBL are significant in comparison with BL. Both S3 and NBL would not be appropriate to be applied to control robots for rehabilitation. BL shows the potential

in accurately decoding EMG signals into smooth assistance even in an experimental scenario with limited participants, duration, and data. This switching mechanism based on a multirealisation of submodels can be an appropriate and practical approach to control robots in clinical rehabilitation.

Furthermore, this chapter attempted to learn the patterns of how the muscles produce motion. The patterns are what our bodies naturally have and are apparently continuous. The motion that participants performed in a tracking task is generally regarded to be continuous, and it should match the continuous force outputs estimated from the decoder model.

During system validation experiments, the brain stands at the highest level in the closed control loop. When a participant receives a visual stimulus, the brain reacts and sends information to the muscles, and controls the arm to follow the reference target. The decision-making model of the brain has been recognised as an example of a choice model, which is realised by a continuous perception-action loop [151].

The proposed bumpless switching system has similarities with the operation of perception-action loops. In particular, the submodel's state is similar to the forward information flow, while the output is associated with body motion. The compatibility between the proposed bumpless switching model and the human perception-action process also indicates the proposed approach is a viable method for revealing human motion intention.

4.5.3 Analysis of the Impact of Outputs Continuity

Considering the application of our method in clinical rehabilitation, we believe it is necessary to investigate bumpless approaches when applying an EMG decoder to promote the active participation of control over the rehabilitation robots.

The above-mentioned results demonstrated the practicality and effectiveness of the proposed bumpless transfer method in decoding EMG signals. Due to the complexity of bio-signal based control systems, it is reasonable and practical to describe such a system by a switching model, i.e., describe the system by several low complexity submodels under a properly designed high-level switching law.

Table 4.1 The MFE, PCC and RNJS values of the S3, NBL and BL decoders, and their differences among decoders in both the testing and verifying phases.

Phase	Output	**MFE (Mean±S.D., N)**			Significance
		S3	NBL	BL	
Testing	O1	1.71±0.97	1.01±0.42	0.97±0.74	b,c
	O2	1.91±1.26	1.09±0.55	1.20±0.90	b,c
	O3	1.65±0.96	1.03±0.43	0.97±0.60	b,c
Verification	O1	4.02±2.74	3.66±2.55	4.60±2.77	
	O2	4.71±2.25	2.64±1.25	5.75±5.32	b
	O3	4.93±3.61	2.09±0.58	3.23±2.63	b,c
Phase	Output	**PCC (Mean±S.D.)**			Significance
		S3	NBL	BL	
Testing	O1	0.76±0.26	0.91±0.10	0.92±0.17	b,c
	O2	0.68±0.48	0.92±0.08	0.93±0.12	b,c
	O3	0.76±0.27	0.89±0.10	0.89±0.14	b,c
Verification	O1	0.17±0.59	0.68±0.24	0.72±0.35	b,c
	O2	0.23±0.48	0.73±0.23	0.60±0.38	b,c
	O3	0.17±0.43	0.82±0.11	0.61±0.57	b,c
Phase	Output	**RNJS (Mean±S.D.)**			Significance
		S3	NBL	BL	
Testing	O1	17.14±13.13	75.20±38.71	16.58±9.60	a,b
	O2	17.94±18.16	85.15±60.88	24.51±23.71	a,b
	O3	21.35±17.02	113.08±69.77	24.58±12.93	a,b
Verification	O1	17.81±11.83	370.00±209.69	20.36±15.68	a,b
	O2	20.02±24.72	188.37±110.80	31.13±52.03	a,b
	O3	27.15±40.00	368.00±185.72	27.25±15.23	a,b

Note: Significant differences between these decoders are represented by the following alphabets. a: NBL-BL, b: S3-NBL, c: S3-BL.

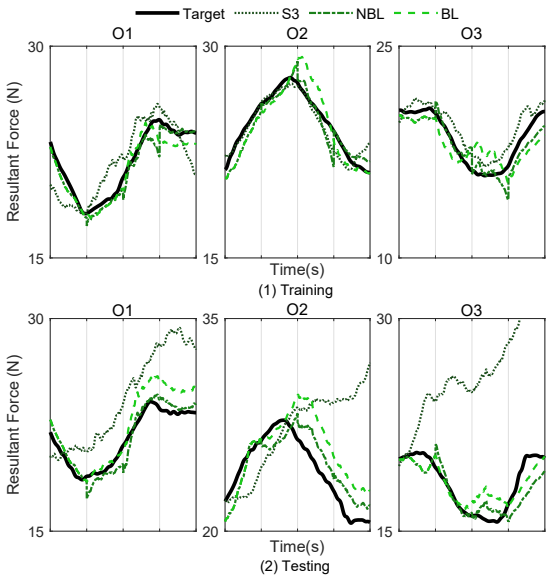

Fig. 4.4 The model outputs of three different decoders (S3, NBL, BL) during the training and testing phases.

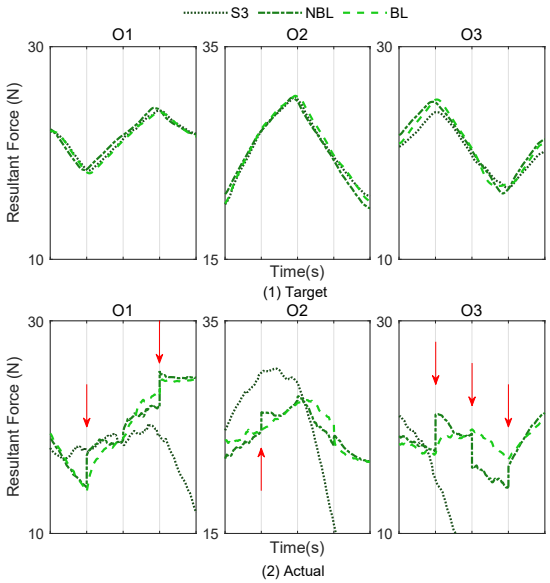

Fig. 4.5 The model outputs of three different decoders (S3, NBL, BL) during the verifying phase.

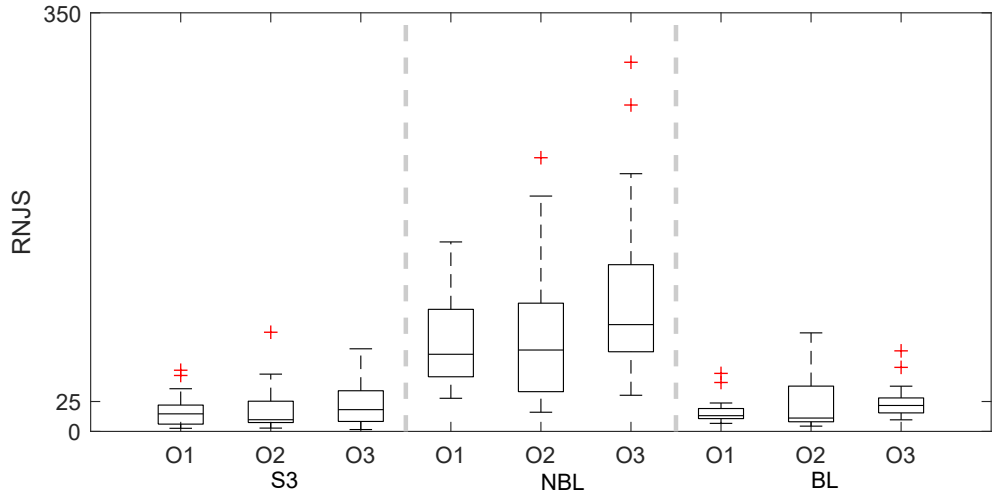

Fig. 4.6 The RNJS of the estimated outputs of the three EMG decoders (S3, NBL, BL) during the testing phase.

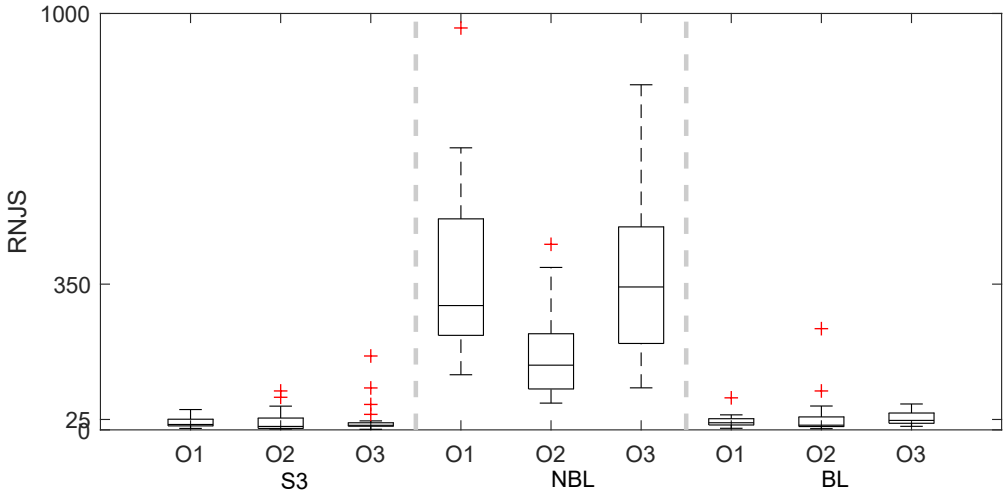

Fig. 4.7 The RNJS of the estimated outputs of the three EMG decoders (S3, NBL, BL) during the verifying phase.

For a switching system, like the EMG decoder we proposed, many researchers in system control place great emphasis on properties of the continuous state and outputs [152], and most of the existing stability criteria for switching systems are under the assumption that both the system states and outputs are continuous.

Under the continuity condition, the stability of the switching system is also affected by other factors, such as the submodel's stability and switching law. It is possible to stabilise the whole system by a well-designed switching law, even if all subsystems are unstable [153]. It is also well known that a switching system may be unstable when switching between two stable submodels. Fortunately, in practice, for a switching system, if its submodels are all stable, under the continuity requirements, the stability of the switching system can always be met if the switching frequency is low enough, i.e., the switching period is long enough. In this study, the identified submodels are all stable. In addition, for a human involved biosignal-based system, the switching frequency is often high.

To ensure the continuity of states and outputs, we applied the multi-realisation theory and proposed a practical bumpless transfer approach for the cable rehabilitation robot. The method we proposed here is to construct a multirealisation form for all subsystems based on their minimal common denominator in order to reduce the complexity of the overall switching system (i.e., reduce the dimension of the switching system). In the multirealisation form, two parameters A_0 and C_0 are fixed for ensuring the continuity of states and outputs during switching. The other two parameters B_i and F_i are changing when switching to different submodels. With this approach, the stability requirement of a switched system is attained without loss of submodel estimation accuracy.

4.6 Conclusion

Compared with the physical sensor-based robot control strategy, the biosensor-based robot control strategy for rehabilitation can more naturally trigger movements by human intention motion.

In this study, we presented a bumpless switching based modelling approach to consecutively estimate required forces of arm motion from EMG signals by switching among simple submodels during complex rehabilitation tasks. The main procedure of the bumpless switching mechanism is first to carve up a complex task into several simple subtasks which are treated by individual subsystem. Then, a simple state-space model for each subtask was individually built. Based on the similar characteristics of the submodels, a generic realisation (multirealisation) for bumpless switching between every two submodels was purposed based on the RMFD.

The proposed bumpless switching mechanism was validated by both offline testing and online experimental verification on seven subjects. The testing results suggest that the method can be applied naturally without any kinematic or dynamic constraints. Moreover, the estimated outputs of the proposed method during verifications are equally accurate and smoother than our previous study, making it suitable for patient rehabilitation applications.

Chapter 5

Continuous Description of Human Motion Intention Based on a Mixed-order Switching Mechanism for a Rehabilitation Robot

5.1 Introduction

User's proactive involvement is vital in both the therapy procedures and the development of rehabilitation technics [124], especially for rehabilitation robotics [125]. Based on advanced rehabilitation theory, biosensor-based robot control strategies imply the user's motion intention and allow triggering movements more naturally. The main focus of biosensor-based robot control strategies mostly locates in the signal selection and decoding method. The surface EMG signal is a great option and has already attracted much attention. EMG signals can be collected easily with noninvasive sensors, and reliably with a close relationship with muscle activities.

Proper intensive physiotherapy is required to improve motor re-learning and recovery levels of the affected limb after stroke. Since different patients need different therapies, it is vital to recognise the actual motion ability that patients remain. For post-stroke

patients who remain partly motion ability, it is essential to evoke their motion intention and help them proactively enrol in rehabilitation with robot assistance.

A few researchers have tried revealing human's motion intention in both static [30] and dynamic manners [126]. However, rarely studies can consecutively map human motion intention from EMG to limb motion in a natural neuromuscular control strategy. The difficulty may cause by the existence of inconsistent motor control patterns among subjects and highly dynamic EMG characteristics. Panagiotis et al. proposed a state-space model with reduced dimensionality of both inputs and outputs which devoted to continuously map the relationship between EMG signals and multi-joint movements [50]. However, the information included in EMG signals may be reduced, and the dynamics of the system will be ignored with the dimension-reduction. Zhang et al. proposed an adaptive estimation method to train a model for accurately mapping two-paired muscle activations and elbow motion for solving subject-specific problems [127]. However, the application of this method is limited in single or two joints, and there still settles a big challenge in keeping signal integrity.

A method was developed without dimension reduction for consecutively estimating multi-joint motion intention in real-time motion from EMG signals during a linear tracking task [128]. The method showed good performance in accuracy and had the potentials in supporting users naturally. But there exists a problem: when the decoder model has a low order, all the important system dynamics can not be represented by the model, but a high order model may lead to an over-fitting problem [154]. A switching mechanism is proposed for expanding application in complex rehabilitation tasks and improving applicability [129]. The method showed better overall performance than the previous one and had potentials in supporting users with consideration of task complexity effects. Another problem is recognised when applying the method in real-time experiments. Between the switching of every two submodels, the estimated outputs are suddenly changed denoted as bump outputs because the models' parameters are varied. The continuity of estimated outputs when switching every task is rarely discussed though there are some researches about switching method for different tasks [44, 86]. Furthermore, to obtain the best model for each subsystem, different orders are tried, and for each order, the model performance on the training data and the robustness testing data were evaluated. Since the best order of every model is different

from each other, a much complicit situation is to switching among parameters whose dimensions are also varied. The overall performance of the previous method is high, and the suddenly changed outputs show slight influence in real-time experiments. However, the influence of bump outputs is ineligible for some healthy subjects, because it may cause a short term response of functionally destabilise posture, or even a long term response of body displacement as compensation [130]. It is totally unacceptable for dyskinesia patients, because it may affect movement stability which is vital during rehabilitation and even cause injury.

For the purpose of exploring the best EMG decoder model during complex tasks, a switching mechanism for carving up the task into several simple subtasks and individually identifying a submodel for each subtask is set up. Since the parameters, orders, and hidden states are different among every model, the 'Bump' appearance of the output may affect the consecutiveness and status of the system. Morse proposed an effective way for improving the inadequate transient response of some switched systems, which is to implement 'Bumpless' transfer between the linear multivariable systems [132]. Hespanha et al. employed an adaptive control algorithm that consists of a group of linear controller models and a high-level switching logic for supervising [131]. A multirealisation problem for a family of linear controller models is solved and applied in MMAC algorithms [133]. Similar to the MMAC application, the proposed switching mechanism uses only one submodel (i.e. a controller) to generate estimated outputs at any instant of time. Furthermore, different submodels may require different orders for acquiring the best performance, reserve most EMG information, and present maximum system dynamics. Thus, the aim of this chapter is to eliminate the 'Bump' appearance of the EMG decoder outputs into a 'bumpless' appearance by finding a general realisation for a group of MIMO subsystems with different orders.

5.2 Models of EMG decoder

The EMG decoder model of each subtask is built up as a linear continuous state-space model. Consider the state-space model for one subsystem (denoted as a submodel) as shown in Eq.3.3.

The state-space submodels for a given task are established by identifying the matrices $\{A_i, B_i, C_i\}$, and the initial state x_0. These parameters are identified in the continuous-time domain by using one of the Subspace Model Identification methods, the Canonical Variate Analysis. As the system under investigation is stable, the stability of the model is added as a compulsory condition during model identification.

For each submodel, the selection of order k by Zhang et al. [155] based on the Minimum Description Length criterion for the trade-off between the simplicity of the model and the model's applicability to the data is referenced. To be more specific, the orders of all four submodels are selected with the consideration of the performance of the singular value during each modelling period. Therefore, the order of each submodel may be different, and the order of the whole decoder model for each subject may be different.

5.3 Multirealisation

As described in Section.4.3, the transfer function matrix $H_i(s)$ ($i \in \{1, 2, 3, 4\}$) can be expressed by MFD [136]. The specific steps of using MFD to find a multirealisation of the four submodels $H_i(s)$ will be described later.

To achieve a simpler transfer function of these subsystems, the minRMFD of these subsystems are calculated as Section.4.3.1. The minRMFD ($\bar{D}(s)$ and $\bar{N}(s)$) of a transfer function can be found after this step.

5.3.1 Multirealisation of Linear Subsystems with Mixed Orders

With the minRMFDs ($\bar{D}_i(s)$ and $\bar{N}_i(s)$) of all subsystems found, a generic multirelisation of the set of subsystems H_i can be achieved by the following method which is simplified based on [134].

A ploynomial matrix $D(s)$ can be written as $D(s) = D^{hc}S(s) + D_{lc}(s)$, where $S(s) \triangleq diag\{s^{k_1}, s^{k_2}, ..., s^{k_m}\}$ is the highest column degree matrix with k_i being the highest degree of the i-th column of $D(s)$, and D^{hc} is the highest degree-coefficient

matrix of $D(s)$, which is constructed from the coefficients of the highest degree polynomials in the columns of $D(s)$, and $D_{lc}(s)$ is the remaining part of the $D(s)$. The operator ($\mathcal{D}_{hc}\{\cdot\}$) is defined as $\mathcal{D}_{hc}\{(D(s)\} = D^{hc}S(s))$.

Assume the minRMFD of a transfer function $H_i(s) = N_i(s)D_i^{-1}(s) = \bar{N}_i(s)\bar{D}_i(s)$ can be found with $\bar{D}_i(s)$ in column reduced form. To simplify the discussion, we can assume that the matrix $D_i(s)$ is a Popov form matrix [136]. With the minRMFDs ($\bar{D}_i(s)$ and $\bar{N}_i(s)$) of all subsystems found, a generic minimal multirealisation of the set of subsystems $H_i(s)$ can be achieved by the following procedure [134].

5.3.1.1 Reform the minRMFD

To derive conditions for the multirealisation of multivariable systems, we first reform the $\bar{D}_i(s)$ into $\tilde{D}_i(s)$ with requirements that the elements of $S(s)$ exist on the diagonal in degree reducing order, and the D_i^{hc} of the $\tilde{D}_i(s)$ are normalised to I, which are implemented by elementary transformation with consideration of every element of each $\bar{D}_i(s)$. The transfer function, therefore, is transformed into:

$$H_i(s) = \bar{N}_i(s)M_i[\bar{D}_i(s)M_i]^{-1} = \tilde{N}_i(s)\tilde{D}_i^{-1}(s) \tag{5.1}$$

where M_i is a real matrix for i-th subsystem for reform the minRMFD.

5.3.1.2 Uniform the Common Highest-degree-coefficient Matrix

As described by the previous research [133], a stable based generic multirealisation can be found with a genic minimal common denominator $D_{ms}(s)$, for which $\mathcal{D}_{hc}\{D_{ms}(s)\} = D_m(s)$ has the form shown in Eq.4.5 and Eq.4.6:

In this step, we try to find out the common D_m^{hc} for every subsystem.

5.3.1.3 Construct a Common RMFD

With the constructed common highest-degree-coefficient denominator $\mathcal{D}_{hc}\{D_{ms}(s)\} = D_m(s)$, it is always possible to transfer the $\mathcal{D}_{hc}\{\tilde{D}_i(s)\}$ by right multiply a polynomial

matrix $\mathcal{D}_{hc}\{\bar{M}_i\}$ for increasing the order of each column, the $\bar{M}_i$ has the following form

$$\mathcal{D}_{hc}\{\bar{M}_i\} = diag\{s^{\Delta k_p^i}\}(p \in 1, ...n), \tag{5.2}$$

where the $\Delta k_p^i = k_{max_p} - k_p^i$ is the order difference in p-th column between $D_m(s)$ and $\mathcal{D}_{hc}\{\tilde{D}_i(s)\}$. After that, a real number g is needed. The number g is for constructing the matrix by $\bar{M}_i = diag\{(sI - g)^{\Delta k_p^i}\}$. The g here is required to be any positive number. The stability of the system after this step is ensured.

When we found the $\bar{M}_i$, the $Dm_i(s)$ and $Nm_i(s)$ of i-th system can be constructed by right multiplying it as follow:

$$H_i(s) = \tilde{N}_i(s)\bar{M}_i[\tilde{D}_i(s)\bar{M}_i]^{-1} = Nm_i(s)Dm_i^{-1}(s) \tag{5.3}$$

where $\mathcal{D}_{hc}\{Dm_i(s)\} = \mathcal{D}_{hc}\{\tilde{D}_i(s)\bar{M}_i\} = D_m(s)$.

After we constructed the new RMFDs for all subsystems, it is ready to multi-realise all the submodels.

5.3.1.4 Construct a Generic Multirealisation

Based on the previous research [133], to implement the multirealisation form, we need to construct $Nm_i(s)$ and $Dm_i(s)$ for the transpose form of $H_i(s)$, i.e.,

$$H_i^T(s) = Nm_i(s) \cdot Dm_i^{-1}(s).$$

Then, construct a stable polynomial matrix $D_{ms}(s)$ such that $\mathcal{D}_{hc}\{D_{ms}(s)\} = D_m(s)$. By using the method in [136] (pp. 403-407), a controller form realisation $\{A_{c0}, B_{c0}, C_{ci}\}$ of $Nm_i(s)D_{ms}^{-1}(s)$ can be found with the pair $\{A_{c0}, B_{c0}\}$ controllable and A_{c0} stable and $C_{ci} = Nm_{ilc}$. Let $K_i = D_{mlc} - Dm_{ilc}$. Then, a generic minimal multirealisation for the set of subsystems $H_i^T(s)$ $(i \in \{1, 2, 3, 4\})$ is $\{A_{c0} + B_{co}K_i, B_{co}, C_{ci}\}$.

Then, the multirealisation form for the original submodels $H_i(s) = H_i^T(s)^T$ can be obtained as $\{A_0 + F_iC_0, B_i, C_0\}$ by letting $A_0 = A_{c0}^T$, $B_i = C_{ci}^T$, $C_0 = B_{c0}^T$, $F_i = K_i^T$ where only the F_i and B_i are needed to be adjusted during switching. As A_0 and C_0

are constant during switching, the stable LTI system with the switching mechanism can ensure bumpless outputs in real-time (i.e., the outputs keep continuous under the switching of F_i and B_i). The obtained generic multirealisation of four subsystems is denoted as $\{A_{Ei}, B_{Ei}, C_E\}$.

5.3.1.5 Find an Expanded Initial State x_{Ei}

Although it is always possible to find the adequate generic multirealisation, the dimension of the initial state x_{Ei} of each subsystem in multirealisation is different from the identified x_i of the initial submodel. Therefore, the following steps are proposed to construct the x_{Ei} based on the multirealisation and x_i.

Firstly, when the order of a submodel raised to the order of the generic multirealisation, the new realisation includes Δk_p^i uncontrollable elements. These elements are related to the extended elements of x_{Ei}. To find out these elements, the generic multirealisation for a subsystem is transformed into controllability staircase form $\{\bar{A}_{Ei}, \bar{B}_{Ei}, \bar{C}_{Ei}\}$ as follow:

$$\begin{cases} \bar{A}_{Ei} = \tilde{M}_i A_{Ei} \tilde{M}_i^T = \begin{bmatrix} \bar{A}_{uci} & 0 \\ \bar{A}_{21} & \bar{A}_{ci} \end{bmatrix} \\ \bar{B}_{Ei} = \tilde{M}_i B_{Ei} = \begin{bmatrix} 0 \\ \bar{B}_{ci} \end{bmatrix} \\ \bar{C}_{Ei} = C_E \tilde{M}_i^T = \begin{bmatrix} \bar{C}_{nci} & \bar{C}_{ci} \end{bmatrix} \\ \bar{C}_{Ei}(sI - \bar{A}_{Ei})^{-1}\bar{B}_{Ei} = \bar{C}_{ci}(sI - \bar{A}_{ci})^{-1}\bar{B}_{ci} \end{cases} \tag{5.4}$$

where $\bar{A}_{ci}, \bar{B}_{ci}, \bar{C}_{ci}$ are the controllable elements, and $\bar{A}_{uci}$ and C_{nci} are the uncontrollable element.

Based on the Eq.5.4, the matrix $\tilde{M}_i$ is also applied in the extended initial state x_{Ei} of the generic multirealisation for reforming it as a controllable form $\bar{x}_{Ei}$ as follows:

$$\bar{x}_{Ei} = \tilde{M}_i^T x_{Ei} = \begin{bmatrix} 0 \\ \bar{x}_{ci} \end{bmatrix}, \tag{5.5}$$

where $\bar{x}_{ci}$ is the controllable element, and the 0 elements are the uncontrollable elements.

Theoretically, the controllable form $\{\bar{A}_{ci}, \bar{B}_{ci}, \bar{C}_{ci}\}$ should equal the identified realisation $\{A_i, B_i, C_i\}$. However, due to the complexity of a real system and the simplification of minRMFD, $\{\bar{A}_{ci}, \bar{B}_{ci}, \bar{C}_{ci}\}$ here has the same the dimension as $\{A_i, B_i, C_i\}$, and their values are related as follows:

$$\begin{cases} \breve{M}_i \bar{A}_{ci} - A_i \breve{M}_i \leq \alpha \\ \breve{M}_i \bar{B}_{ci} - B_i \leq \beta \\ \bar{C}_{ci} - C_i \breve{M}_i \leq \gamma. \end{cases} \tag{5.6}$$

With the restrictions that $\alpha, \beta, \gamma \geq 0$ and $\alpha + \beta + \gamma \leq e^{-10}$, it is always possible to find the matrix $\breve{M}_i$ that best fit the relationship between two forms.

After that, the controllable element $\bar{x}_{ci}$ of $\bar{x}_{Ei}$ is also related to the identified initial state x_i by $\breve{M}_i$ as:

$$\bar{x}_{ci} = \breve{M}_i^T x_i. \tag{5.7}$$

Combining Eq.5.5 and Eq.5.7, the extended initial state x_{Ei} for each subsystem can be calculated and applied with the generic multirealisation $\{A_{Ei}, B_{Ei}, C_E\}$.

This general bumpless switching method with mix-order submodels is denoted as 'GBL' in the following sections.

5.3.2 Other Switching Mechanisms

5.3.2.1 A Simplified Bumpless Switching Mechanism

In terms of the whole system, the dimensions of the inputs and outputs always keep the same in any submodels, while the dimensions of the hidden state x_i are different from each other. To realise bumpless outputs, adjustments on C_i can compensate for the gap between the final state of the previous submodel and the initial state of the present submodel. This method needs to be implemented separately according to two situations.

When the order of the submodel (k_i) equal the dimension of output (here is 3), construct O_i matrix that equals C_i matrix, i.e.

$$O_i = C_i. \tag{5.8}$$

When k_i is larger than the dimension of output, construct O_i by grouping a zero matrix $Q_i \in \mathbb{R}^{(k_i-3)\times 3}$, an element matrix $I_i \in \mathbb{R}^{(k_i-3)\times(k_i-3)}$ and C_i into a square matrix as follows:

$$\begin{cases} \bar{Q}_i = \begin{bmatrix} Q_i & I_i \end{bmatrix} \\ O_i = \begin{bmatrix} C_i \\ \bar{Q}_i. \end{bmatrix} \end{cases} \tag{5.9}$$

Use O_i to reform all parameters as follows:

$$\begin{cases} \bar{x}_i = O_i x_i \\ \bar{A}_i = O_i A_i O_i^{-1} \\ \bar{B}_i = O_i B_i \\ \bar{C}_i = C_i O_i^{-1}. \end{cases} \tag{5.10}$$

The output matrix $\bar{C}_i$ is an element matrix but may differ from each submodel. With this $\bar{C}_i$, the outputs would be only affected by the hidden state $\bar{x}_i$.

When applying this simplified switching method, the initial hidden state of the first submodel is given as the reformed $\bar{x}_0$ from the modelling phase. With the new realisation $\{\bar{A}_i, \bar{B}_i, \bar{C}_i\}$ and hidden state $\bar{x}_i$, when the time flows to the switch point between every two models, denote the order of the first model as m and the order of the second model as n: 1) if $m = n$, the hidden state keeps changing without additional processing; 2) if $m < n$, keep the first m states the same, and add the extra $(n - m)$ state from the reformed $\bar{x}_i$ of the certain submodel; 3) if $m > n$, keep the first n states the same, and throw away the rest states. With this method, bumpless outputs can also be realised while the hidden state is not continuous. This simplified bumpless switching mechanism is denoted as 'SBL' in the following sections.

5.3.2.2 A Zero Initial State Switching Mechanism

Another method to ensure a bumpless method is to set the x_0 as a zero matrix while the initial state of the first model is given from the modelling phase. This method is applied to investigate the impact of the initial states in overall model performance and denoted as 'ZISBL' in the following sections.

5.3.2.3 A Bump Switching Mechanism

A switching mechanism is directly switching the four submodels by time without any additional processes on parameters. The outputs thus are not continuous, but the overall accuracy is proved to be relatively good [129]. This bump switching mechanism method is denoted as 'NGBL' in the following sections.

5.3.2.4 A Single State Space Model without Switching Mechanism

In comparison, a single state space model is also trained for applying in the whole task. Since the orders of all submodels are not exceeding 6, the order of the single state space model is selected as six. This six-order single model is denoted previously as 'S6' and in the following sections.

5.4 Experiments

A cable-based upper limb rehabilitation robotic system is used to provide assistance to participants. The details of the robotic system are described in Section.2.4 and showed in Fig.5.1.

The muscle activations are calculated from full-wave rectified EMG envelops [50], normalised to the MVC values [110] and a EMG-muscle activation models [111–113]. The EMG-driven forces which related to human motion intention and further calculated the driven torques of the three motors are computed from the human-robot dynamics model [94] by using the motion system. In order to match the frequency of muscle activations (system inputs) and the EMG-driven forces (system outputs) from the

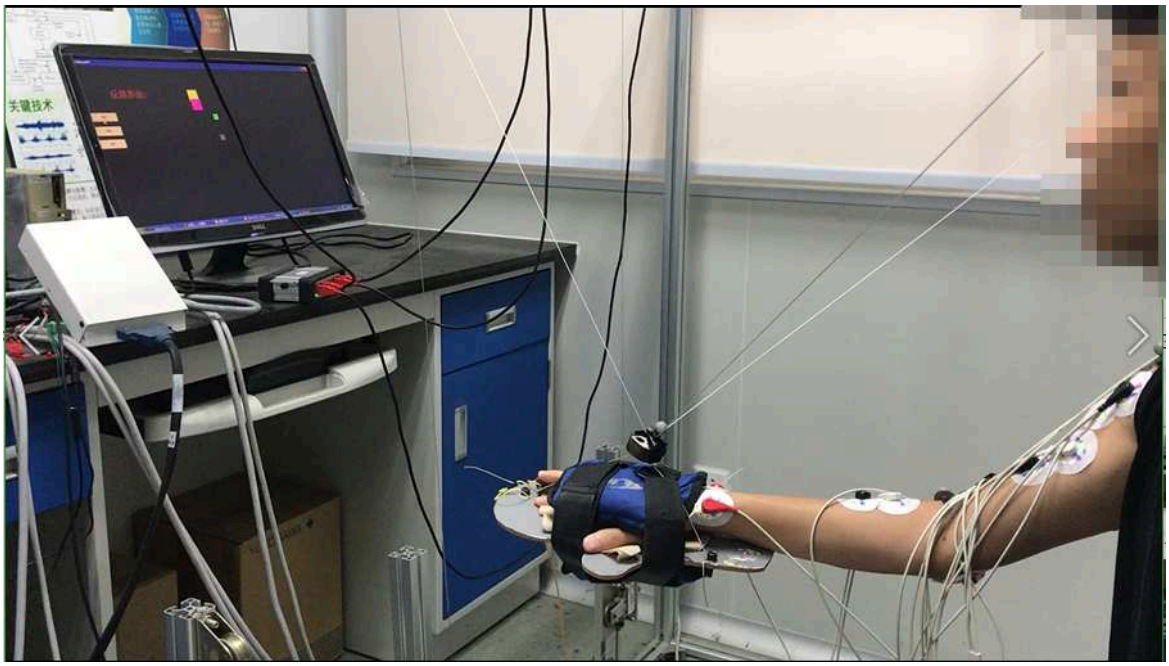

Fig. 5.1 An experimental scenario.

human-robot dynamics model, the muscle activations are further decimation into 100 Hz. The dynamic model is applied to calculate the EMG-driven forces on the wrist (the decoder outputs) during the human-robot cooperation movements of the arm and splint.

5.4.1 EMG-based Human-robot Cooperation Controller

The human-robot cooperation controller based on an EMG decoder is used for controlling the robot. The EMG decoder is trained to estimate the EMG-driven forces along with the cables from muscle activations. The six muscle activations are the inputs, and the EMG-driven forces are the outputs of the decoder system.

In this chapter, the designed complex task is still the tracking of a square shape preset trajectory in a horizontal plane with four rectilinear movements (i.e. the four subtasks) in different directions of 3D space. The length of each rectilinear movement is $\sqrt{0.02}m$.

The switching mechanism for carving up the task into subtask is also applied. A total of four different ordered linear state-space models as submodels with six-input

and three-output are built up for this task. For subtask decoder models, each of them can seem as a subsystem. The switching mechanism in the chapter can be realised directly by time series (bump) and by a general bumpless realisation. As a comparison, the 6-order single model for the whole task is also built up and applied.

5.4.2 Participants

Five healthy participants (aged 25.0 $\pm$ 0.6 yrs) were recruited. All participants signed the written informed consent forms. This study was approved by the Human Ethics Committee of the First Affiliated Hospital of Sun Yat-Sen University ([2013]C-096).

Based on biomechanics literature [116], the surface EMG signals of six muscles (BIC, TRI, DA, DM, DP, and BR), which are mainly responsible for analysing the upper limb motions, are recorded by the EMG acquisition system.

5.4.3 Experimental Protocol

The efficiency of the proposed general bumpless transfer method will be verified by both numerical analysis and real-time experiments with seven participants. The impact of the initial state will also be verified with three participants. Numerical analysis (mainly modelling) consists of the EMG decoder model *training* phase and model *testing* phase by simulation. The experiments are mainly for the real-time EMG-based control performance in the $verifying$ phase.

The data for the training phase and the testing phase are collected according to the following procedures. Each participant is asked to track a moving cursor shown on the screen by using his/her arm for 20 seconds in total. The trajectory of the moving cursor is the preset square shape trajectory in the horizontal plane. The cursor moves for 5 seconds during each rectilinear movement. Each participant is asked to track the cursor, which repeatedly moves along the square shape trajectory nine times as nine trials. Six trails are randomly selected for the training phase, and three trials are for the testing phase.

The data for *model training* is processed for training four submodels. These models may have different orders and order selection is based on model performance during the training phase as described in Section 5.3.

In the model testing phase, the EMG signals are also processed as the input, and the trained models are used to estimate the outputs. The estimated outputs are compared to the targeted output to assess the accuracy of the models. As noted before, during the testing stage, the muscle activities contain no response to the tracking error through human visual feedback.

In the experimental verification stage, the participants are instructed to place their forearms in the splint. All three models are applied in the EMG-based controller and for realising the human-robot cooperation movements. During this phase, each participant is asked to tracking the cursor three times as three trials. All participants are required to finish the task with *robot assistance* estimated by every model together with their muscle contributions. The performance of different models can be assessed in a real-time feedback loop. In this loop, the human 3D motion intent, estimated by using the identified models, as reflected in the human visual feedback in real-time to reduce the tracking error as indicated in the computer screen.

5.5 Results and Discussion

The muscle activations are analysed to explore the motion ability difference between the modelling in offline phases (i.e., training phase and testing phase) and the online verifying phase. To evaluate the performance of different models, the model $fitness$, output smoothness are calculated, analysed, and compared.

5.5.1 Model Fitness

Based on the EMG decoder models, the target outputs from the joint positions and estimated outputs from the models with the same inputs can be calculated.

The Root Mean Squared Logarithmic Error (RMSLE) value is calculated to evaluate the model. RMSLE can measure the ratio between outputs target and estimation

according to the following equation:

$$RMSLE = \sqrt{\frac{1}{N}\sum_{i=1}^{N}(|(\log(y_i+1) - \log(\hat{y}_i+1)|)^2} \tag{5.11}$$

where y_i is the estimation value, $\hat{y}_i$ is the estimation value in each output at i-th sampling instant, and N is the number of samples.

The Concordance Correlation Coefficient (ρ_c) between the targeted and estimated outputs is calculated for measuring how well the estimation compares to the targets as follow [156]:

$$\rho_c = \frac{2s_{xy}}{s_x^2 + s_y^2 + (\bar{x} - \bar{y})^2} \tag{5.12}$$

where $\bar{x}$ and $\bar{y}$ are the mean values of the targeted and estimated outputs, the s_x^2 and s_y^2 are their variances and $s_{xy} = \frac{1}{N}\sum_{n=1}^{N}(x_n - \bar{x})(y_n - \bar{y})$ is the covariance.

Furthermore, for measuring how successful the model fit is in explaining the variation of the data, the adjusted coefficient of determination noted as the adjusted R-squared (R_{adj}^2) is calculated as follow [157]:

$$R_{adj}^2 = 1 - \frac{(N-1)(1-R^2)}{N-p} \tag{5.13}$$

and

$$R^2 = \frac{SS_{regression}}{SS_{total}} = \frac{\sum_{i=1}^{N}(f_i - \bar{y})^2}{\sum_{i=1}^{N}(y_i - \bar{y})^2} \tag{5.14}$$

where y_i is the observed value, and f_i is the estimation value in each output at i-th sampling instant, and $\bar{y}$ is the mean values of y_i, and N is the number of samples, and p is the number of parameters of a model. The R_{adj}^2 is a rescaling of R^2 by Dof. Thus it can evaluate models with consideration of the quantities difference of model parameters.

The results of the RMSLE, ρ_c and R_{adj}^2 are shown in Table.5.1.

The model outputs of the four different models during the training and testing phases are shown in Fig.5.2. The model outputs of four different models during verifying phases are shown in Fig.5.3.

Table 5.1 The comparison between the RMSLE, ρ_c, R^2_{adj} and NJS values of three models (NGBL, GBL and S6) during training, testing and verifying phases.

Phase	Output	**RMSLE (Median(IQR))**			Significance
		NGBL	GBL	S6	
Training	O1	0.01(0.01)	0.02(0.01)	0.05(0.05)	a,b,c
	O2	0.01(0.01)	0.02(0.01)	0.03(0.01)	b,c
	O3	0.01(0.01)	0.02(0.03)	0.05(0.04)	b
Testing	O1	0.03(0.01)	0.03(0.01)	0.08(0.05)	b,c
	O2	0.03(0.02)	0.03(0.03)	0.06(0.03)	b,c
	O3	0.03(0.02)	0.04(0.03)	0.08(0.01)	b,c
Verifying	O1	0.23(0.26)	0.15(0.14)	0.78(2.03)	b,c
	O2	0.13(0.22)	0.11(0.05)	0.25(0.55)	
	O3	0.15(0.09)	0.12(0.07)	0.67(0.55)	b,c
Phase	Output	ρ_c **(Median(IQR))**			Significance
		NGBL	GBL	S6	
Training	O1	0.99(0.01)	0.97(0.03)	0.90(0.12)	a,b
	O2	1.00(0.01)	0.98(0.02)	0.94(0.05)	a,b,c
	O3	0.99(0.03)	0.97(0.09)	0.89(0.13)	b
Testing	O1	0.94(0.05)	0.95(0.04)	0.65(0.36)	b,c
	O2	0.96(0.06)	0.95(0.11)	0.85(0.11)	b,c
	O3	0.94(0.06)	0.92(0.08)	0.74(0.27)	b,c
Verifying	O1	0.34(0.50)	0.35(0.18)	-0.03(0.02)	b,c
	O2	0.47(0.26)	0.46(0.37)	0.11(0.33)	c
	O3	0.41(0.27)	0.67(0.18)	0.01(0.23)	b,c
Phase	Output	R^2_{adj} **(Median(IQR))**			Significance
		NGBL	GBL	S6	
Training	O1	0.98(0.02)	0.95(0.07)	0.76(0.32)	a,b
	O2	0.99(0.03)	0.95(0.06)	0.88(0.11)	b,c
	O3	0.98(0.07)	0.94(0.17)	0.69(0.32)	b
Testing	O1	0.86(0.12)	0.88(0.09)	0.56(0.83)	b,c
	O2	0.91(0.16)	0.89(0.17)	0.68(0.44)	b,c
	O3	0.87(0.15)	0.80(0.25)	0.42(0.26)	b,c
Verifying	O1	-4.61(9.44)	-2.72(4.28)	-88.92(121.96)	b,c
	O2	-0.35(3.51)	0.02(0.62)	-3.35 (58.98)	c
	O3	-0.92(1.89)	-0.18(0.98)	-36.31(72.28)	b,c
Phase	Output	**RNJS (Median(IQR)**			Significance
		NGBL	GBL	S6	
Training	O1	34.81(22.36)	15.92(5.44)	26.76(40.77)	a
	O2	30.20(13.92)	11.69(9.69)	19.97(10.04)	a,b
	O3	39.15(24.11)	21.11(10.00)	22.91(21.66)	a
Testing	O1	41.37(27.16)	14.82(6.82)	28.66(30.39)	a,b
	O2	34.25(16.51)	15.23(18.88)	23.01(11.81)	a,b
	O3	45.69(66.07)	19.44(8.63)	29.06(25.66)	a
Verifying	O1	265.80(242.68)	32.71(23.07)	7.65(21.13)	a,b
	O2	217.30(244.84)	20.76(18.19)	13.43(22.80)	a,b
	O3	316.34(174.73)	22.33(15.11)	13.81(13.16)	a,b

Note: 1) IQR:Interquartile Range; 2) Significant differences between these models are represented by the following alphabets: ***a:NGBL-GBL****, b:NGBL-S6, c:GBL-S6.*

As expected, both the general bumpless switching mechanism and the simplified bumpless switching mechanism can effectively estimate motion needed forces without any sudden changes. However, it is not surprising to find that the modelling fitness of among the bump, the general bumpless, and the simplified bumpless method didn't show any difference. It is because of the high accuracy obtained by each subtask model and the gap of sudden change during switching was averaged into the whole task.

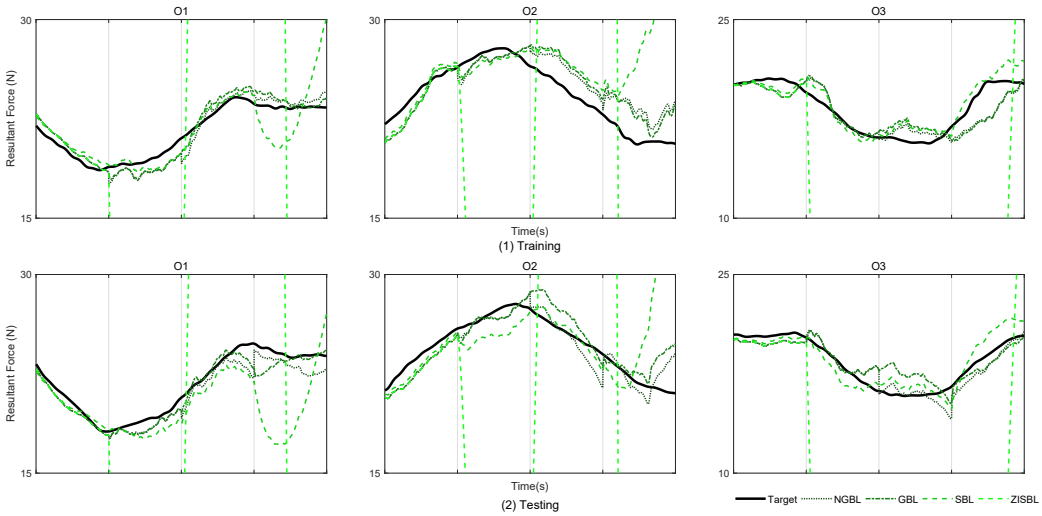

Fig. 5.2 The model outputs of three different models during the training and testing phases.

5.5.2 Output Smoothness

In order to quantify the smoothness of the outputs for controlling the motor groups, NJS of the outputs during the simulation and real-time experiments was adopted to represent movement smoothness in 3D space [142] and calculated as Eq.4.8.

The RNJS of the outputs estimated by different EMG decoder models is calculated for comparing with desired outputs from the dynamics models as Eq.4.9.

The results of the $RNJS$ during both testing and verifying phases are shown in Table.5.1.

The difference between GBL and NGBL is significant among all outputs in all three phases, while the values of $RNJS$ of the NGBL model are the highest. The smoothness

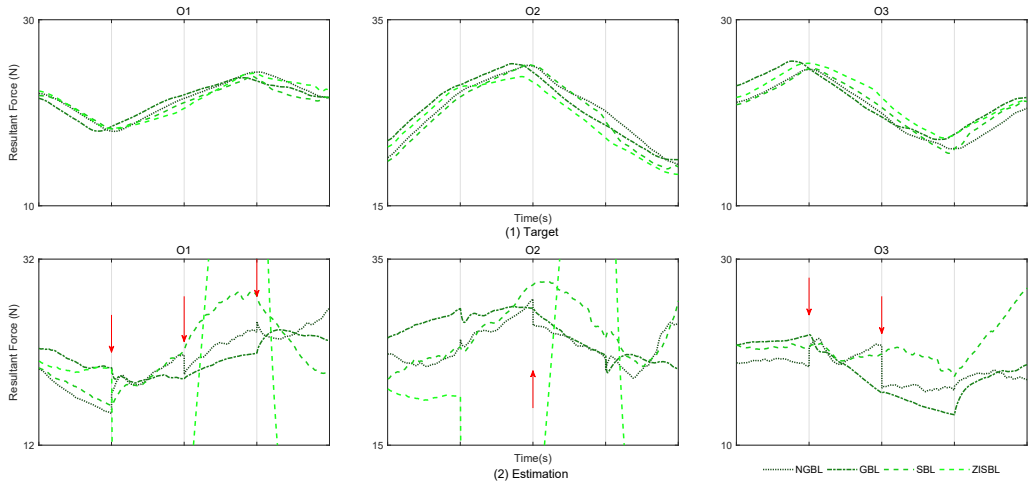

Fig. 5.3 The model outputs of three different models during the verifying phase.

of the bumpless outputs perfectly kept the same level to the same-ordered bumpless method and 3-order single model in our previous study [129]. The results demonstrated that no matter what the order of each submodel is, the bumpless estimated forces are well performed. Therefore, it is obvious that, although the bump model can relatively estimate the outputs, it can not offer the smoothness of the outputs and therefore will highly affect the application in real-life rehabilitation.

5.5.3 Effects of Different Initial States

The results of the $RMSEL$, ρ_c, R^2_{adj}, and $RNJS$ among four different models (NGBL, GBL, SBL, ZISBL) within three subjects are shown in Fig.5.4, Fig.5.5, Fig.5.6, and Fig.5.7.

The effects of different initial states showed thoroughly from the results. It is apparent that the best performance of the results is: a small value of $RMSELE$, a small value of NJS, a value of ρ_c that close to 1 and also a value of R^2_{adj} that close to 1. With these requirements, it is clear to clarify the best selection of the initial state is processed in GBL, which is realised by the proposed advanced general bumpless switching mechanism.

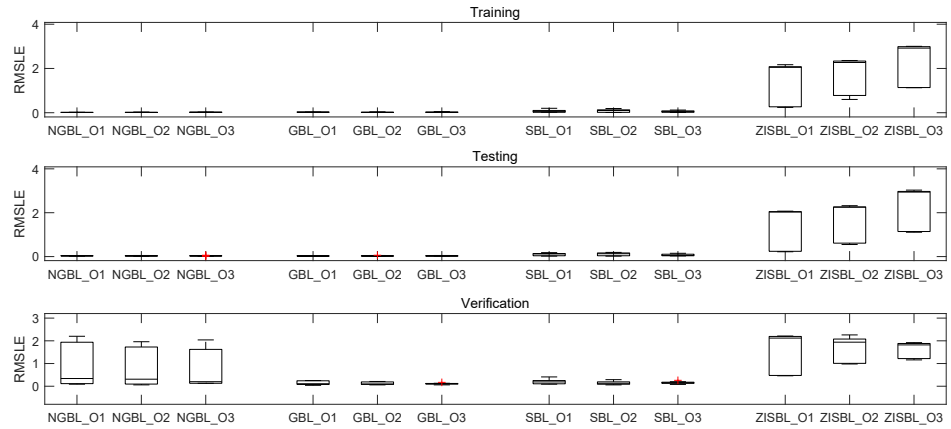

Fig. 5.4 Results of $RMSLE$ among four different models within three subjects.

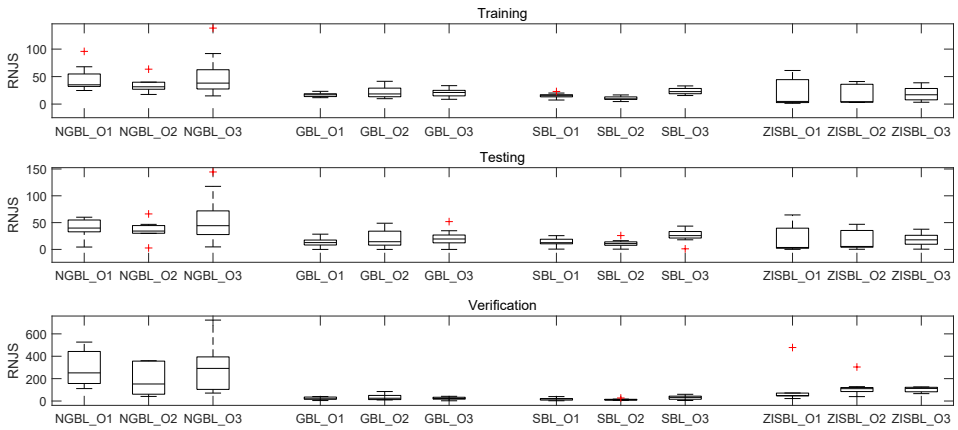

Fig. 5.5 Results of $RNJS$ among four different models within three subjects.

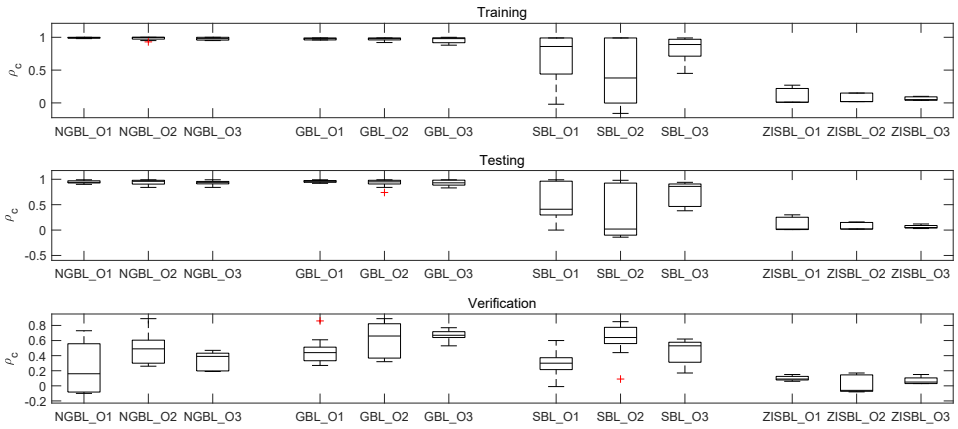

Fig. 5.6 Results of ρ_c among four different models within three subjects.

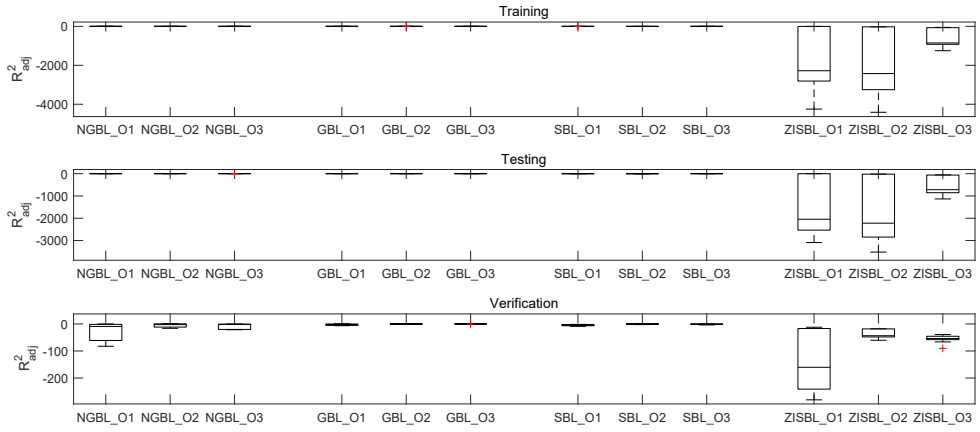

Fig. 5.7 Results of R^2_{adj} among four different models within three subjects.

5.5.4 Statistical Analysis

Based on the results, the results of $RMSEL$, ρ_c, R^2_{adj}, and $RNJS$ of different models is non-normal distribution. Therefore, to analyse the influence of different decoder models, the difference of these parameters are evaluated by using the Kruskal-Wallis nonparametric test with pairwise multiple comparisons with significance level at 0.05. Statistical work is performed using SPSS 19.0 (SPSS Inc., USA).

5.6 Conclusion

In this study, a mathematical method was proposed to realise a general bumpless transfer among EMG decoder models with different orders. An order transformation which aimed to reform models based on the common order among all models is applied to form a multirealisation of different ordered linear systems. With the multirealisaion, selecting proper initial states of each model is vital for ensuing no bump connection between every two models. The effect of initial states is investigated among four models with different selections. The results indicated that the initial states, based on the proposed order transformation method, have the best performance. Overall, this advanced general bumpless switch mechanism together with EMG decoder models can effectively estimate the motion needed forces from EMG signals with high accuracy and smoothness, which was validated by numerical simulation and real-time experiments.

Chapter 6

Continuous Estimation of Motion Intention based on EMG Signals Using a Time-variant Long Short-term Memory Network

6.1 Introduction

Due to the noninvasiveness and relative robustness in the collection of the surface EMG signal, there has been a focus in the field of prostheses, exoskeleton, stroke rehabilitation, and robot control. Specifically, EMG decoders are mostly used to estimate motion intention from EMG signals and are highly concerned with control strategy research. There are two main design schemes for them: pattern recognition and direct control [81]. The pattern recognition scheme in myoelectric control is more likely to extract and classify basic patterns that happen during motion. However, despite its reliability in results, the outputs of the scheme are predefined motion classes, the number of patterns that can be chosen is limited [83]. The requirements of the coordination of multiple physiological degrees of freedom across multiple joints and the continuity among different classes are intractable issues that needed to be addressed

[84]. However, in many areas, especially rehabilitation and robot control, simultaneous and continuous control of multiple DoFs is necessary.

For a direct control scheme, the main aim is to estimate forces or torques in time series for simultaneously controlling robotics or prostheses directly from EMG signals or their characteristics. Many myoelectric control methods based on linear system approaches have been proposed, i.e. a dimensionality-reduction technique with a linear system model [50], an adaptive muscle-to-force model based on EMG patterns [158], a decoder model based on Kalman filter and ridge regression [149]. Although the linear system modelling methods are easier to be realised and only required individual data for training parameters, the nonlinearity of EMG signals is not fully considered, and more DoFs are needed to be represented.

With the development of nonlinear system methods and deep learning methods in biological signals, lots of methods that can solve many complex problems such as the non-stationarity of EMG signals across sessions and achieve much better performance are also reported, i.e., a decoder model based on kernel ridge regression [88], and a three domains fuzzy wavelet neural network algorithm [89]. In another aspect, some researchers take advantage of both classification, and regression approaches [159]. A decision from the classification scheme was used to trigger a task-specific EMG decoding model based on a linear system method that outperforms a 'general' model. Moreover, some studies also combined different deep learning methods such as convolutional neural network, RNN, and LSTM to obtain a much general and robust algorithm with even better performance in decoding EMG signals [83, 91]. Machine learning methods with enormous data support have shown great power for myoelectric control while some variabilities such as fatigue, and physiological factors of EMG signals still need more investigation [92].

Generally, deep learning methods try to extract features on multiple levels of representation and learn very complex functions with the composition of several layers. An advantage also shows in the learning procedure where layer features can be learned without human designing [93], and also no physiological significance needs to be related. It is much easier to be applied in real and commercial rather than traditional linear system methods which require dedicated design based on biomedical experts.

Although most of the mentioned research has demonstrated impressive power in force estimation, and controlling prostheses and rehabilitation robots, the complexity and its requirements in data size, and time cost training procession are key points in results.

This chapter aims to develop an approach based on deep learning technology and time-variant thoughts in decoding EMG signals and applied in real-time rehabilitation robot testing. LSTM is a method that can be effective in capturing temporal dependencies based on learning contextual information from past inputs [160, 161]. However, most recent studies in myoelectric control have only applied conventional selected features rather than deep temporal or spatial features in their regression process. For the purpose of identifying the temporal information during continuous muscle contractions of a whole movement, an LSTM-based model was applied at every time instance and treats the process of EMG signals to motion forces as a time-variant system. Furthermore, two models based on LSTM were trained by data of one or three designed tracking tasks in three-dimensional space. Two models based on linear system methods were also trained by data of every task. The comparisons among different models were analysed to reveal the contributions of different methods. A total of seven healthy participants took part in experiments to perform three different tracking tasks in three-dimensional space when without or with robot assistance. From experimental results, it could be observed that the deep learning-based methods outperform linear system based methods in most tasks. At the same time, they both contribute to the myoelectric controlled robot being used in a rehabilitation process.

The remainder of this chapter is structured as follows. Section 6.2 describes the proposed time-variant LSTM-based method and introduces the experimental setups. Section 6.3 presents estimation results in both offline and online testing phases. Section 6.4 compares and discusses the results from different methods and their contributions, respectively. Section 6.5 draws the overall conclusion whilst presents our future works.

6.2 Materials and Methods

The platform was used to provide assistance to participants, as shown in Fig.6.1, and its details are described in Section.2.4.

Fig. 6.1 An experimental scenario. (a) The platform structure (b) Electrodes placements, markers placements, and three tracking tasks.

6.2.1 EMG-based Human-Robot Cooperation Controller

The human-robot cooperation controller based on an EMG decoder was used for controlling the robot [129]. The EMG decoder (Fig.6.2 (b-d)) was trained to estimate the EMG-driven forces along the cables from muscle activations. The muscle activations were obtained by basic EMG processing and EMG-activation model based on a previous research [60]. The arm and robot dynamic models were built for reckoning the voluntary forces driven by muscle's EMG from the kinetics of arm together with the end-effector on the basis of arm and robot structure. The EMG-driven forces would be further transferred into a motor torque for driving the motor group.

6.2.1.1 EMG-activation Model

The EMG to muscle activation model was built for calculating the muscle activated levels from the amplified EMG signals measured by the EMG acquisition system. First, the amplified EMG signals were full-wave rectified by a 4th order Butterworth low-pass filter to obtain the envelope of amplified EMG signals [50]. Then, the envelop magnitude of each muscle was normalised to the values of its MVC [110]. The neural activations were obtained from the normalised envelope of EMG signals in real-time by a second-order discrete-time linear model [111]. The muscle activations were then

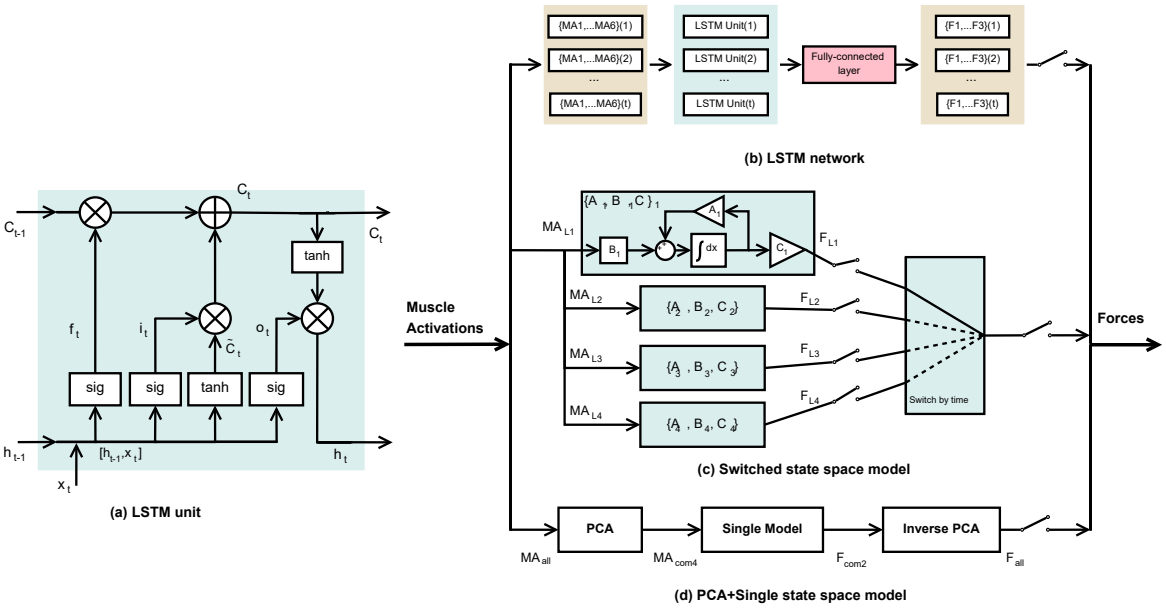

Fig. 6.2 The detailed architecture of the real-time EMG decoding method with the PCA-SS model, the switched system model, and the LSTM-based method. (a) LSTM unit, (b-d) Three methods to train an EMG decoder.

obtained by the coupled relationship between it and the neural activations. The relationship was presented by first-order dynamics [112] and by a non-linear function at low levels of force [113]. The muscle activations were further decimated into 100 Hz to match the frequency of the EMG-driven forces.

6.2.1.2 Arm and Robot Dynamics Analysis

A dynamic model was used to calculate the EMG-driven forces on the hand during the human-robot cooperation movements of the arm and the end-effector. The palm was the contact point between the robot and the arm. During the modelling phase, the assistance from the robot was *unavailable*. Therefore, the forces were driven by EMG on the hand and consist of the motion driven forces and the forces for resisting the effects of arm gravities. During the verifying phase, the cables would drive the arm and the end-effector moving together for executing the task. The forces provided by the motor along the cables were estimated by the EMG decoder model based on the real-time EMG. The kinetics of the robot was applied for calculating the forces along the cables and further the driven torques of the motor group as described in [94].

6.2.2 Participants

Seven healthy participants (aged 26.3 ± 1.4 yrs) were recruited in the data collection phase. Three of them also participated in real-time experiments. All participants have signed the written informed consent forms. This study was approved by the Human Ethics Committee of the first affiliated Hospital of Sun Yat-Sen University ([2013]C-096).

Based on biomechanics literature [116], the surface EMG signals of six muscles (BIC, TRI, DA, DM, DP, and BR), which are mainly responsible for analysing the upper limb motions, were recorded by the EMG acquisition system. The EMG signals, positions of the shoulder and elbow, and the position of the end-effector together with the hand were recorded simultaneously.

6.2.3 Experimental Protocol and Dataset Construction

In this chapter, the experiment design aims to investigate the performance of LSTM-based EMG decoder in a single complex task and multiple complex tasks that do not consider the task difference. We also expected to compare the performances of this deep learning method with some traditional linear system methods and find their difference. Base on the aims, two distinct data preparation for the deep learning method and linear system methods were designed according to the procedure described as follows.

For both methods, the basic task requirements were the same. Participants were required to finish the same groups of tracking tasks with the best accuracy and stability as follows: A target as a yellow cursor shows and moves on the screen, as shown in Fig.6.1(2). The trajectory of the moving yellow cursor varies depending on the different tasks: (a) triangle-shaped task in the sagittal plane, (b) square-shaped task in transversal plane, and (c) circle-shaped task in the frontal plane in Fig.6.3. In all tasks, the cursor moves for 20 seconds with a constant velocity. The actual position of the hand in the specific plane is linked in a red cursor. The specific plane also varies depending on the tasks. Both the yellow and red cursors only move in two dimensions of the specific plane of each task. As a secondary reference, a grey cursor that represents the third dimension besides the task plane is fixed to instruct how far

the actual movement is away from the specific plane. A green cursor is the actual position of the hand in the third dimension and only moves in this dimension.

The difference between the two methods locates in model training dataset construction. For the linear system methods, the models should be trained based on personnel data. In this case, ten repeating trials of every task were merged as a training dataset for each participant. Each participant had an individual switched state space model (denoted as 'MMSS') and an individual PCA based state space model (denoted as 'PCASS') based on his/her own training dataset for every task. There were three participants involved in the dataset constructions of these linear system methods.

For the deep learning methods, to build up a larger dataset for thoroughly activating parameters, seven participants, including the previous three, were involved. Three training datasets were constructed with these participants in three tasks for training LSTM-based models (denoted as 'LSTMS'). In this case, every 15 repeating trials of seven participants in each task were merged and randomised as a training dataset. To investigate whether the LSTM-based method could be used in random tasks, the data of all participants in three tasks were merged and randomised as an expanded dataset. This dataset was for training LSTM-based models for random tasks (denoted as 'LSTMT'). To ensure the dataset properness, noise addition is used to enlarger these datasets. Five groups of additive noises were added and enlarged the size of the datasets into five times larger.

The effectiveness of the mentioned four models was verified using numerical analyses and real-time verifications with the three participants involved in model training dataset constructions of both methods. The numerical analysis consisted of the performance analysis of reapplying decoder models in *training* phase and applying in offline model *testing* phase. The offline testing data were collected together with the training data and were grouped with five trials in each task per participant. In these phases, each participant was asked to move his/her hand to track the yellow cursor on the screen without the robot's assistance. The robot provided zero assistance to the participants, as the force feedback loop was open.

In both phases, the EMG signals were also processed as the input, and the trained models were used to estimate the outputs. The estimated outputs were compared to

the targeted output to assess the accuracy of the models. As noted earlier, during the testing stage, the muscle activities did not respond to the tracking error through human visual feedback.

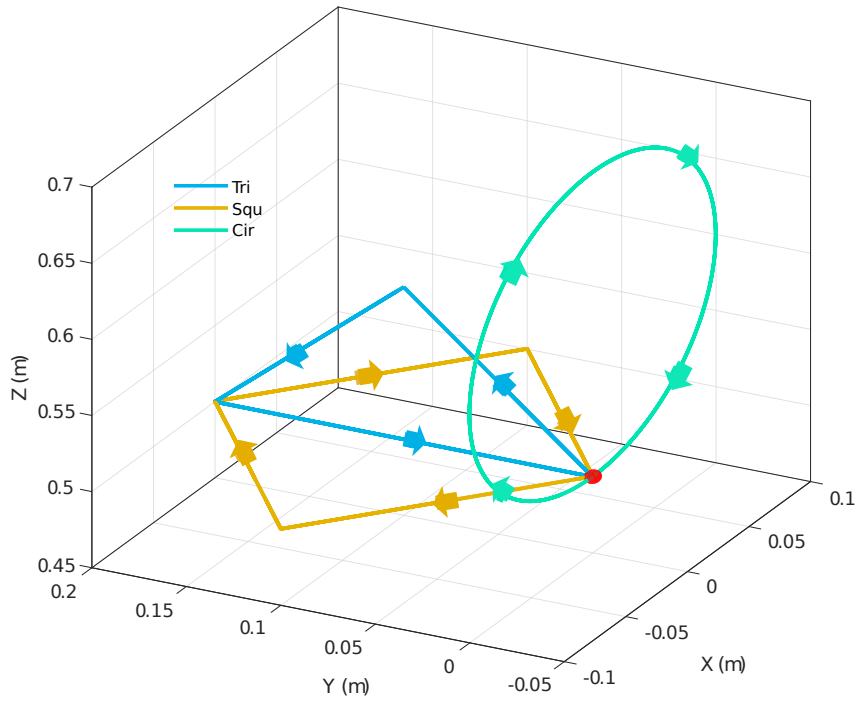

Fig. 6.3 The three tasks in space. Tri: A triangle-shaped task in the sagittal plane. Squ: A square-shaped task in the transversal plane. Cir: A circle-shaped task in the frontal plane. The red marker is the start point of all tasks.

In the real-time verifications, the three participants were instructed to hold the end-effector by hand. Three models (LSTMS, LSTMT, and PCASS) were applied in the EMG-based controller to realise the human-robot cooperation movements. Therefore, the robot provided assistance based on EMG signals as the force feedback loop was closed. During this phase, each participant could control the end-effector to track the target cursor with *robot assistance* estimated by each model together with their muscle contributions. They were asked to repeat five trials. The performance of different models was assessed in a real-time feedback loop. In this loop, the human 3D motion intent, estimated using the identified models, was reflected in the human visual feedback in real-time to reduce the tracking error as indicated on the computer screen.

6.2.4 Models for Force Estimation

6.2.4.1 Long Short-term Memory Network

Long short-term memory network is a type of RNN. It was proposed by Hochreiter and Schmidhuber [160] and has been applied well in many aspects of biosignal related filed, like posture classifications [162] and musculoskeletal force prediction [163]. The strength of it locates in modelling temporal sequences and avoiding problems related to long-term dependence.

Comparing to a standard RNN network, the LSTM network has a more complex cell structure than a simple neural network. A standard LSTM unit is shown in Fig.6.2.(a). Suppose the six muscle activations $x_t = (MA1_t, MA2_t, ..., MA6_t)$ as the inputs and denote inputs as $x = (x_1, x_2, ..x_t)$, where t is the time step, the hidden state h, and the real outputs $y = (y_1, y_2, ..y_t)$ where $y_t = (F1_t, F2_t, F3_t)$ can be computed by following equations.

Three gate units ('forget gate layer', 'input gate layer' and 'output gate layer') grouped in a cell and were computed respectively. The 'forget gate layer' f_t decides to discard what information from the present input x_t and the previous hidden state h_{t-1}:

$$f_t = \sigma(W_f \cdot [h_{t-1}, x_t] + b_f). \tag{6.1}$$

The 'input gate layer' i_t together with $\widetilde{C}_t$ identifies what the information from the present input x_t and the previous hidden state h_{t-1} would be added to the present cell state vector C_t:

$$i_t = \sigma(W_i \cdot [h_{t-1}, x_t] + b_i), \tag{6.2}$$

$$\widetilde{C}_t = tanh(W_C \cdot [h_{t-1}, x_t] + b_C), \tag{6.3}$$

$$C_t = f_t \cdot C_{t-1} + i_t \cdot \widetilde{C}_t. \tag{6.4}$$

The 'output gate layer' o_t decides what the information from the present input x_t and the previous hidden state h_{t-1} would be computed by

$$o_t = \sigma(W_o \cdot [f_t, x_t] + b_o). \tag{6.5}$$

The present hidden state h_t is decided by both present cell state vector C_t and output gate o_t as follow:

$$h_t = o_t \cdot tanh(C_t). \tag{6.6}$$

The real output y_t is computed by a fully-connected layer shown in Fig.6.2(b) as follow:

$$y_t = W_y h_t \tag{6.7}$$

where $\sigma(\cdot) = \frac{1}{1+e^{-x}}$ is the standard logistic sigmoid function, and $tanh(\cdot) = \frac{e^x - e^{-x}}{e^x + e^{-x}}$ is the hyperbolic tangent function, and W_i, W_C and W_o are the input layer, hidden layer, and output layer weight matrices, and b_i, b_C, b_o are the bias matrices of these layers, and W_y is the fully-connected layer weight matrix.

In this study, we treat the relationship between muscle activations and forces in every time instance as a subsystem. In other words, a real-time process of estimating forces in a tracking task is treated as a time-variant system. In this case, a total of 2000 LSTM networks at all time instances are training. All networks have the same structure in layers, but their parameters have no relationships. The input of this network is six channels EMG features, and the output is three channels forces. The LSTM layer contains ten hidden units and the fully-connected layer with an input of three and an output of three maps network internal parameters to three forces.

The subsystem parameters are trained by minimising the following loss functions. The first one is to minimise the sum of square errors in each iteration:

$$e_i = \sum_{i=1}^{n} (\frac{1}{m} \sum_{j=1}^{m} (y_i - p_i)^2), \tag{6.8}$$

where $p_i = [F1_i, F2_i, F3_i]$ is the real forces at ith iteration during training, and n is the batch size. The second loss function is to ensure the sum of square errors during

the whole task to balance the overall accuracy among all instance,

$$e_a = \sum_{t=1}^{T}(\frac{1}{m}\sum_{j=1}^{m}(y_t - p_t)^2), \tag{6.9}$$

where $p_t = [F1_t, F2_t, F3_t]$ is the real forces at its instance t, and $T = 2000$. The procedure to minimise these two functions is: a) calculate the errors of every time step by Eq.6.8; b) calculate the errors of all instance by Eq.6.9; c) if the result of a) is not minimised enough, update parameters at each time step. Else, check the results of b); d) if the result of b) is not minimised enough, repeat a) and find which subsystem has relatively low accuracy and repeat c). To minimise training error, the stochastic gradient descent optimiser is applied for back propagation through time.

6.2.4.2 Switched State Space Model

One linear system method for decoding EMG signals that we proposed previously is used and compared with the deep learning method. This method named the switched state space models [129] is to identify a system in the state-space form. In this chapter, a whole task is divided into four parts, and each part is treated as a subsystem, as shown in Fig.6.2(c). Therefore, four linear six-inputs and three-outputs continuous time-invariant model Eq.3.3 is applied to map the relationship between the muscle activations and the voluntary motion forces. If taking the whole task as the entirety, it can also be treated as a time-variant system which is similar to the LSTM-based method.

There also needs a process of model training phase to identify the parameters of the state-space model.

The state space model for a given task T_i can be established by identifying the matrices $\{A_i, B_i, C_i\}$, and the initial state x_{0_i} using a model training dataset. These parameters are identified in the continuous-time domain using one of the subspace model identification methods, the canonical variate analysis [115]. The stability of the model is added as a compulsory condition during model identification. In this study, to reduce transient behaviour due to switching, the initial value x_{0_i} for each subsystem T_i is adjusted within the range identified in the training phase. This adjustment can

reduce the discontinuity of the output during switching so as to improve the transient switching dynamics.

6.2.4.3 PCA-based State Space Model

To make a comparison with other approaches, we have applied the dimension reduction method of Panagiotis K. Artemiadis et al. [109] for the development of EMG decoder models in our study shown in Fig.6.2(d). This method is also based on the state space model identification. A PCA redundancy reduction is applied to the inputs (six-channel EMG signals) and the outputs (three-channel forces). The reduction is decided by reconstruction accuracy, which required as 95%. In this chapter, at least four components are needed to reconstruct the EMG, and at least two components are required for reconstructing the forces from the PCA analysis. By using the state-space modelling approach, we establish a second-order (i.e., with two hidden states), four-input two-output model. This method treats the whole task as a time-invariant system and focusing on learning the main contribution parts.

6.2.5 Performance Assessment and Statistical Analysis

To evaluate the performance of the mentioned four models ('LSTMS', 'LSTMT', 'MMSS', 'PCASS'), the model $fitness$, the trajectory tracking error, and the muscle activations were calculated, analysed, and compared.

6.2.5.1 Model Fitness

The target outputs from the joint positions and estimated outputs from the models with the same inputs can be calculated.

The MFE is defined as the gap between the target outputs and estimated outputs. To evaluate the model accuracy, the RMS value of MFE was calculated as Eq.3.4.

Furthermore, the PCC between the targeted and estimated outputs was also calculated according to [117].

6.2.5.2 Trajectory Tracking Results in Online Testing

The desired preset trajectory of the task and the actual trajectories completed by participants were drawn as secondary results for the analysis of the overall performance.

6.2.5.3 Muscle Activation

The muscle activations of the six selected muscles of one subject who was supported by robots in finishing the three kinds of tasks were drawn to show their differences.

6.2.5.4 Statistical Analysis

To visually show the performance differences among different models in training, offline testing, and online testing phases, the mean and SD values of these evaluation parameters were calculated for all seven participants.

To analyse the influence of different models in model fitting accuracy, the difference of the MFE and PCC was evaluated using the Kruskal-Wallis nonparametric test with pairwise multiple comparisons. The significance level of all statistical tests was 0.05. In the online testing phase, only the model that can support all participants to complete the task was compared. Statistical work was performed using SPSS 19.0 (SPSS Inc., USA).

6.3 Results

The full results of the nonparametric tests of MFE and PCC that conducted on the training, offline testing, and online testing performance to compare the four models, are listed in Table.6.1, Table.6.2, and Table.6.3.

Table 6.1 The MFE and PCC values of the LSTMS, LSTMT, MMSS and PCASS models, and their differences in training, offline testing, and online testing of the triangle shape task.

Phase	Output	**MFE (Mean±S.D., N)**				Significance
		LSTMS	LSTMT	MMSS	PCASS	
Training	O1	0.82±0.38	1.31±0.43	0.91±0.46	1.50±0.67	a,c
	O2	0.86±0.66	1.25±0.58	0.63±0.29	2.53±1.42	a,c,d,e,f
	O3	1.04±0.77	2.11±0.58	0.71±0.39	2.88±1.85	a,c,d,f
Offline	O1	0.86±0.35	1.37±0.41	0.93±0.35	1.59±0.44	a,c,d
	O2	0.94±0.74	1.31±0.60	0.63±0.23	2.71±1.17	c,d,f
	O3	1.21±0.85	2.19±0.62	0.72±0.23	2.81±1.29	a,c,d,f
Online	O1	1.95±0.40	2.05±0.82		3.07±0.54	c,e
	O2	2.28±1.20	1.92±0.72		1.56±0.67	
	O3	3.06±1.11	1.99±0.82		3.75±0.98	a,e
Phase	Output	**PCC (Mean±S.D.)**				Significance
		LSTMS	LSTMT	MMSS	PCASS	
Training	O1	0.90±0.10	0.29±0.36	0.86±0.10	0.23±0.45	a,c,d,f
	O2	0.89±0.12	0.61±0.23	0.90±0.08	0.24±0.29	a,c,d,e,f
	O3	0.85±0.15	0.78±0.15	0.80±0.22	0.40±0.33	a,c,d,f
Offline	O1	0.89±0.10	0.28±0.39	0.84±0.09	0.29±0.40	a,c,d,f
	O2	0.85±0.16	0.52±0.28	0.90±0.06	0.15±0.35	a,c,d,f
	O3	0.77±0.24	0.74±0.25	0.86±0.14	0.40±0.33	c,e,f
Online	O1	0.73±0.14	0.07±0.48		0.27±0.45	a,c
	O2	0.81±0.11	0.43±0.22		0.22±0.34	a,c,e
	O3	0.80±0.12	0.77±0.17		-0.35±0.24	c,e

Note: Significant differences between these models are represented by the following alphabets. a: LSTMS-LSTMT, b: LSTMS-MMSS, c: LSTMS-PCASS, d: LSTMT-MMSS, e: LSTMT-PCASS, f: MMSS-PCASS.

Table 6.2 The MFE and PCC values of the LSTMS, LSTMT, MMSS and PCASS models, and their differences in training, offline testing, and online testing of the square shape task.

Phase	Output	**MFE (Mean±S.D., N)**				Significance
		LSTMS	LSTMT	MMSS	PCASS	
Training	O1	0.68±0.29	1.53±0.80	1.12±1.03	1.66±0.48	a,c,f
	O2	1.37±0.70	1.57±0.62	3.48±2.73	6.09±6.37	a,b,c,e
	O3	1.17±0.62	1.71±0.56	1.63±1.14	4.81±4.02	a,c,e,f
Offline	O1	0.68±0.28	1.60±0.91	1.05±0.88	1.49±0.56	a,c
	O2	1.43±0.65	1.59±0.74	3.18±2.80	5.69±5.77	c,e
	O3	1.17±0.60	1.70±0.50	1.46±0.94	4.49±3.63	a,c
Online	O1	1.76±0.53	2.95±1.64		3.26±0.65	c
	O2	3.27±1.02	3.53±1.38		9.85±4.60	c,e
	O3	1.95±1.15	4.15±1.30		11.92±8.31	a,c
Phase	Output	**PCC (Mean±S.D.)**				Significance
		LSTMS	LSTMT	MMSS	PCASS	
Training	O1	0.92±0.09	0.82±0.11	0.79±0.25	-0.06±0.28	a,c,e,f
	O2	0.81±0.15	0.69±0.25	0.29±0.48	0.16±0.23	a,b,c,d,e
	O3	0.73±0.28	0.63±0.37	0.45±0.44	0.03±0.26	a,c,e
Offline	O1	0.93±0.06	0.83±0.11	0.78±0.29	0.13±0.29	a,c,d,f
	O2	0.76±0.19	0.64±0.34	0.35±0.53	0.24±0.20	c,e
	O3	0.70±0.28	0.58±0.34	0.58±0.28	0.12±0.23	c,e
Online	O1	0.80±0.13	0.27±0.37		0.23±0.47	a,c
	O2	0.03±0.32	-0.04±0.36		-0.04±0.28	
	O3	0.43±0.35	-0.23±0.39		0.17±0.12	a,c,e

Note: Significant differences between these models are represented by the following alphabets. a: LSTMS-LSTMT, b: LSTMS-MMSS, c: LSTMS-PCASS, d: LSTMT-MMSS, e: LSTMT-PCASS, f: MMSS-PCASS.

Table 6.3 The MFE and PCC values of the LSTMS, LSTMT, MMSS and PCASS models, and their differences in training, offline testing, and online testing of the circle shape task.

Phase	Output	**MFE (Mean±S.D., N)**				Significance
		LSTMS	LSTMT	MMSS	PCASS	
Training	O1	1.22±0.82	2.14±0.88	1.60±0.89	1.82±0.90	a,c
	O2	1.06±0.71	1.72±0.89	1.42±0.62	3.50±1.60	a,b,c,f
	O3	0.62±0.37	2.49±1.55	0.99±0.42	3.17±1.32	a,b,c,d,f
Offline	O1	1.07±0.57	1.65±0.74	2.52±1.26	2.15±0.72	a,b,c
	O2	1.00±0.49	1.39±0.82	2.05±0.74	3.64±1.52	b,c,d,e
	O3	0.68±0.27	2.11±1.53	1.24±0.34	3.04±1.10	a,b,c
Online	O1	2.12±0.94	3.00±1.74		5.27±1.85	c,e
	O2	2.07±0.94	3.09±1.67		6.05±2.17	c,e
	O3	1.11±0.55	3.54±1.61		8.66±3.09	a,c,e
Phase	Output	**PCC (Mean±S.D.)**				Significance
		LSTMS	LSTMT	MMSS	PCASS	
Training	O1	0.91±0.18	0.53±0.30	0.85±0.10	0.04±0.44	a,b,c,d,e,f
	O2	0.92±0.09	0.52±0.33	0.76±0.18	0.16±0.25	a,b,c,d,e,f
	O3	0.95±0.11	0.84±0.26	0.94±0.04	0.16±0.38	a,b,c,e,f
Offline	O1	0.94±0.09	0.54±0.30	0.78±0.09	-0.02±0.32	a,b,c,f
	O2	0.89±0.07	0.67±0.26	0.62±0.20	0.03±0.30	a,b,c,e
	O3	0.96±0.07	0.87±0.16	0.90±0.05	0.16±0.32	a,b,c,e
Online	O1	0.84±0.23	-0.22±0.29		-0.74±0.14	a,c,e
	O2	0.78±0.11	-0.05±0.46		-0.76±0.19	a,c,e
	O3	0.96±0.04	0.80±0.10		-0.92±0.08	a,c,e

Note: Significant differences between these models are represented by the following alphabets. a: LSTMS-LSTMT, b: LSTMS-MMSS, c: LSTMS-PCASS, d: LSTMT-MMSS, e: LSTMT-PCASS, f: MMSS-PCASS.

6.3.1 Offline Testing Results

As shown in Table.6.1 that contains the results of the triangle task, the smallest RMSE and closest PCC would be found either in LSTMS or MMSS, while both LSTMT and PCASS show relative worse performance in both evaluation parameters.

As shown from the results of a square shape task in Table.6.2, the best model is the LSTMS with notable advantages in both RMSE and PCC. The performance of LSTMT is the best of the rest three models but not that significant.

The results of the circle task as shown in Table.6.3 reveal that LSTMS is the best model for this task, while PCASS is the worst one. The difference between MMSS and LSTMT are not significant in most outputs.

6.3.2 Online Testing Results

The muscle activations of one participant with three different models and three tasks in the online testing phase are shown in Fig.6.4, Fig.6.5, Fig.6.6. When we look at one task, it is clear that there are differences, but the overall trend of each muscle in time-domain is similar even with different assistance from different models. In contrast, when looking at the same models, the trends of different tasks are notably different from each other.

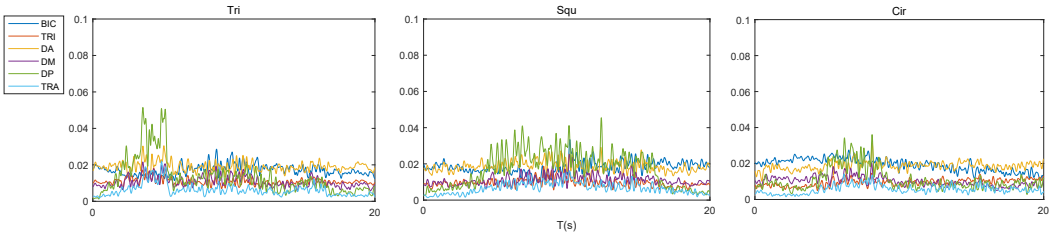

Fig. 6.4 Muscle activities during an online verification movement with robot assistance decoded by LSTMS.

The tracking trajectories of online experiments where one participant completed three tasks with robot assistance estimated by different models are shown in Fig.6.7, Fig.6.8, Fig.6.9. It is clear that the completeness of the circle task is the best among the three tasks, and there is no difference among the three models in this task. There

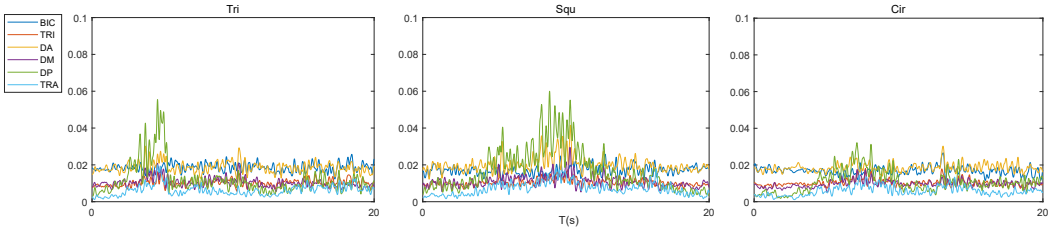

Fig. 6.5 Muscle activities during an online verification movement with robot assistance decoded by LSTMT.

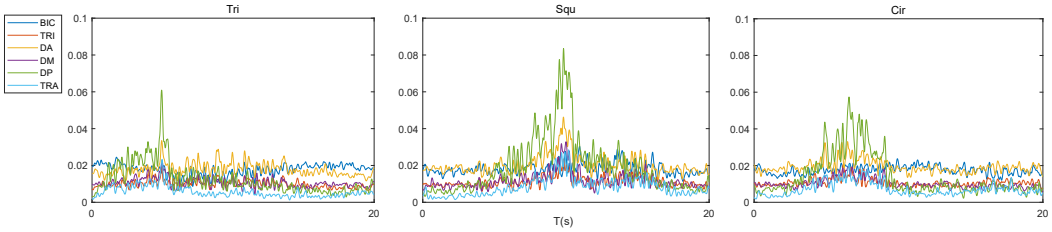

Fig. 6.6 Muscle activities during an online verification movement with robot assistance decoded by PCASS.

are only slight differences among the three models, no matter in triangle and square tasks. Nevertheless, the tracking error in the third dimension is significantly larger than in the two main dimensions of all three tasks. However, it should be pointed out that the results of tracking accuracy are only used to display how successful healthy people deal with different assistance in the same task.

The results of model fitness in online experiments are all listed in Table.6.1, Table.6.2, Table.6.3. Among all three tasks, the values of RMSE of different models show the following order: $LSTMS < LSTMT < PCASS$. In contrast, the order of values of PCC is $LSTMS > LSTMT > PCASS$. As a result, LSTMS is the best model in online experiments.

When comparing the results of different tasks, the PCC values of square tasks in both LSTMS and LSTMT are lower than that of the other two tasks. The difference for PCASS is that the lowest PCC values of this model locate in circle tasks. The values even mean there are negative relationships between estimated forces and target forces.

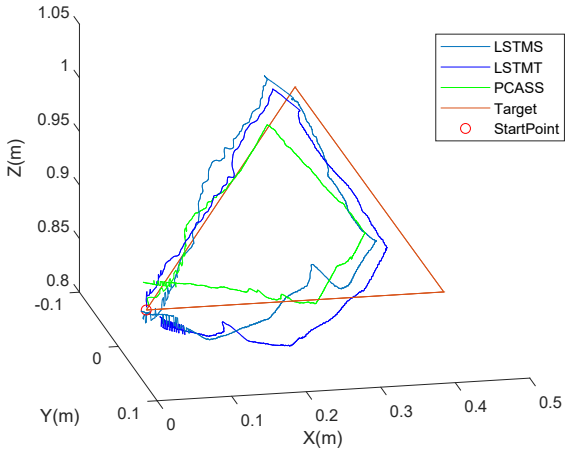

Fig. 6.7 Triangle task trajectories with the three decoders (LSTMS, LSTMS, PCASS).

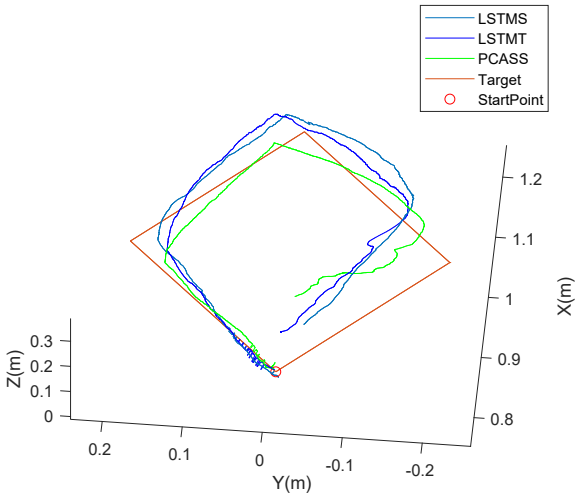

Fig. 6.8 Square task trajectories with the three decoders (LSTMS, LSTMS, PCASS).

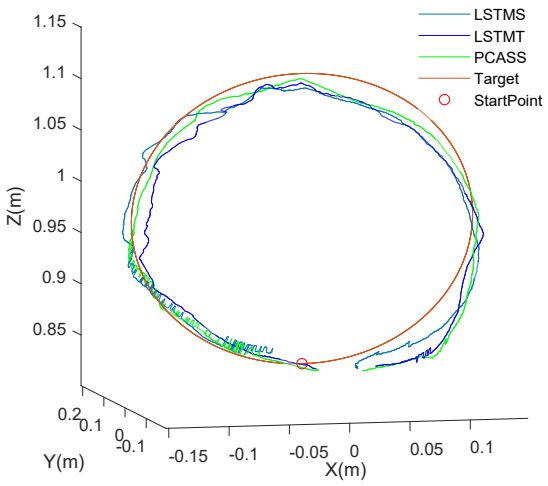

Fig. 6.9 Circle task trajectories with the three decoders (LSTMS, LSTMS, PCASS).

A difference between the performance of LSTMS and LSTMT is that LSTMS mostly shows balanced performance in all three outputs, while LSTMT can well estimate only one or two outputs.

Finally, although we have not applied the MMSS in the online testing, the results of its real-time verification can be found in our previous study [129]. The previous results showed a significant drop was found between the results of offline and online testing, but it would still have general performance. With the good performance of MMSS in most of the tasks during offline testing, we would able to discuss the differences among the four models in the next part.

6.4 Discussions

In this chapter, an LSTM-based method for building an EMG decoder model is proposed and applied in an EMG controlled robotic system with online testing. The performance of two models based on this method was validated and compared to two linear system based decoder models. From the mentioned results in offline testing, the LSTM-based model for a single task has the highest model fitting accuracy and estimation correlation. In contrast, the switched state space model and the LSTM-based model for multiple tasks show slightly worse performance in one or more tasks.

Based on the results of three models in online testing, only the LSTM-based model for a single task keeps a balanced high accuracy and correlation in all three outputs of most tasks. However, from the figures of muscle activations shown in Fig.6.4, Fig.6.5, and Fig.6.6, and tracking trajectories shown in Fig.6.7, Fig.6.8, and Fig.6.9 of online testing, we can only find a subtle difference among the three models. To understand the results, we shall never underestimate the healthy subject's power. Although they were not told about models' differences, these subjects could feel the assistance difference provided by the robot. As reported orally, some assistance supported their movements in tracking while some were no use. Nevertheless, subjects were all able to handle the assistance and controlled the end-effector to complete the tasks as their best. That is to say, it is the healthy muscle function that enables them to complete the task with models that have worse performance. In a nutshell, for clinical application in the future, an EMG decoder model that is precise and accurate in online testing is a fundamental and vital requirement.

EMG signals are superpositions of Motor Unit Action Potentials (MUAPs). Characteristics of EMG signals are impacted by the number of recruited motor units and the firing rate of the MUAPs. To map the complicated relationship between forces for motion and EMG signals is a challenging task, especially in different tasks and different subjects. It is not a posture classification research that needs specific features to be extracted for strong relationships to be found among features and outputs [164, 165]. Motion forces need to be estimated and applied to subjects by robots simultaneously when the EMG signals are collected in every collection interval. In this study, the LSTM-based method, which does not require any secondary characteristic extraction method in time and frequency domain, is different from many related works [166, 91, 83]. The main motivation of this method is to take the relationship between muscle activities and motion forces during a tracking task as a time-varying process. In every time interval of the process, a subject receives the visual stimulation and consciously focuses on narrowing the gap between their hand and the target. We cut off the process into 2000 pieces, which we called subsystems. To build up a model for each subsystem is to identify how the subject's MUAPs are firing and how many motor units are recruited with the same target stimulation. By connecting all subsystems and controlling the overall performance, the whole process shows the potential in

estimating motion forces, which are the terminal outputs of the neural-muscle system during movements. It should be pointed out that, although the idea of the method seems simple and its results are good as expected, the cost of it is the overly complex structure and complicated model parameters.

Comparing the results of different models, we proposed two ideas for applying these methods in a rehabilitation process and fulfilling different requirements. Firstly, the apparent advantages of LSTM-based method are nonnegligible. Its extremely high accuracy and trend prediction in both offline and online tests should be valued. Nevertheless, the cost of training an LSTMS/LSTMT model is tremendous. A similar situation is also reported in research about a nonlinear method of building an EMG decoder to control prosthetic devices and the difference between linear and nonlinear approaches [88]. Cumbersome parameters and lengthy data for build up a large enough database are necessary for deep learning methods. The complex training process and waiting time are indispensable parts of the method. However, strict requirements for the completion of the task always lead to muscle fatigue in healthy people and further challenge its clinical application with patients. From the results of MMSS, we can see that this kind of method which is based on linear systems can achieve a certain accuracy in most complex tasks in the offline testing phase, and maintain a certain degree of accuracy in the online test [129]. It is evident that it is not as good as the LSTM-based method in task universality and robustness. However, the linear system-based method has much lower data volume requirements, modelling complexity, and physical strength requirements than the deep learning-based method.

When comparing these two kinds of methods, it is not difficult to find that the difference between them can cope with the needs in two directions of the rehabilitation training process. In the early stage of robot-assisted rehabilitation, it is impossible to obtain enough data, especially when the number of subjects is limited. Collect the data of the current subject directly, use a linear system method to establish an individual model that is only applicable to the subject, and support the subject with a certain degree of appropriate assistance. This is an excellent solution to assist subjects in regaining their motion abilities. Only until sufficient data are available from a broad range of subjects, the deep learning-based method can be used to build a universal

model suitable for most people and most tasks. The universal model might be useful to fulfil the subject's demand for regaining their motion ability.

In this article, we have no intention to compare the advantages and disadvantages of different methods or decide which is the only way we should use. We tend to explore the applicability and value of different methods in building an EMG decoder to control a robot for rehabilitation purposes. Even nowadays, when learning and big data analysis are so prevalent, we should still pay attention to the excellent contribution that linear systems can make and give full play to their advantages. In this chapter, the PCASS method does not exert its effectiveness in these tasks, but this does not mean the method is not useful. We have tried to apply it in linear tracking tasks, and well performance has been obtained. Similarly, the LSTMT model we built in this chapter does not achieve its function well. Its unbalanced output accuracy may lead to excessive multi-directional force differences in the assistance, which in turn damages the subject. Therefore, it is not applicable to reality at present, but we still regard it as a potential development in the future. On the basis of larger datasets and more sophisticated model design and training, one model that can correctly identify the needs of different subjects in different tasks may be built. More works on testing the time-invariant LSTM-based model in the properness of the dataset size and model overfitting risk are planned. In conclusion, through this chapter, we hope to explore the application of linear system methods and deep learning methods in EMG signals so that different needs can be met and the application value of different methods can be tapped.

6.5 Conclusion

An LSTM-based EMG decoder modelling method was proposed, and its performance was validated by both offline testing and online testing to control an EMG-based rehabilitation robot. Two LSTM-based models were built for decoding EMG signals in a single task and multiple tasks. The model fitness performances of the LSTM-based models were compared to the linear system based models which are a switched state space model and a PCA-based state space model. The LSTM-based model

for a single task outperformed the other three models in both testing phases. The relatively high performance of the switched state space model in the offline testing phase shows its ability in identifying motion intention from EMG signals of individuals. The performance of the LSTM-based model for multiple tasks shows its potential in some outputs and some tasks. Future works would be focusing on how to balance the database size and EMG decoder model selections in different periods of rehabilitation with robot assistance. Furthermore, more forward-looking evidence points to improve the usability of the LSTM-based model for multiple tasks which aims to investigate the EMG decoding insight in various muscle activities thoroughly.

Chapter 7

The Effect of Assistance from an EMG-based Control Robot on Upper Limb Muscle Synergies

7.1 Introduction

Some studies have found that motor commands from the neural system are generated by combining some synergies which represent the activation levels of a group of muscles [167]. This combination allows for the coordinated recruitment of different muscles with specific relative amplitude balances. A common consequence of stroke is the incoordination of motion, which has been clinically characterised as 'abnormal muscle synergies'. This incoordination would appear to be a relatively tight coupling of motion at adjacent joints, due to the co-activation of muscles. The occurrence of covariation in various coupled joints tend, termed as the kinematic synergies, may also result from muscle synergies [168].

Surface EMG signals can respond to users' intentions and have been used for prostheses and rehabilitation robot control [169, 101]. With the growing demand for the application of EMG-based rehabilitation robot control, many researchers have been committed to transforming EMG-based control into clinical and industrial applications [170]. However, since rehabilitation robot control and human-robot

interface applications both require reliable simultaneous control of multiple DoFs robot movements through EMG signals, EMG-based control has been difficult in industrial applications [81]. In the research on real-time EMG-based prosthesis control, the simultaneous pattern recognition controller in tasks with 2 DoFs has significantly enhanced performance [171]. For achieving simultaneous EMG-based control, it is first necessary to identify complex interactions between a group of motion recruited muscles, which is also commonly referred to as the identification and analysis of 'muscle synergy' [47].

Muscle synergy is regarded as a combination of neurophysiological entities and coordinated by the motor cortex area and the afferent system [172]. It is also evidently considered as the low-level discrete elements for the simplification of motor control. The analysis of muscle synergy contributes to learning the nature of motor control and motor learning. Muscle synergy is capable of describing the activation pattern of a group of co-activated muscles during specific tasks. The pattern is specified by a vector containing muscles and their relative activations to each other. It is assumed by studies [173, 174] that each synergy's activation vector is modulated by a single neural command signal from the CNS. A group of muscles related to specific movements would be recruited within one synergy, while different synergies for the same and different movements may contain the same muscle. Therefore, muscle synergies are considered to be used for predicting human arm static postures and movements with multiple DoFs [175]. Using linearly combined muscle synergies to describe motion for motor control problems means that fewer dimensions are needed than those using all muscles' amplitude [176]. Specific to the EMG-based control, muscle synergy is performed by the user as a high-level control input without care of any nervous system source[175]. However, due to the inter-user and intra-user characteristic differences [177] and nonlinearity [110] with the EMG signals, the existing analysis of muscle synergy on robot control problems are quite different. The control schemes proposed based on these analyses are difficult to provide reliable control systems robustly.

Ajiboyel et al. [178] used the Non-negative Matrix Factorisation (NMF) algorithm to extract muscle synergies among a group of eight muscles. The training dataset contains these muscles' activity recordings during 33 static postures. These extracted synergies are reported can predict muscles' activities during 20 new static postures.

Jiang et al. [179] proposed a simultaneous and proportional EMG-based control for wrist movements with two DoFs. This approach NMF to extract control signals (i.e., muscle synergies) with few dimensions from muscle activations of some forearm muscles. Dipietro et al. [180] found that there are significant differences in muscle activation patterns among different reach-to-grasp strategies. The neural command signals from human CNS modulate different muscle activation patterns to both controlling reach-to-grasp movements to different positions and deal with various objects. Berger et al. [181] found that within the three control methods based on force signals, EMG signals, and muscle synergies, there is no difference between the errors of the initial movement direction and the endpoint. This may indicate that muscle synergy for robot control may be an effective strategy.

The analysis based on muscle synergy may reveal the underlying mechanism of the strategy of the nervous system on motor control. The main purpose of this chapter is to explore whether the robot control method based on EMG will affect the nervous system by coordinating the muscles during arm movements in 3D space. The muscle activities are recorded from six upper arm muscles when subjects are performing a tracking task with different assistance conditions. The natural completion means performing tasks without any assistance, and the robot-assisted completion means performing tasks with assistance from a cable-based rehabilitation robot. The provided assistance is estimated from the recorded EMG signals and applied to subjects by a human-robot cooperation strategy. This chapter aims to investigate the possibility of describing a multi-joint multi-directional tracking task for human arms through a linear combination of six upper arm muscle activation patterns. We hypothesised that the results might prove the existence of a modular neural control mechanism for revealing how the CNS controls the movement of the human arm with assistance or not.

The rest of this chapter is organised as follows: In Section 7.2, the system architecture, experiment settings, EMG signal collections and procession, and muscle synergy extraction method are introduced and analysed. Section 7.3 gives the results. Section 7.4 discusses and concludes this chapter.

7.2 Method

The platform was used to provide assistance to participants, as shown in Fig.7.1, and its details are described in Section.2.4.

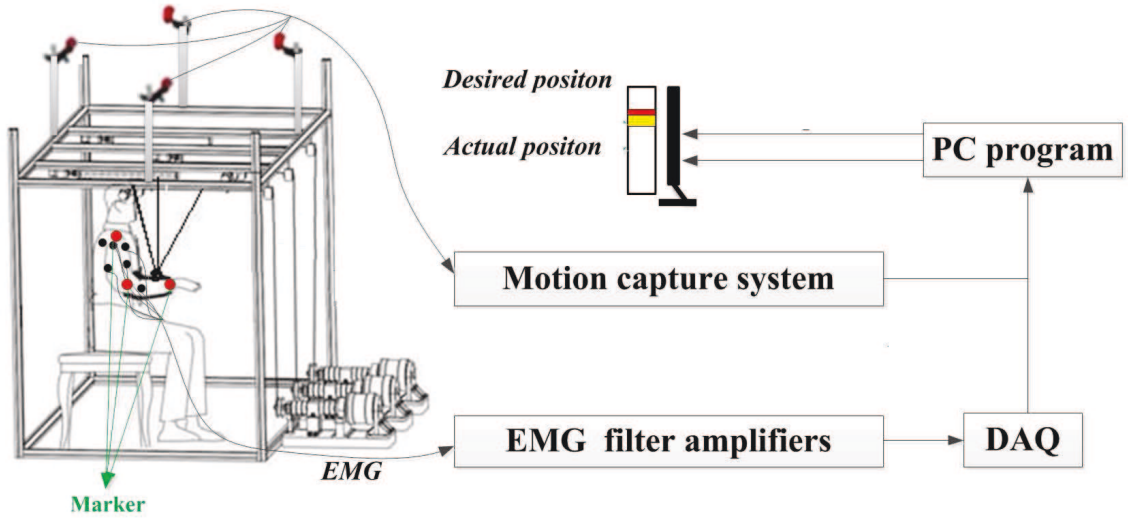

Fig. 7.1 The architecture of the cable-based rehabilitation robot in muscle synergy analysis regarding robot assistance effects.

7.2.1 EMG Signals Collection and Processing

An EMG-based control scheme is proposed to estimate the movement-needed force based on the EMG signals and to assist participants in finishing the tasks [128]. The scheme consists of EMG signal processing and EMG-based human-robot cooperation control strategy.

- EMG signal collection. Based on biomechanics literature [116], a group of six muscles, which mainly contribute to upper limb movements, are recorded by the data acquisition system of the robot from participants: BIC, TRI, DA, DM, DP, and BIC. The paired surface EMG electrodes are used for recording one muscle's activities. The electrodes regarding the six muscles are placed on the specific skin surface of participants following the instructions in [116]. The reference electrodes are placed on the skin surface of the bones area around the joints.

- EMG signal processing. The raw EMG signals are amplified to 5000 times and filtered by a 4th-order Bandpass Butterworth filter ($10 - 400$ Hz). Each muscle's MVC of each participant is tested to be used as the baseline of EMG normalisation. The envelope of each muscle during the MVC test is regarded as the maximal muscle activation. The envelopes of muscle activities during arm movements can be normalised within 0 to 1 relative to the maximal muscle activation. The normalised muscle activity envelopes will be used as a data basis for synergies extraction.

- EMG-to-activation model.For obtaining muscle activations from the processed EMG signals in real-time, an EMG-to-activation model is built based on a model between processed EMG signals and neural activations [111] and a model between the neural activations and the muscle activations [113]. To map muscle activations to the movement-needed force of the upper limb joints in real-time, the EMG decoder model is built based on a three order state space model [128]. The EMG decoder model is embedded in a human-robot cooperation robot control strategy, which can support participants to finish experiments with estimated assistance from the robot.

7.2.2 Muscle Synergy Analysis

Muscle synergy is defined by a vector of relative muscle activation levels among a group of muscles, which is calculated based on the full-wave rectified and normalised EMG envelope curves. For extracting synergies and their activation coefficients from the normalised EMG envelope curves, the NMF algorithm is commonly used. NMF assumes that a muscle activation pattern consists of some muscles during a period is composed of a linear combination of groups of muscle synergies, and these synergies are recruited by a group of coefficients [182]. A muscle synergy represents the relative contributions of the involved muscles in a pattern. In different muscle synergies, the same muscle has different levels of relative contribution.

Under the non-negative constraint condition, the objective function is alternately optimised to find the local optimal solution of the NMF problem [183]. Since the muscle synergy is defined as the relative activation degree of different muscles, each

synergy is considered to be positive. Therefore, the non-negative constraints of BNMF are confirmed and used here. The muscle activation pattern can be regarded as a matrix M:

$$M_j(t) = \sum_{i=1}^{N} h_{ij} \cdot w_i(t) + \epsilon_j(t), \tag{7.1}$$

where M_j is the j-th ($j \in (1, 6)$ normalised EMG envelope, h_{ij} is the time-independent weight of j-th muscle in i-th muscle synergy, $w_i(t)$ is the time-varying basic activation patterns vector for showing the amplitude and duration time of the i-th synergy, N is the number of synergies, and $\epsilon_j(t)$ is the error matrix of j-th muscle in time series.

The detailed extraction of muscle synergy by BNMF is described in the following sections.

7.2.2.1 Construct an Envelope Matrix

The six normalised muscle envelopes (BR, BIC, TRI, DA, DM and DP) which are recorded during participants finishing tasks with and without robot assistance, are arranged in sequence to form an envelope matrix M.

7.2.2.2 BNMF Decomposition

For each synergy, the h_j and w_j matrices are randomly initialised. In the process of alternation optimisation, the method proposed by Paatero [184] is used to alternately update the matrix H and W, respectively, with a squared error as the objective function. After step by step reconstruction, the matrices can be updated by minimising the residual error E_r between the initial envelope matrix M and the reconstructed envelop matrix M_{Re}. The reconstructed envelop matrix is calculated by multiplying the final updated H and W. The termination condition is set by limiting the iteration as 10000 for sufficiently minimise the errors.

7.2.2.3 Quantity of Muscle Synergies

The number of synergies (i.e., N) is determined with the range from 1 to $n-1$ (here it is from 1 to 5). To evaluate the extracted muscle synergies' quality and to determine

the quantity, one commonly used measure is the Variance Accounted For (VAF) metric [185] calculated by Eq.7.2.

$$VAF = 1 - \frac{\sum_{ij} (M - M_{Re})_{ij}^2}{\sum_{ij} M_{ij}^2} \tag{7.2}$$

where M_{Re} is the reconstructed EMG envelops from the final updated H and W, and M is the initial envelope matrix.

The VAF metric is capable of quantifying how much EMG signal variability can be explained by the extracted muscle synergies [186]. A high VAF value indicates a correct reconstruction of the EMG envelopes with enough variability, while a low VAF value suggests that the synergies do not explain most EMG variance [187]. The number of synergies can be chosen as the least number of synergies that could account for greater than 95% of the overall VAF. The threshold setting is the same as the previous study used for assessing upper limb motor dysfunction [188].

In this step, the number of muscle synergies, i.e., the N-value determination conditions is set as: 1) record the N if the average VAF value of each group is over 90% in each muscle; 2) record the N if the sum of the error matrix $\epsilon(t)$ among each group is less than 0.05; by comparing N value from these two conditions and finding the greater one as the number of muscle synergies.

7.2.2.4 Similarity of Muscle Synergies

To examine the similarity of muscle synergies under different conditions, the relationship of extracted muscle synergies was measured by calculating the PCC). For the same participant executing the task under each condition, the relationship between obtained synergies during repeated experiments was tested to confirm what synergies are recruited individually. For different participants, the relationship between several extracted synergies was tested under the same condition to confirm the similarities and differences under this condition. Similarly, the comparison among all extracted muscle synergies under different conditions is to determine the similarities and differences under different conditions. Two muscle synergies from different participants during the same condition,

which can seem like the same one, should have their correlation $PCC > 85\%$. Two muscle synergies from different conditions, which can seem like the same one, should have their correlation $PCC > 90\%$.

7.2.3 Experiment

7.2.3.1 Data Processing

Three infrared reflection markers are attached to the skin surface of the centre of the shoulder, the elbow, and the wrist. The EMG signals and position signals are recorded simultaneously.

7.2.3.2 Participants

Twelve healthy participants (six women and six men, mean age 24.75 ± 0.92 yrs) with no experience with this robot were invited to join this study after providing written informed consent. All participants were able to lift their upper limbs with right-handed and declared that they have no health issue. All participants provided their informed consent before participating in this study. The human ethics committee approved all experimental procedures at Sun Yat-sen University.

7.2.3.3 Procedure

Participants were seated at a chair and were softly tied to decrease extra compensation from the trunk. Each participant went through three rounds of tracking the moving marker shown on the screen. The marker moves in a square trajectory for a total of 20 seconds (each rectilinear movement moves for 5 seconds). During the first round, which was the modelling round, the robot offered no assistance to participants. The muscle activations and motion-needed forces calculated by the arm dynamic model were used to identify the parameters of the state space model after this round. During the second round, participants were asked to finish tracking movements naturally without the robot. For the third round, participants were assisted by the robot with

the EMG-based control. Every round required the participant to execute six trials consecutively.

7.2.4 Envelop Evaluation and Statistical Analysis

To evaluate the performance of the two groups, EMG envelop analysis for the task and mean muscle activations during the natural and robot-assisted movements are calculated and compared.

EMG envelops for four rectilinear movements of the task are analysed for each participant. Furthermore, the mean muscle activations of the six muscles are used to evaluate the muscular effort during the four rectilinear movements in both groups.

The similarity and difference between the two conditions are evaluated by correlation analysis to analyse whether the assistance from the EMG-based controlled robot affects the neural control mechanism on the same arm tracking task. The comparisons of EMG envelop of each muscle between two conditions are analysed by the pair-T test with consideration of the individual difference of EMG signals. A significance level of 0.05 is set for all statistical tests. The statistical work is conducted with SPSS 19.0 (SPSS Inc., USA).

7.3 Result

7.3.1 Muscle Excitation Level

The EMG activities of natural and robot-assisted movements during the whole task in all six muscles are shown in Fig.7.2. The EMG envelops' waveforms of this task show similar increasing tendency like other horizontal arm movements in previous studies [189]. The amplitudes of the BIC and BR activities are higher in natural movements than that in robot-assisted movements in this example. For other muscles, no significant difference between the two movements is found. Among the four stages, the activities of all six muscles shown different trends, but there is no significant difference among the averages of the activity in all stages during both movements shown in Fig.7.3.

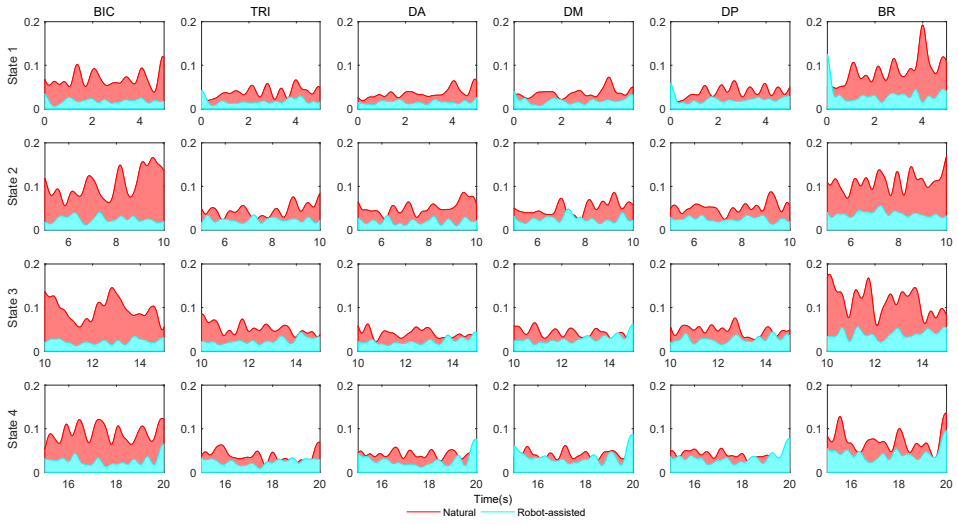

Fig. 7.2 Muscle activity for six muscles from left to right during different stages of the whole task. The red and blue represent the modelling and verifying phase, respectively. The activities of the two phases were superimposed by each other.

7.3.2 Quantity of Muscle Synergy

According to the definition of synergistic quantity, eleven participants of the twelve healthy participants had two muscle synergies, and one participant had three synergies during the natural movements. Relatively, ten participants had two muscle synergies, and two participants had three synergies during the robot-assisted movements.

7.3.3 Natural Movements

Among the muscle synergies extracted by all twelve participants, the muscle synergy NSYN1 was found in six participants, the muscle synergy NSYN2 was found in five participants, and the muscle synergy NSYN3 and NSYN4 were found in four participants. Six muscle synergies (NSYN5, NSYN6, NSYN7, NSYN8, NSYN9, NSYN10) were unique. NSYN5 and NSYN7 were from one participant, and NSYN8 and NSYN9 were from one participant, and NSYN6 and NSYN10 were from two participants, respectively. Therefore, NSYN1 was found to be the most common muscle synergy during the natural arm tracking movements. The results are shown in Fig.7.4(1).

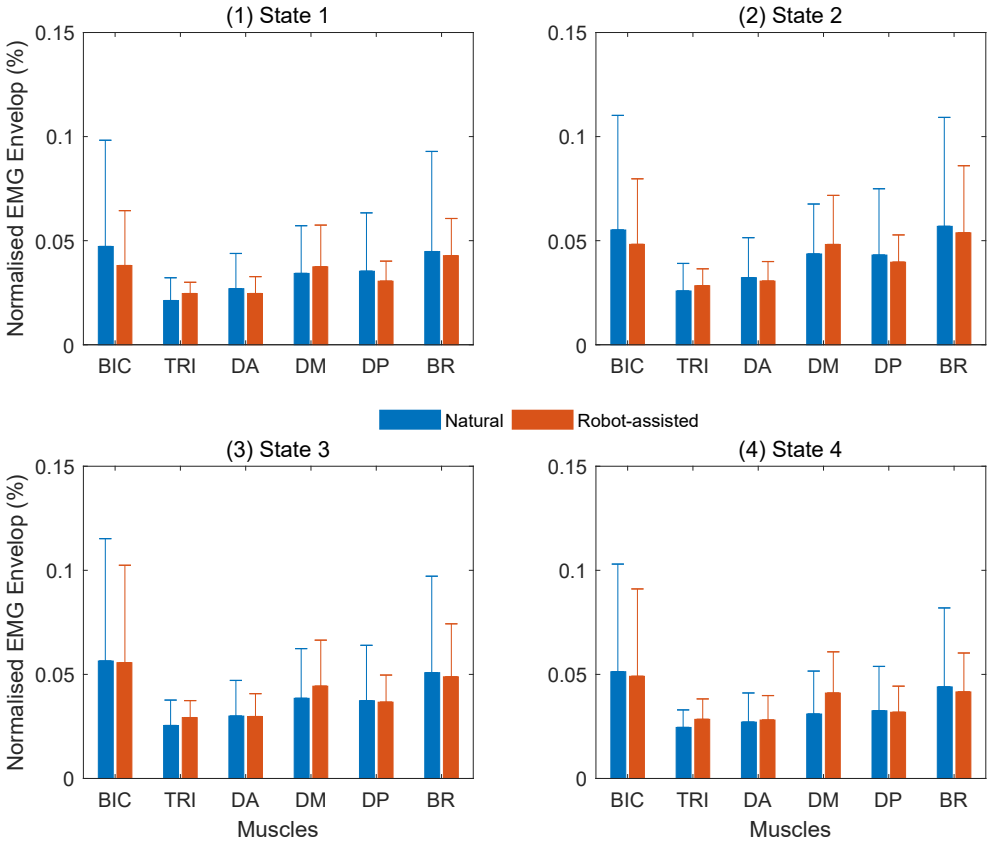

Fig. 7.3 The average muscle excitation in different stages and movements.

7.3.4 Movements with Robot Assistance

Among the twelve participants, the muscle synergy RSYN1 was found in eight participants, the muscle synergies RSYN2 and RSYN3 were found in five participants, the muscle synergies RSYN4, RSYN5, and RSYN6 were found in two participants. The muscle synergies RSYN7, RSYN8, and RSYN9 were unique from three different participants, respectively. Therefore, RSYN1 was found to be the most common muscle synergy during the robot-assisted arm tracking movements. The results are shown in Fig.7.4(2).

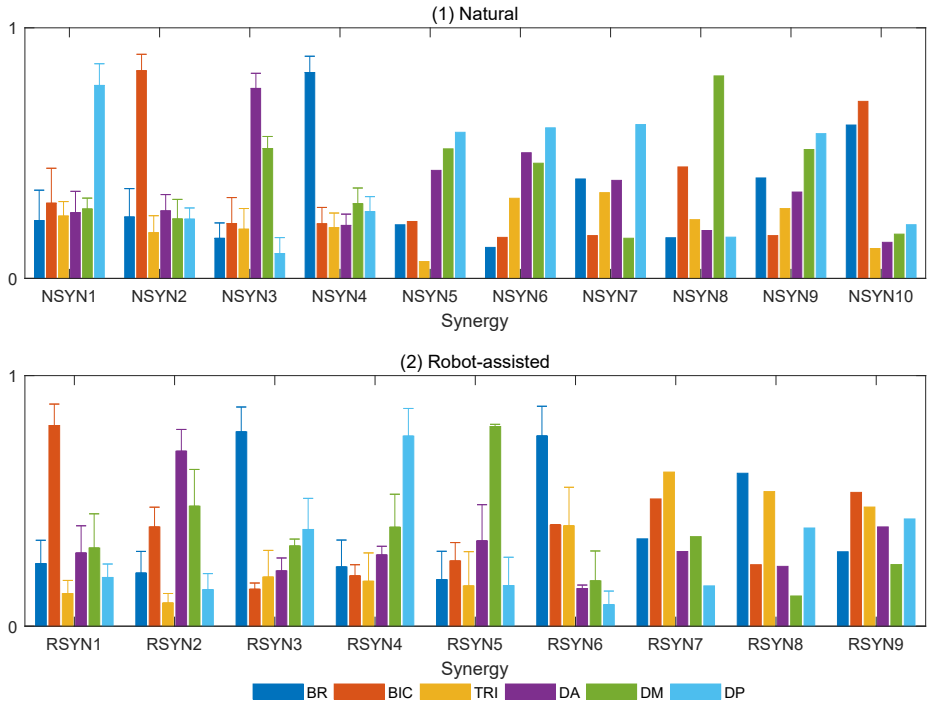

Fig. 7.4 The muscle synergies of two conditions.

7.3.5 Common Muscle Synergy with/without Robot Assistance

By comparing all calculated muscle synergy correlations, there were significant correlations ($PCC > 90\%$) found between five pairs of synergies from two conditions, i.e., NSYN1-RSYN4, NSYN2-RSYN1, NSYN3-RSYN2, NSYN4-RSYN3, and NSYN8-

RSYN5. Most of these muscle synergies were the common muscle synergies under different assistance conditions, and details are shown in Table.7.1.

Table 7.1 PCC between natural and robot assisted conditions.

	RSYN1	RSYN2	RSYN3	RSYN4	RSYN5
NSYN1	-18.38%	-35.69%	1.47%	**93.69%**	-26.65%
NSYN2	**98.09%**	20.90%	-38.08%	-29.20%	-8.51%
NSYN3	-0.07%	**91.98%**	-33.43%	-19.84%	58.95%
NSYN4	-18.38%	-25.96%	**96.15%**	-13.98%	-15.82%
NSYN8	34.51%	34.10%	-27.96%	-6.67%	**90.35%**

The five common synergies between two conditions are shown in Fig.7.5. By observing the experimental results, movements with different conditions have similar similarities in the relative activation of different muscles. The difference among these common synergies mainly lies in the relative activation level of the primary muscle, i.e., the DP of NSYN1(6)-RSYN4(2), the BIC of NSYN2(5)-RSYN1(8), the DA of NSYN3(4)-RSYN2(5), the BR of NSYN4(4)-RSYN3(5), and the DM of NSYN8(1)-RSYN5(2). The number in brackets is the number of participants who recruit this synergy during the movements. Overall, DA, DP, and BIC, BR, the four major contributors to upper extremity muscle activation based on the synergies.

7.4 Discussion

The human-robot cooperation control strategy based on EMG signals is realised based on a state space modelled EMG decoder. The control strategy tried to simultaneously control a cable-based upper limb rehabilitation robot to assist participants in finishing a multi-joint multi-directional arm tracking task. The muscle synergies are analysed when participants are finishing the square-shaped horizontal tracking task. Two assistance conditions during the task are designed to validate whether robot assistance would affect what muscle synergies as motor control indicators from the CNS to muscles are recruited. The similarity synergies between natural and robot-assisted movements show that the robot with the human-robot cooperation control strategy can assist participants in their arm movements without affecting the contribution of major muscle groups.

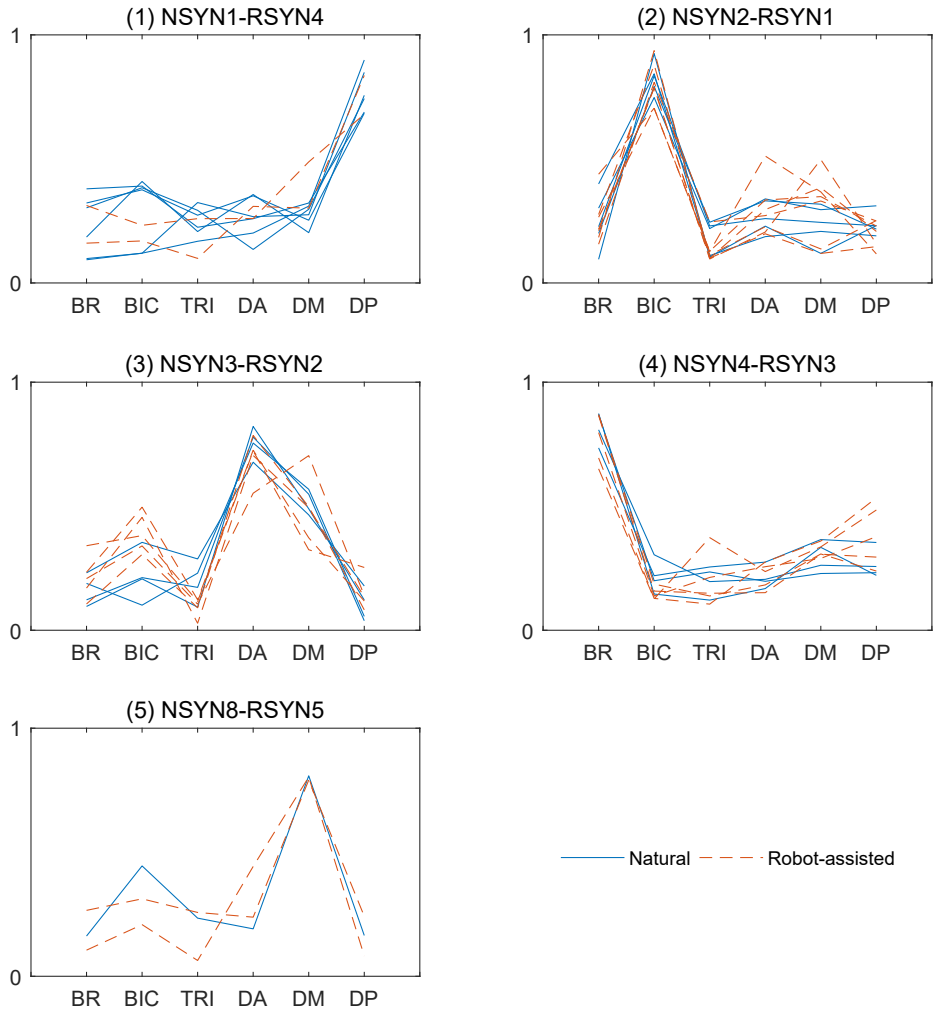

Fig. 7.5 Common muscle synergies of the natural and robot-assisted movements.

In addition to the same muscle synergy, there are still several muscle synergies without significant similarity. The reasons for this may be: 1) Participants actually recruit more muscles except for the recorded six muscles. The six upper limb muscles selected in this chapter mainly cover the upper extremities and are mostly used to control the movement of the elbow and some of the shoulder joints. The performance of four muscles as major contributors are relatively consistent with the previous studies (DA, DP in [189] and BR, BIC of elbow flexor synergy in [190]). However, in the actual multi-directional movements, shoulder replacement exercise is common in the control of the upper limbs. Therefore, more muscles mainly contribute to shoulder movement but are not recruited in this study. The situation leads to the problem of muscle synergy incompleteness; 2) The impact of the number and choice of muscles on synergy analyses [191]. It may be related to whether participants have finished the movements ideally as experimenters required. Different neurologic indicators can instruct the same kinematic performance. 3) There are significant individual differences in healthy participants due to personal muscle strength and muscle control during exercise [177].

7.5 Conclusion

This chapter explores whether robot assistance from a cable-based robot with the EMG-based human-robot cooperation control strategy influences the nervous system's motor control strategy. The analysis of muscle synergies for arm movements finished naturally and with robot-assistance is completed to investigate the differences and similarities. The results revealed that the same muscles provide the major muscular contribution, and groups of the same synergies are recruited under both conditions. It is indicated that the robot with the myoelectric control strategy could provide physiologically appropriate assistance to the participant without affecting natural instructions from the neural system. It may be predictable that this myoelectric control strategy is capable of controlling a rehabilitation robot to provide proper assistance to patients without influencing their own voluntary residual motor efforts in rehabilitation. Clinical tests will be conducted to verify the feasibility of this EMG-based human-robot cooperation control strategy.

Chapter 8

The Effects of Different Tracking Tasks on Muscle Synergy through Visual Feedback

8.1 Introduction

A typical hypothesis for movement generation is the existence of muscle synergy which is recruiting a set of muscles in performing activities at different relative levels by the CNS [192]. The muscle synergies during a task are combined by both shared and task-specific synergies with the indication from the motor cortical areas and the afferent systems [172]. The synergy theory facilitates in both motor control and motor learning by contributing in exploration about how the motor system constructing a large set of movements.

The muscle synergies as putative modules of muscle system are typically identified and extracted from EMG signals by dimensionality reduction algorithms such as NMF [193]. The purpose of any algorithms for the procedure is improving the accuracy of the modular decompositions for reconstructing the EMG data. Most of the previous researches try to explore what kinds of task-specific muscle synergies are indicated during vast tasks and contribute to motion classification and motion analysis [194, 195]. The task complexity in [194, 195] is relatively singular (e.g. one direction rectilinear

motion) because of the muscle synergies need to be extracted within a period of time. Whether muscle synergies of a complex task can be extracted with high accuracy needs to be explored. For active rehabilitation, when participants complete tasks through virtual interactions, whether their efforts on improving task competition will affect the neural system in controlling movements is unclear.

For these reasons, in this study, three complex tracking tasks together with visual interaction are designed. The BNMF with an extra initial estimation is applied to extract primary muscle synergies from grouping processed EMG recordings during these tasks. The main purpose of this chapter is to identify the effects on muscle synergy for these designed tasks. Both task variety (TV) and tracking accuracy (TA) by visual feedback are considered for evaluating their effects by statistic analysis. The results of this study indicate that only the TV affected the synergies adopted by the neural system, but both TV and TA affected the durations and magnitudes of the primary synergies.

8.2 Method

8.2.1 Experiment Design

Three target movements with different shapes (Triangle, Square and Circle) in different dimensions are designed as shown in Fig.8.1. The target movements are coding into a cursor's moving trajectories. The target cursor moves in a two-dimensional surface as displayed in a screen for providing a continuous visual stimulation. The actual position of the wrist is also displayed as a cursor. Intuitively, when the participant is executing a task, he receives two different visual effects. One is the target cursor's trajectory which is defined as the TV, and the other one is the gap between the target and actual cursors which is defined as the TA by visual feedback. The TV has three values corresponding to different tasks. The level of TA is processed later.

The start position of every task is the same. The length of the long side of the isosceles triangle is $0.2m$, and the short sides are $\sqrt{0.2}m$. The length of the square sides is $\sqrt{0.2}m$. The radius of the circle is $0.1m$. The duration time of every task is 20

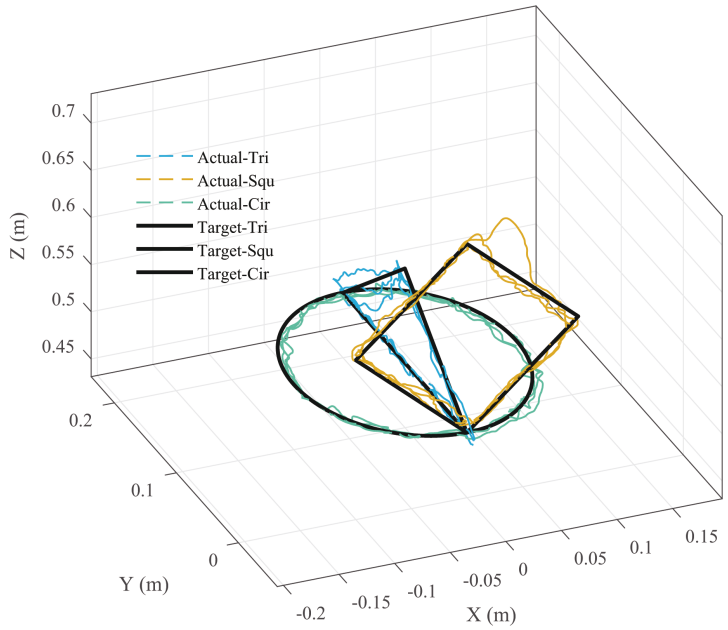

Fig. 8.1 The trajectories of three target tasks and actual tracking movements. Tri: Triangle, Squ: Square, Cir: Circle.

seconds, and the cursor moves with constant velocity during each task. All three tasks are required to finish three times as three trails.

8.2.2 Data Acquisition and Processing

One healthy female is recruited and signed the written informed consent form with approvement from the Human Ethics Committee of Sun Yat-sen University. The raw EMG signals are bandpass filtered ($10 - 400$ Hz), full-wave rectified, and Butterworth low-pass filtered (20 Hz cutoff) into EMG envelops. The EMG envelops were down-sampled for synchronising.

For accurately extracting the muscle synergies, the down-sampled EMG envelops during every tracking task are separated into 40 samples. For each sample, there is a total of 50 EMG envelop data points of each muscle for 0.5 seconds. Similarly, the Average (AVG), SD and RMS values of TA in two main dimensions (D_1, D_2) during each sample is calculated. For the level of TA during the whole task, the TA in D_1, D_2 and their square root (D_{12}, i.e. the linear gap between two cursors) are grouped into 17

levels with evenly spaced. Similarly, the level of TA of all envelop samples, the AVG, STD and RMS of TA in D_1, D_2 are grouped.

8.2.3 Muscle Synergy Extraction

The muscle synergies during every EMG envelops sample are extracted by BNMF algorithm from the EMG envelop samples as follows [47, 196] in Eq.7.1:

For choosing the minimum number of muscle synergies and selecting the most precise synergies and their patterns, the root-mean-square residual (D) between the original EMG envelopes and the reconstructed EMG envelopes ($M_{Re} = H \times W$) is used for evaluation. The value of D is required as smaller than 10^{-4} [47]. The VAF is used to evaluate how accurate the algorithm is [195, 190]. The VAF is calculated as Eq.7.2, and is required as larger than 99.95%.

During the synergy extraction, the residual and VAF values of the repeated multiplicative BNMF algorithm with random initial estimation show high variance. Therefore, an initial estimation of synergies and their patterns are found by using the multiplicative algorithm ($Iiterations = 10, replicate = 10$). With the initial estimation, the alternating least squares algorithm can rapidly estimate synergies and their patterns with better parameters' performance without high variance [197].

The number of extracted synergies of a task is constrained by the mean values of both D and VAF during all samples. The synergies of different samples are compared by using PCC for similarity. Only those synergies with PCC values higher than 85% are regarded the same. The mean values of the same synergies are defined as the primary synergies.

8.2.4 Statistic Analysis

The effects of the TV values and the levels of AVG, SD and RMS of TA in two main dimensions on the primary muscle synergies (H) are analysed by two-way ANOVA statistic test in sample orders. Similarly, the effects of the TV values and the levels of

TA in D_1, D_2 and D_{12} on the activation patterns of primary muscle synergies (W) are analysed by two-way ANOVA statistic test in time series.

8.3 Results and Discussion

8.3.1 BNMF with the Advanced Procedure

The results of D and VAF (Fig.8.2) showed that the advanced procedure of BNMF for extracting muscle synergy could improve the estimation accuracy. Therefore, the extraction standard can only be applied for selecting the synergy number after using the BNMF with the initial estimation.

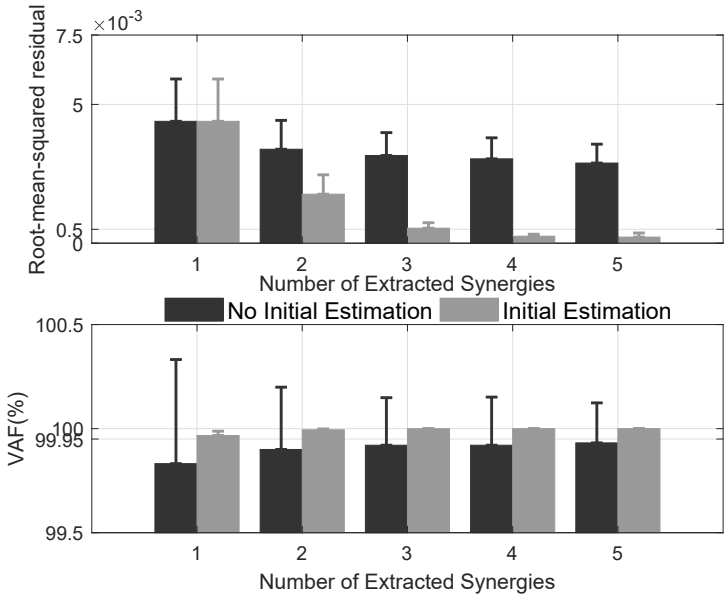

Fig. 8.2 The root-mean-squared residual and VAF of BNMF without or with initial estimation for extracting synergies.

8.3.2 Muscle Synergies and Patterns

The primary muscle synergies and their activation patterns during the first 5 seconds of a trail of triangle task is shown in Fig.8.3 as an example. The number of muscle synergies was nine of all 120 samples but only four synergies were extracted in each

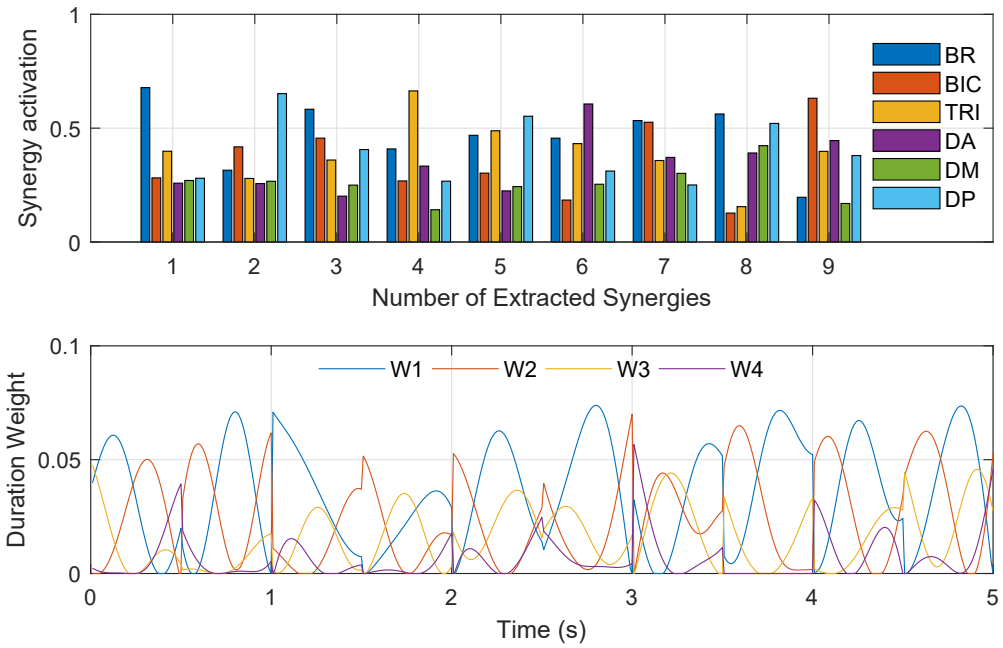

Fig. 8.3 Muscle synergies and basic activation patterns (W1-4).

example of this task. The first and second synergies were found in over 90 samples, and the third and fourth were found in over 50 samples. The rest synergies were found in no more than 20 samples. For the basic activation patterns, the four lines were for the primary synergies of each sample. The results can be supported by Delis et al. in task discrimination objectives by synergy difference [195].

8.3.3 Effects on Muscle Synergy

The effects of the TV and the TA by visual feedback on the primary muscle synergies and their basic activation patterns are summarised in Table.8.1. In the Table.8.1, the D_1, D_2, D_{12} are the TA in the two main dimensions and their square root, and the AVG, SD and RMS are the average, standard deviation and root mean square of TA.

The TV highly affected primary muscle synergies. For the combined elbow synergies, the AVG and RMS of TA levels in the D_1 dimension also affected what kind of synergies is indicated by the CNS system. Both the TV and TA in D_1, D_2 and D_{12} affected the basic activation patterns of those primary muscle synergies. It indicated that no

matter what primary synergies were indicated, the onset, offset and duration of the most important synergies changed with different tasks and the varying gap between actual and target positions [119].

Table 8.1 Effects of TV and TA on Muscle synergies (H) and patterns (W).

H	**TV**	D_1			D_2		
		AVG	SD	RMS	AVG	SD	RMS
M1-6	< 0.05						
M_E	< 0.05	0.05		< 0.05			
M_S	0.05						
W	**TV**	D_1	D_2	D_{12}	**Effects Order**		
W1	< 0.001	< 0.001	< 0.001	< 0.001	$TV < D_2 < D_1 < D_{12}$		
W2	< 0.001	< 0.001	< 0.001	< 0.001	$TV < D_1 \approx D_2 < D_{12}$		
W3	< 0.001	< 0.001	< 0.001	< 0.001	$TV < D_1 < D_2 < D_{12}$		
W4 *	< 0.001	< 0.001	< 0.001	< 0.001	$TV < D_1 < D_{12} < D_2$		
W5 *	< 0.001	0.003	< 0.001	< 0.001	$TV < D_1 < D_{12} < D_2$		

Note: '*' means the duration W is not full rank because the number of extracted synergies is from three to five. $M1-6$ means the synergy of all six muscles. M_E and M_S are synergy values of the elbow muscles (BIC, TRI and BR) and the shoulder muscles (DA, DM and DP).

8.4 Conclusions

This chapter attempts to demonstrate the effects of TV and the TA by visual feedback on muscle synergy and their activation patterns. The statistic analysis showed that the muscle synergies are highly related TV but their durations and activations are affected by both TV and TA. For further study, the results may suggest that during early rehabilitation for patients with neural system injury, it is essential to provide diversity tasks for evacuating different synergies to be utilised, but during later rehabilitation, the accuracy of visual tracking feedback should be advised to reach high accuracy tracking motion for acquiring synergies similar to healthy people.

Chapter 9

Conclusions and Future Work

9.1 Conclusions

In this section, we first summarise the significance of the four proposed EMG decoders and their contributions to robot-assisted rehabilitation. The contributions of the muscle synergy analysis of the robot assistance effect and task effect are also summarised. Finally, we conclude the dissertation. The main contributions of the four proposed EMG decoders are as follows:

An EMG decoder named the switching decoder including a switching mechanism together with LTI state space submodels is innovatively proposed to decode EMG signals during complex arm movements. This decoder can investigate the relationship between multiple EMG signals and multiple motion-needed forces without any dimension-reduction techniques. With the switching mechanism, several simple submodels with low order are capable of dealing with the system variation for complicated movements, because the mechanism reduces the model complexity. The decoder with the direct switching mechanism and submodels can predict the voluntary motion intention with high accuracy from multiple-channel EMG signals. With the EMG decoder, a human-robot cooperation control strategy is designed to control a cable-based upper limb rehabilitation robot. The robot with the control strategy is able to help users to finish multi-joint arm movements with lower muscle effort and higher task completion rates.

A bumpless switching mechanism for ensuring the outputs' continuity when switching among submodels is creatively proposed. With this bumpless switching mechanism, an EMG decoder named the bumpless decoder is developed. Both the bumpless switching mechanism and the direct switching mechanism carve up a complex task into several simple subtasks which are treated by simple state-space models individually. Both the bumpless decoder and the switching decoder have equal degrees of accuracy in decoding EMG signals to motion needed forces because their submodels have high efficacy. In contrast to the switching decoder, the bumpless decoder has significant smoother estimation and a continuous hidden state when switching among submodels. The bumpless switching mechanism is realised by constructing a multirealisation for submodels with the same order, which is firstly proposed and applied in the rehabilitation robot control field. This mechanism can be applied in a natural manner without any kinematic or dynamic constraints. The bumpless decoder has the potential to be applied in clinical robot-assisted rehabilitation because the robot assistance to patients occurs smoothly without the safety risks caused by 'bump' behaviour.

Based on the bumpless switching mechanism, a general multirealisation is first proposed to realise a general bumpless switching mechanism for submodels with different orders. A novel order transformation method which aims to reform submodels into a common order without affecting model accuracy is developed to form the general multirealisation. A general decoder constructed by the general bumpless switching mechanism and different-ordered submodels is applied and evaluated by robot-assisted movements. Like the bumpless decoder, the general decoder can decode EMG signals to motion needed forces smoothly and accurately. The difference between the two decoders is the mechanisms and the submodels' order. The general decoder is not limited by order selection because the general multirealisation is realised by individually giving the initial state of each submodel without considering its continuity. Having investigated the effect of the initial state on the whole system, we see the proposed order transformation method can both maintain the EMG decoder's accuracy and allocate the fittest initial state to every different-ordered submodel. This general decoder can effectively decode the motion needed forces from the EMG signals with high accuracy and smoothness, and it has a broader application in clinical rehabilitation.

The three proposed decoders are all constructed by a switching mechanism and several submodels based on the linear system method, i.e. the state space modelling method. The submodels are only used to decode EMG signals in a specific stage of a complex task for rehabilitation. These submodels can be trained easily and quickly with limited training data while they are built up for each subject and each task. Combined with a well-designed switching mechanism, the decoders perform very well both on the model fitting error and the correlation coefficient. The bumpless decoder and general decoder diminish 'bump' behaviour during submodel switching, while also having a range of scope in clinical rehabilitation.

An LSTM-based EMG decoder modelling method is creatively proposed to deal with modelling problems related to subject-dependent EMG characteristics. The method is motivated by the requirement of real-time robot control in rehabilitation and the function of the LSTM network and time-variant system. The LSTM-based method can be used to build a decoder with good estimation performance for a single task, which means the decoder is subject-independent as designed. After using the method to decode EMG signals in multiple tasks, the decoder performed well in estimation during offline testing. It also displayed great potential in realising an omnipotent decoder with task-independence and subject-independence. Furthermore, more forward-looking evidence reveals that improving the usability of one EMG decoder for multiple tasks may contribute to a thorough investigation of the decoder's nature in various muscle activities.

Since the performance of all decoders were validated by both offline testing and online testing to control an EMG-based rehabilitation robot, the comparison of these decoders is outlined as follows:

- The advantage of a linear system is that there are fewer data requirements and higher degrees of accuracy.
- The linear system-based method may be suitable for early-stage patients who have limited motion function and need to enhance their motion controllability.
- The advantage of the nonlinear system-based method, i.e., the LSTM-based method, is that it deals with the EMG differences between subjects and tasks.

- The nonlinear system-based method can improve the modelling efficiency for patients with similar motor abilities and similar rehabilitation aims.
- The nonlinear system-based method may be suitable for post-stage patients who have regained most of their motion function and need to enlarge their motion area by random tasks.

With these different EMG decoder models, a better fitting model can decode EMG signals when applying them in different shapes of arm tracking tasks. For a single task with a simple trajectory in one dimension, one state-space model has displayed satisfying results. A switched system state-space model has shown an approval decoding performance for a single task with a complex trajectory in more than two dimensions. For multiple tasks that need to be finished within one visit, the time-variant LSTM method has a high potential to be applied, especially when there are various subjects and enough data.

To explore whether robot assistance influences human motor control, we analysed and compared muscle synergies during robot-assisted motion and natural arm motion. The results proved that with appropriate robot assistance during arm motion, users' motor control systems can recruit the same muscle synergies as those during natural motion. It indicates that a robot that could conduct tasks alongside human voluntary motor effort is a crucial part of robot-assisted rehabilitation. Simultaneously, this muscle synergy analysis of the robot assistance effect proves that the proposed human-robot cooperation EMG-based control strategy is efficient without changing the user's manner of motor control.

To demonstrate the effects of task variety and the tracking accuracy by visual feedback on muscle synergy and their activation patterns, we statistically analysed their correlations. The muscle synergies are highly related to task variety. The duration and activation of synergies are affected by both task variety and tracking accuracy. The results suggest that during early rehabilitation for patients with neural system injury, it is essential to provide a diversity of tasks for evaluating different synergies. Moreover, during later rehabilitation stages, the tasks should be finished with high accuracy for the purpose of acquiring synergies that are similar to healthy people.

In conclusion, the proposed decoders based on linear system and nonlinear system methods have a range of application. All of these decoders can be applied in the area of rehabilitation robot control. With the synergy analysis on task tracking accuracy and task variety, the proposed decoders can satisfy different requirements and applications in various stages of rehabilitation. The cable-based robot with the EMG-based control strategy based on these newly proposed EMG decoders can continuously help users during multi-joint movements. Indeed, the synergy analysis revealed that the assistance provided by this cable-base robot with an EMG-based control strategy would not affect the user's own manner of motor control. At the same time, all EMG decoders show high potential to provide users with safe, smooth, and accurate assistance during repetitive exercise.

9.2 Future Work

There are many areas that can still be explored based on our current project.

- In Chapters 4 and 5, it was shown that these newly proposed EMG decoder models can be generalised to other multi-joint rehabilitation robots for patients who suffer from neurological diseases, such as stroke and cerebral palsy. As the next step, we aim to apply the proposed method to young patients (20-30 yrs) who have had a stroke in the previous year but they perform high scores in basic motion ability assessments after passive rehabilitation. In addition, these patients must be able to sit on a chair for at least 30 minutes and hold their affected arms for at least 1 minute.

- In Chapter 6, to achieve better clinical application, a more extensive and balanced dataset for training the LSTM-based decoder is needed for subjects of both sexes who have different motor ability levels, tasks, ages, and handedness. With a more complicated network based on the time-variant LSTM-based method, the motion intention included in EMG signals can be revealed and used for the purpose of indicating to the robots. For improvements in modelling efficiency, works could also focus on how to balance the database size and model selections in different

periods of rehabilitation. More works on testing the time-invariant LSTM-based model in the properness of the dataset size and model overfitting risk are planned.

- In Chapter 7, based on the EMG decoders and muscle synergy analysis, it was found that the intention analysis method was highly related to the rehabilitation tasks, and we all know the importance of completing several tasks during a rehabilitation program. How then do we solve the problem of transfer control systems when the tasks change within a program? In the future, it would be useful to integrate the kinetics signals, kinematics and, EMG signals as a variable and to design a scheme for selecting a fit control system during different tasks. It is also important to explore, verify and deepen the understanding of how muscle synergy performs with robot assistance from different EMG decoders.

- Another prospective area for exploration is to design a therapeutic program that can meet the requirements of an 'assist-as-needed' rehabilitation theory. Users' control efficacy and movement quality in each program stage can be evaluated and used as 'no ceiling' scaled criteria and the feedback components for automatically choosing adequate tasks. Furthermore, to realise a smooth transfer between control systems of different programs and different tasks is an important goal.

All of this information could be productively explored in future works of rehabilitation robot control strategy based on the results of this doctoral research.

References

[1] N. Hogan, H. I. Krebs, A. Sharon, and J. Charnnarong, "Interactive robotic therapist," Nov. 14 1995. US Patent 5,466,213.

[2] D. J. Reinkensmeyer, L. E. Kahn, M. Averbuch, A. McKenna-Cole, *et al.*, "Understanding and treating arm movement impairment after chronic brain injury: progress with the arm guide," *Journal of rehabilitation research and development*, vol. 37, no. 6, p. 653, 2000.

[3] J. E. Speich and J. Rosen, "Medical robotics," *Encyclopedia of biomaterials and biomedical engineering*, vol. 983, p. 993, 2004.

[4] T. Nef, M. Mihelj, and R. Riener, "Armin: a robot for patient-cooperative arm therapy," *Medical & biological engineering & computing*, vol. 45, no. 9, pp. 887–900, 2007.

[5] R. Beer, D. Mayhew, C. Bredfeldt, and B. Bachrach, "Technical evaluation of the macarm: A cable robot for upper limb neurorehabilitation," in *2008 2nd IEEE RAS & EMBS International Conference on Biomedical Robotics and Biomechatronics*, pp. 942–947, IEEE, 2008.

[6] C. Fanin, P. Gallina, A. Rossi, U. Zanatta, and S. Masiero, "Nerebot: a wire-based robot for neurorehabilitation," in *ICORR'03*, pp. 23–27, HWRS-ERC, 2003.

[7] G. Rosati, P. Gallina, S. Masiero, and A. Rossi, "Design of a new 5 dof wire-based robot for rehabilitation," in *9th International Conference on Rehabilitation Robotics, 2005. ICORR 2005.*, pp. 430–433, IEEE, 2005.

[8] A. I. of Health and Welfare, "Australia's health 2018 (cat. no. aus 221; australia's health series no. 16)," 2018.

[9] D. A. Economics, "No postcode untouched: Stroke in australia 2017 report (nsf1586)," 2017.

[10] D. A. Economics, "The economic impact of stroke in australia," 2013.

[11] A. I. of Health, *Australia's health 2012: the thirteenth biennial health report of the Australian Institute of Health and Welfare*. AIHW, 2012.

[12] S. J. Ball, I. E. Brown, and S. H. Scott, "Medarm: a rehabilitation robot with 5dof at the shoulder complex," in *Advanced intelligent mechatronics, 2007 IEEE/ASME international conference on*, pp. 1–6, IEEE, 2007.

[13] R. L. Birkenmeier, E. M. Prager, and C. E. Lang, "Translating animal doses of task-specific training to people with chronic stroke in 1-hour therapy sessions: a proof-of-concept study," *Neurorehabilitation and neural repair*, vol. 24, no. 7, pp. 620–635, 2010.

[14] P. B. of Australia, "Managing risk to the public: Regulation at work in australia," 2017.

[15] C. E. Lang, J. R. MacDonald, and C. Gnip, "Counting repetitions: an observational study of outpatient therapy for people with hemiparesis post-stroke," *Journal of Neurologic Physical Therapy*, vol. 31, no. 1, pp. 3–10, 2007.

[16] L. G. Richards, K. C. Stewart, M. L. Woodbury, C. Senesac, and J. H. Cauraugh, "Movement-dependent stroke recovery: a systematic review and meta-analysis of tms and fmri evidence," *Neuropsychologia*, vol. 46, no. 1, pp. 3–11, 2008.

[17] H. Krebs, N. Hogan, B. Volpe, M. Aisen, L. Edelstein, and C. Diels, "Overview of clinical trials with mit-manus: a robot-aided neuro-rehabilitation facility," *Technology and Health Care*, vol. 7, no. 6, pp. 419–423, 1999.

[18] J. Rosen and J. C. Perry, "Upper limb powered exoskeleton," *International Journal of Humanoid Robotics*, vol. 4, no. 03, pp. 529–548, 2007.

[19] A. H. Stienen, E. E. Hekman, F. C. Van der Helm, G. B. Prange, M. J. Jannink, A. M. Aalsma, and H. Van der Kooij, "Freebal: dedicated gravity compensation for the upper extremities," in *Rehabilitation Robotics, 2007. ICORR 2007. IEEE 10th International Conference on*, pp. 804–808, IEEE, 2007.

[20] W. M. Nunes, L. A. O. Rodrigues, L. P. Oliveira, J. F. Ribeiro, J. C. M. Carvalho, and R. S. Gonçalves, "Cable-based parallel manipulator for rehabilitation of shoulder and elbow movements," in *Rehabilitation Robotics (ICORR), 2011 IEEE International Conference on*, pp. 1–6, IEEE, 2011.

[21] E. Ottaviano, G. Castelli, and G. Cannella, "A cable-based system for aiding elderly people in sit-to-stand transfer#," *Mechanics Based Design of Structures and Machines*, vol. 36, no. 4, pp. 310–329, 2008.

[22] C. J. Walsh, K. Endo, and H. Herr, "A quasi-passive leg exoskeleton for load-carrying augmentation," *International Journal of Humanoid Robotics*, vol. 4, no. 03, pp. 487–506, 2007.

[23] A. B. Zoss, H. Kazerooni, and A. Chu, "Biomechanical design of the berkeley lower extremity exoskeleton (bleex)," *IEEE/ASME Transactions On Mechatronics*, vol. 11, no. 2, pp. 128–138, 2006.

[24] J. F. Veneman, R. Kruidhof, E. E. Hekman, R. Ekkelenkamp, E. H. Van Asseldonk, and H. Van Der Kooij, "Design and evaluation of the lopes exoskeleton robot for interactive gait rehabilitation," *IEEE Transactions on Neural Systems and Rehabilitation Engineering*, vol. 15, no. 3, pp. 379–386, 2007.

[25] H. Vallery, E. H. Van Asseldonk, M. Buss, and H. Van Der Kooij, "Reference trajectory generation for rehabilitation robots: complementary limb motion estimation," *IEEE transactions on neural systems and rehabilitation engineering*, vol. 17, no. 1, pp. 23–30, 2009.

[26] R. Ronsse, N. Vitiello, T. Lenzi, J. van den Kieboom, M. C. Carrozza, and A. J. Ijspeert, "Human-robot synchrony: flexible assistance using adaptive oscillators," *IEEE Transactions on Biomedical Engineering*, vol. 58, no. 4, pp. 1001–1012, 2011.

[27] T. Lenzi, S. M. M. De Rossi, N. Vitiello, and M. C. Carrozza, "Intention-based emg control for powered exoskeletons," *IEEE transactions on biomedical engineering*, vol. 59, no. 8, pp. 2180–2190, 2012.

[28] H. I. Krebs, J. J. Palazzolo, L. Dipietro, M. Ferraro, J. Krol, K. Rannekleiv, B. T. Volpe, and N. Hogan, "Rehabilitation robotics: Performance-based progressive robot-assisted therapy," *Autonomous robots*, vol. 15, no. 1, pp. 7–20, 2003.

[29] A. Frisoli, C. Procopio, C. Chisari, I. Creatini, L. Bonfiglio, M. Bergamasco, B. Rossi, and M. C. Carboncini, "Positive effects of robotic exoskeleton training of upper limb reaching movements after stroke," *Journal of neuroengineering and rehabilitation*, vol. 9, no. 1, p. 36, 2012.

[30] H.-J. Yu, A. Lee, and Y. Choi, "Human elbow joint angle estimation using electromyogram signal processing," *IET signal processing*, vol. 5, no. 8, pp. 767–775, 2011.

[31] D. Ferris, G. Sawicki, and A. Domingo, "Powered lower limb orthoses for gait rehabilitation," *Topics in spinal cord injury rehabilitation*, vol. 11, no. 2, pp. 34–49, 2005.

[32] J. Patton, S. L. Small, and W. Zev Rymer, "Functional restoration for the stroke survivor: informing the efforts of engineers," *Topics in stroke rehabilitation*, vol. 15, no. 6, pp. 521–541, 2008.

[33] H. K. Hameed, W. Z. W. Hassan, S. Shafie, S. A. Ahmad, and H. Jaafar, "A review on surface electromyography-controlled hand robotic devices used for rehabilitation and assistance in activities of daily living," *JPO: Journal of Prosthetics and Orthotics*, vol. 32, no. 1, pp. 3–13, 2020.

[34] T. S. Buchanan, D. G. Lloyd, K. Manal, and T. F. Besier, "Neuromusculoskeletal modeling: estimation of muscle forces and joint moments and movements from measurements of neural command," *Journal of applied biomechanics*, vol. 20, no. 4, pp. 367–395, 2004.

[35] J. Lobo-Prat, P. N. Kooren, A. H. Stienen, J. L. Herder, B. F. Koopman, and P. H. Veltink, "Non-invasive control interfaces for intention detection in active movement-assistive devices," *Journal of neuroengineering and rehabilitation*, vol. 11, no. 1, p. 168, 2014.

[36] C.-Y. Chu and R. M. Patterson, "Soft robotic devices for hand rehabilitation and assistance: a narrative review," *Journal of neuroengineering and rehabilitation*, vol. 15, no. 1, p. 9, 2018.

[37] M. Zecca, S. Micera, M. C. Carrozza, and P. Dario, "Control of multifunctional prosthetic hands by processing the electromyographic signal," *Critical Reviews in Biomedical Engineering*, vol. 30, no. 4-6, 2002.

[38] L. Marchal-Crespo and D. J. Reinkensmeyer, "Review of control strategies for robotic movement training after neurologic injury," *Journal of neuroengineering and rehabilitation*, vol. 6, no. 1, p. 20, 2009.

[39] J. Huang, W. Huo, W. Xu, S. Mohammed, and Y. Amirat, "Control of upper-limb power-assist exoskeleton using a human-robot interface based on motion intention recognition," *IEEE transactions on automation science and engineering*, vol. 12, no. 4, pp. 1257–1270, 2015.

[40] C. Fleischer and G. Hommel, "A human-exoskeleton interface utilizing electromyography," *IEEE Transactions on Robotics*, vol. 24, no. 4, pp. 872–882, 2008.

[41] R. Song and K. Tong, "Using recurrent artificial neural network model to estimate voluntary elbow torque in dynamic situations," *Medical and Biological Engineering and Computing*, vol. 43, no. 4, pp. 473–480, 2005.

[42] K. Kiguchi, S. Kariya, K. Watanabe, K. Izumi, and T. Fukuda, "An exoskeletal robot for human elbow motion support-sensor fusion, adaptation, and control," *IEEE Transactions on Systems, Man, and Cybernetics, Part B (Cybernetics)*, vol. 31, no. 3, pp. 353–361, 2001.

[43] O. Fukuda, T. Tsuji, M. Kaneko, and A. Otsuka, "A human-assisting manipulator teleoperated by emg signals and arm motions," *IEEE Transactions on Robotics and Automation*, vol. 19, no. 2, pp. 210–222, 2003.

[44] L. Dipietro, M. Ferraro, J. J. Palazzolo, H. I. Krebs, B. T. Volpe, and N. Hogan, "Customized interactive robotic treatment for stroke: Emg-triggered therapy," *IEEE transactions on neural systems and rehabilitation engineering*, vol. 13, no. 3, pp. 325–334, 2005.

[45] E. Cavallaro, J. Rosen, J. C. Perry, S. Burns, and B. Hannaford, "Hill-based model as a myoprocessor for a neural controlled powered exoskeleton arm-parameters optimization," in *Robotics and Automation, 2005. ICRA 2005. Proceedings of the 2005 IEEE International Conference on*, pp. 4514–4519, IEEE, 2005.

[46] S. Yao, Y. Zhuang, Z. Li, and R. Song, "Adaptive admittance control for an ankle exoskeleton using an emg-driven musculoskeletal model," *Frontiers in neurorobotics*, vol. 12, p. 16, 2018.

[47] A. d'Avella, A. Portone, L. Fernandez, and F. Lacquaniti, "Control of fast-reaching movements by muscle synergy combinations," *Journal of Neuroscience*, vol. 26, no. 30, pp. 7791–7810, 2006.

[48] A. Phinyomark, H. Hu, P. Phukpattaranont, and C. Limsakul, "Application of linear discriminant analysis in dimensionality reduction for hand motion classification," *Measurement Science Review*, vol. 12, no. 3, pp. 82–89, 2012.

[49] C. W. Antuvan, F. Bisio, F. Marini, S.-C. Yen, E. Cambria, and L. Masia, "Role of muscle synergies in real-time classification of upper limb motions using extreme learning machines," *Journal of neuroengineering and rehabilitation*, vol. 13, no. 1, p. 76, 2016.

[50] P. Artemiadis and K. Kyriakopoulos, "Emg-based control of a robot arm using low-dimensional embeddings," *IEEE Transactions on Robotics*, vol. 2, no. 26, pp. 393–398, 2010.

[51] A. B. Ajiboye and R. F. Weir, "A heuristic fuzzy logic approach to emg pattern recognition for multifunctional prosthesis control," *IEEE Transactions on Neural Systems and Rehabilitation Engineering*, vol. 13, no. 3, pp. 280–291, 2005.

[52] G. Wang, Y. Zhang, and J. Wang, "The analysis of surface emg signals with the wavelet-based correlation dimension method," *Computational and mathematical methods in medicine*, vol. 2014, 2014.

[53] L. K. Osterkamp, "Current perspective on assessment of human body proportions of relevance to amputees," *Journal of the American Dietetic Association*, vol. 95, no. 2, pp. 215–218, 1995.

[54] L.-C. Hsu, W.-W. Wang, G.-D. Lee, Y.-W. Liao, L.-C. Fu, and J.-S. Lai, "A gravity compensation-based upper limb rehabilitation robot," in *American Control Conference (ACC), 2012*, pp. 4819–4824, IEEE, 2012.

[55] C. G. Burgar, P. S. Lum, P. C. Shor, H. M. Van der Loos, *et al.*, "Development of robots for rehabilitation therapy: The palo alto va/stanford experience," *Journal of rehabilitation research and development*, vol. 37, no. 6, pp. 663–674, 2000.

[56] P. S. Lum, C. G. Burgar, P. C. Shor, M. Majmundar, and M. Van der Loos, "Robot-assisted movement training compared with conventional therapy techniques for the rehabilitation of upper-limb motor function after stroke," *Archives of physical medicine and rehabilitation*, vol. 83, no. 7, pp. 952–959, 2002.

[57] F. Ozkul and D. Barkana, "Design and control of an upper limb exoskeleton robot rehabroby," *Towards autonomous robotic systems*, pp. 125–136, 2011.

[58] R. J. Sanchez, J. Liu, S. Rao, P. Shah, R. Smith, T. Rahman, S. C. Cramer, J. E. Bobrow, and D. J. Reinkensmeyer, "Automating arm movement training following severe stroke: functional exercises with quantitative feedback in a gravity-reduced environment," *IEEE Transactions on neural systems and rehabilitation engineering*, vol. 14, no. 3, pp. 378–389, 2006.

[59] A. H. Stienen, E. E. Hekman, G. B. Prange, M. J. Jannink, F. C. van der Helm, and H. van der Kooij, "Freebal: design of a dedicated weight-support system for upper-extremity rehabilitation," *Journal of Medical Devices*, vol. 3, no. 4, p. 041009, 2009.

[60] R. Song, K.-y. Tong, X. Hu, L. Li, *et al.*, "Assistive control system using continuous myoelectric signal in robot-aided arm training for patients after stroke," *IEEE transactions on neural systems and rehabilitation engineering*, vol. 16, no. 4, pp. 371–379, 2008.

[61] G. Xu, A. Song, and H. Li, "Control system design for an upper-limb rehabilitation robot," *Advanced Robotics*, vol. 25, no. 1-2, pp. 229–251, 2011.

[62] T. S. Olsen, "Arm and leg paresis as outcome predictors in stroke rehabilitation.," *Stroke*, vol. 21, no. 2, pp. 247–251, 1990.

[63] L. S. Cardoso, R. M. E. da Costa, A. Piovesana, M. Costa, L. Penna, A. Crispin, J. Carvalho, H. Ferreira, M. L. Lopes, G. Brandão, *et al.*, "Using virtual environments for stroke rehabilitation," in *2006 International Workshop on Virtual Rehabilitation*, pp. 1–5, IEEE, 2006.

[64] R. Riener, M. Wellner, T. Nef, J. Von Zitzewitz, A. Duschau-Wicke, G. Colombo, and L. Lunenburger, "A view on vr-enhanced rehabilitation robotics," in *2006 International Workshop on Virtual Rehabilitation*, pp. 149–154, IEEE, 2006.

[65] H. I. Krebs, N. Hogan, M. L. Aisen, and B. T. Volpe, "Robot-aided neurorehabilitation," *IEEE transactions on rehabilitation engineering*, vol. 6, no. 1, pp. 75–87, 1998.

[66] P. S. Lum, C. G. Burgar, and P. C. Shor, "Evidence for improved muscle activation patterns after retraining of reaching movements with the mime robotic system in subjects with post-stroke hemiparesis," *IEEE Transactions on Neural Systems and Rehabilitation Engineering*, vol. 12, no. 2, pp. 186–194, 2004.

[67] G. Rosati, P. Gallina, and S. Masiero, "Design, implementation and clinical tests of a wire-based robot for neurorehabilitation," *IEEE Transactions on Neural Systems and Rehabilitation Engineering*, vol. 15, no. 4, pp. 560–569, 2007.

[68] R. Loureiro, F. Amirabdollahian, M. Topping, B. Driessen, and W. Harwin, "Upper limb robot mediated stroke therapy gentle/s approach," *Autonomous Robots*, vol. 15, no. 1, pp. 35–51, 2003.

[69] F. Amirabdollahian, R. Loureiro, E. Gradwell, C. Collin, W. Harwin, and G. Johnson, "Multivariate analysis of the fugl-meyer outcome measures assessing the effectiveness of gentle/s robot-mediated stroke therapy," *Journal of NeuroEngineering and Rehabilitation*, vol. 4, no. 1, p. 4, 2007.

[70] D. Mayhew, B. Bachrach, W. Z. Rymer, and R. F. Beer, "Development of the macarm-a novel cable robot for upper limb neurorehabilitation," in *Rehabilitation Robotics, 2005. ICORR 2005. 9th International Conference on*, pp. 299–302, IEEE, 2005.

[71] S. Masiero, A. Celia, M. Armani, G. Rosati, B. Tavolato, C. Ferraro, and M. Ortolani, "Robot-aided intensive training in post-stroke recovery," *Aging clinical and experimental research*, vol. 18, no. 3, pp. 261–265, 2006.

[72] F. Shahmiri and R. Gentry, "A survey of cable-suspended parallel robots and their applications in architecture and construction," 2016.

[73] W. Meng, Q. Liu, Z. Zhou, Q. Ai, B. Sheng, and S. S. Xie, "Recent development of mechanisms and control strategies for robot-assisted lower limb rehabilitation," *Mechatronics*, vol. 31, pp. 132–145, 2015.

[74] B. Cesqui, P. Tropea, S. Micera, and H. I. Krebs, "Emg-based pattern recognition approach in post stroke robot-aided rehabilitation: a feasibility study," *Journal of neuroengineering and rehabilitation*, vol. 10, no. 1, p. 75, 2013.

[75] Y. Zhuang, Y. Leng, J. Zhou, R. Song, L. Li, and S. Su, "Voluntary control of an ankle joint exoskeleton by able-bodied individuals and stroke survivors using emg-based admittance control scheme," *IEEE Transactions on Biomedical Engineering*, 2020.

[76] R. H. Fereydooni, H. Siahkali, H. A. Shayanfar, and A. H. Mazinan, "semg-based variable impedance control of lower-limb rehabilitation robot using wavelet neural network and model reference adaptive control," *Industrial Robot: the international journal of robotics research and application*, 2020.

[77] A. G. Feleke, L. Bi, and W. Fei, "Emg-based 3d hand motor intention prediction for information transfer from human to robot," *Sensors*, vol. 21, no. 4, p. 1316, 2021.

[78] R. Colombo, F. Pisano, A. Mazzone, C. Delconte, S. Micera, M. C. Carrozza, P. Dario, and G. Minuco, "Design strategies to improve patient motivation during robot-aided rehabilitation," *Journal of neuroengineering and rehabilitation*, vol. 4, no. 1, p. 3, 2007.

[79] K. Kiguchi, T. Tanaka, and T. Fukuda, "Neuro-fuzzy control of a robotic exoskeleton with emg signals," *IEEE Transactions on fuzzy systems*, vol. 12, no. 4, pp. 481–490, 2004.

[80] F. Zhang, P. Li, Z.-G. Hou, Z. Lu, Y. Chen, Q. Li, and M. Tan, "semg-based continuous estimation of joint angles of human legs by using bp neural network," *Neurocomputing*, vol. 78, no. 1, pp. 139–148, 2012.

[81] A. D. Roche, H. Rehbaum, D. Farina, and O. C. Aszmann, "Prosthetic myoelectric control strategies: a clinical perspective," *Current Surgery Reports*, vol. 2, no. 3, p. 44, 2014.

[82] A. Phinyomark, P. Phukpattaranont, and C. Limsakul, "Feature reduction and selection for emg signal classification," *Expert systems with applications*, vol. 39, no. 8, pp. 7420–7431, 2012.

[83] P. Xia, J. Hu, and Y. Peng, "Emg-based estimation of limb movement using deep learning with recurrent convolutional neural networks," *Artificial organs*, vol. 42, no. 5, pp. E67–E77, 2018.

[84] Y. Yu, C. Chen, X. Sheng, and X. Zhu, "Multi-dof continuous estimation for wrist torques using stacked autoencoder," *Biomedical Signal Processing and Control*, vol. 57, p. 101733, 2020.

[85] J. Potvin, R. Norman, and S. McGill, "Mechanically corrected EMG for the continuous estimation of erector spinae muscle loading during repetitive lifting," *European journal of applied physiology and occupational physiology*, vol. 74, no. 1-2, pp. 119–132, 1996.

[86] Y. M. Aung and A. Al-Jumaily, "semg based ann for shoulder angle prediction," *Procedia Engineering*, vol. 41, pp. 1009–1015, 2012.

[87] B. Lim, S. Ra, and F. C. Park, "Movement primitives, principal component analysis, and the efficient generation of natural motions," in *Robotics and Automation, 2005. ICRA 2005. Proceedings of the 2005 IEEE International Conference on*, pp. 4630–4635, IEEE, 2005.

[88] J. M. Hahne, F. Biessmann, N. Jiang, H. Rehbaum, D. Farina, F. C. Meinecke, K.-R. Müller, and L. C. Parra, "Linear and nonlinear regression techniques for simultaneous and proportional myoelectric control," *IEEE Transactions on Neural Systems and Rehabilitation Engineering*, vol. 22, no. 2, pp. 269–279, 2014.

[89] J. Luo, C. Liu, and C. Yang, "Estimation of emg-based force using a neural-network-based approach," *IEEE Access*, vol. 7, pp. 64856–64865, 2019.

[90] C. Choi, S. Kwon, W. Park, H.-d. Lee, and J. Kim, "Real-time pinch force estimation by surface electromyography using an artificial neural network," *Medical engineering & physics*, vol. 32, no. 5, pp. 429–436, 2010.

[91] Y. Chen, C. Dai, and W. Chen, "Cross-comparison of emg-to-force methods for multi-dof finger force prediction using one-dof training," *IEEE Access*, vol. 8, pp. 13958–13968, 2020.

[92] D. Farina, N. Jiang, H. Rehbaum, A. Holobar, B. Graimann, H. Dietl, and O. C. Aszmann, "The extraction of neural information from the surface emg for the control of upper-limb prostheses: emerging avenues and challenges," *IEEE Transactions on Neural Systems and Rehabilitation Engineering*, vol. 22, no. 4, pp. 797–809, 2014.

[93] Y. LeCun, Y. Bengio, and G. Hinton, "Deep learning," *nature*, vol. 521, no. 7553, pp. 436–444, 2015.

[94] J. Yang, H. Su, Z. Li, D. Ao, and R. Song, "Adaptive control with a fuzzy tuner for cable-based rehabilitation robot," *International Journal of Control, Automation and Systems*, vol. 14, no. 3, pp. 865–875, 2016.

[95] M. A. Nicolelis, "Brain–machine interfaces to restore motor function and probe neural circuits," *Nature Reviews Neuroscience*, vol. 4, no. 5, pp. 417–422, 2003.

[96] Z. W. Chen and T. P. Hu, "A reconstructed digit by transplantation of a second toe for control of an electromechanical prosthetic hand," *Microsurgery: Official Journal of the International Microsurgical Society and the European Federation of Societies for Microsurgery*, vol. 22, no. 1, pp. 5–10, 2002.

[97] M. Lotze, C. Braun, N. Birbaumer, S. Anders, and L. G. Cohen, "Motor learning elicited by voluntary drive," *Brain*, vol. 126, no. 4, pp. 866–872, 2003.

[98] R. Riener, M. Guidali, U. Keller, A. Duschau-Wicke, V. Klamroth, and T. Nef, "Transferring armin to the clinics and industry," *Topics in spinal cord injury rehabilitation*, vol. 17, no. 1, pp. 54–59, 2011.

[99] S. Masiero, A. Celia, G. Rosati, and M. Armani, "Robotic-assisted rehabilitation of the upper limb after acute stroke," *Archives of physical medicine and rehabilitation*, vol. 88, no. 2, pp. 142–149, 2007.

[100] D. Zanotto, G. Rosati, S. Minto, and A. Rossi, "Sophia-3: A semiadaptive cable-driven rehabilitation device with a tilting working plane," *IEEE Transactions on Robotics*, vol. 30, no. 4, pp. 974–979, 2014.

[101] L. Marchal-Crespo and D. J. Reinkensmeyer, "Review of control strategies for robotic movement training after neurologic injury," *Journal of neuroengineering and rehabilitation*, vol. 6, no. 1, p. 20, 2009.

[102] P. M. Rossini and G. Dal Forno, "Integrated technology for evaluation of brain function and neural plasticity," *Physical Medicine and Rehabilitation Clinics*, vol. 15, no. 1, pp. 263–306, 2004.

[103] M.-K. Chang, "An adaptive self-organizing fuzzy sliding mode controller for a 2-dof rehabilitation robot actuated by pneumatic muscle actuators," *Control Engineering Practice*, vol. 18, no. 1, pp. 13–22, 2010.

[104] T. Proietti, V. Crocher, A. Roby-Brami, and N. Jarrassé, "Upper-limb robotic exoskeletons for neurorehabilitation: a review on control strategies," *IEEE reviews in biomedical engineering*, vol. 9, pp. 4–14, 2016.

[105] C. Loconsole, S. Dettori, A. Frisoli, C. A. Avizzano, and M. Bergamasco, "An emg-based approach for on-line predicted torque control in robotic-assisted rehabilitation," in *Haptics Symposium (HAPTICS), 2014 IEEE*, pp. 181–186, IEEE, 2014.

[106] M. H. Rahman, C. Ochoa-Luna, M. Saad, and P. Archambault, "Emg based control of a robotic exoskeleton for shoulder and elbow motion assist," *J Aut Con Eng*, vol. 3, no. 4, 2015.

[107] K. Nizamis, J. Lobo-Prat, A. Q. Keemink, R. Carloni, A. H. Stienen, and B. F. Koopman, "Switching proportional emg control of a 3d endpoint arm support for people with duchenne muscular dystrophy," in *Rehabilitation Robotics (ICORR), 2015 IEEE International Conference on*, pp. 235–240, IEEE, 2015.

[108] P. K. Artemiadis, P. T. Katsiaris, M. V. Liarokapis, and K. J. Kyriakopoulos, "On the effect of human arm manipulability in 3d force tasks: Towards force-controlled exoskeletons," in *Robotics and Automation (ICRA), 2011 IEEE International Conference on*, pp. 3784–3789, IEEE, 2011.

[109] P. K. Artemiadis and K. J. Kyriakopoulos, "A switching regime model for the emg-based control of a robot arm," *IEEE Transactions on Systems, Man, and Cybernetics, Part B (Cybernetics)*, vol. 41, no. 1, pp. 53–63, 2011.

[110] F. E. Zajac, "Muscle and tendon properties models scaling and application to biomechanics and motor," *Critical reviews in biomedical engineering*, vol. 17, no. 4, pp. 359–411, 1989.

[111] D. G. Lloyd and T. F. Besier, "An emg-driven musculoskeletal model to estimate muscle forces and knee joint moments in vivo," *Journal of biomechanics*, vol. 36, no. 6, pp. 765–776, 2003.

[112] A. Huxley, "Muscular contraction.," *The Journal of physiology*, vol. 243, no. 1, pp. 1–43, 1974.

[113] K. Manal and T. S. Buchanan, "A one-parameter neural activation to muscle activation model: estimating isometric joint moments from electromyograms," *Journal of biomechanics*, vol. 36, no. 8, pp. 1197–1202, 2003.

[114] P. K. Artemiadis and K. J. Kyriakopoulos, "Emg-based teleoperation of a robot arm using low-dimensional representation," in *2007 IEEE/RSJ International Conference on Intelligent Robots and Systems*, pp. 489–495, IEEE, oct 2007.

[115] W. E. Larimore, "Canonical variate analysis in identification, filtering, and adaptive control," in *29th IEEE Conference on Decision and control*, pp. 596–604, IEEE, 1990.

[116] J. R. Cram, *Cram's introduction to surface electromyography*. Jones & Bartlett Learning, 2011.

[117] M. M. Mukaka, "A guide to appropriate use of correlation coefficient in medical research," *Malawi Medical Journal*, vol. 24, no. 3, pp. 69–71, 2012.

[118] T. Öberg, "Muscle fatigue and calibration of EMG measurements," *Journal of Electromyography and Kinesiology*, vol. 5, no. 4, pp. 239–243, 1995.

[119] K. Nazarpour, A. Barnard, and A. Jackson, "Flexible cortical control of task-specific muscle synergies," *Journal of Neuroscience*, vol. 32, no. 36, pp. 12349–12360, 2012.

[120] S. Kwon, Y. Kim, and J. Kim, "Movement stability analysis of surface electromyography-based elbow power assistance," *IEEE Transactions on Biomedical Engineering*, vol. 61, no. 4, pp. 1134–1142, 2014.

[121] E. Mastinu, P. Doguet, Y. Botquin, B. Håkansson, and M. Ortiz-Catalan, "Embedded system for prosthetic control using implanted neuromuscular interfaces accessed via an osseointegrated implant," *IEEE transactions on biomedical circuits and systems*, vol. 11, no. 4, pp. 867–877, 2017.

[122] K. Suzuki, G. Mito, H. Kawamoto, Y. Hasegawa, and Y. Sankai, "Intention-based walking support for paraplegia patients with robot suit hal," *Advanced Robotics*, vol. 21, no. 12, pp. 1441–1469, 2007.

[123] R. Song, K.-y. Tong, X. Hu, and W. Zhou, "Myoelectrically controlled wrist robot for stroke rehabilitation," *Journal of neuroengineering and rehabilitation*, vol. 10, no. 1, p. 52, 2013.

[124] R. Loureiro, C. Collin, and W. Harwin, "Robot aided therapy: challenges ahead for upper limb stroke rehabilitation," in *Proceed of Intl Conf on Disability, Virtual Reality and Assoc Tech*, pp. 33–39, 2004.

[125] R. Holt, S. Makower, A. Jackson, P. Culmer, M. Levesley, R. Richardson, A. Cozens, M. M. Williams, and B. Bhakta, "User involvement in developing rehabilitation robotic devices: An essential requirement," in *200s7 IEEE 10th International Conference on Rehabilitation Robotics*, pp. 196–204, June 2007.

[126] A. Ajoudani, N. Tsagarakis, and A. Bicchi, "Tele-impedance: Teleoperation with impedance regulation using a body–machine interface," *The International Journal of Robotics Research*, vol. 31, no. 13, pp. 1642–1656, 2012.

[127] Q. Zhang, R. Hosoda, and G. Venture, "Human joint motion estimation for electromyography (emg)-based dynamic motion control," in *2013 35th Annual International Conference of the IEEE Engineering in Medicine and Biology Society (EMBC)*, pp. 21–24, IEEE, 2013.

[128] Y. Huang, Y. Chen, J. Niu, and R. Song, "Emg-based control for three-dimensional upper limb movement assistance using a cable-based upper limb rehabilitation robot," in *International Conference on Intelligent Robotics and Applications*, pp. 273–279, Springer, 2017.

[129] Y. Huang, R. Song, A. Argha, A. V. Savkin, B. G. Celler, and S. W. Su, "Continuous description of human 3d motion intent through switching mechanism," *IEEE Transactions on Neural Systems and Rehabilitation Engineering*, 2019.

[130] H. Diener, J. Dichgans, F. Bootz, and M. Bacher, "Early stabilization of human posture after a sudden disturbance: influence of rate and amplitude of displacement," *Experimental Brain Research*, vol. 56, no. 1, pp. 126–134, 1984.

[131] J. Hespanha, D. Liberzon, A. Stephen Morse, B. D. Anderson, T. S. Brinsmead, and F. De Bruyne, "Multiple model adaptive control. part 2: switching," *International Journal of Robust and Nonlinear Control: IFAC-Affiliated Journal*, vol. 11, no. 5, pp. 479–496, 2001.

[132] A. S. Morse, "Control using logic-based switching," in *Trends in control*, pp. 69–113, Springer, 1995.

[133] B. D. Anderson, S. W. Su, and T. S. Brinsmead, "Multirealization of linear systems," *IEEE Transactions on Circuits and Systems II: Express Briefs*, vol. 52, no. 8, pp. 442–446, 2005.

[134] S. W. Su, B. D. Anderson, and T. S. Brinsmead, "Minimal multirealization of mimo linear systems," *IEEE transactions on automatic control*, vol. 51, no. 4, pp. 690–695, 2006.

[135] L. Ljung, "System identification toolbox for use with matlab," vol. 21, 01 2011.

[136] T. Kailath, *Linear systems*, vol. 156. Prentice-Hall Englewood Cliffs, NJ, 1980.

[137] S. Wang and E. Davison, "A minimization algorithm for the design of linear multivariable systems," *IEEE Transactions on automatic control*, vol. 18, no. 3, pp. 220–225, 1973.

[138] J. Basilio and B. Kouvaritakis, "An algorithm for coprime matrix fraction description using sylvester matrices," *Linear Algebra and its Applications*, vol. 266, pp. 107–125, 1997.

[139] G. D. Forney, Jr, "Minimal bases of rational vector spaces, with applications to multivariable linear systems," *SIAM Journal on Control*, vol. 13, no. 3, pp. 493–520, 1975.

[140] S. Kung and T. Kailath, "Fast projection methods for minimal design problems in linear system theory," *Automatica*, vol. 16, no. 4, pp. 399–403, 1980.

[141] A. Saadatkhah, "Minimal right matrix fraction description." https://www.mathworks.com/matlabcentral/fileexchange/35771-minimal-right-matrix-fraction-description. 2012.

[142] N. Hogan and D. Sternad, "Sensitivity of smoothness measures to movement duration, amplitude, and arrests," *Journal of motor behavior*, vol. 41, no. 6, pp. 529–534, 2009.

[143] Y. Huang, Q. Yang, Y. Chen, and R. Song, "Assessment of motor control during three-dimensional movements tracking with position-varying gravity compensation," *Frontiers in neuroscience*, vol. 11, p. 253, 2017.

[144] K.-E. Hagbarth, J. Hägglund, E. Wallin, and R. Young, "Grouped spindle and electromyographic responses to abrupt wrist extension movements in man," *The Journal of physiology*, vol. 312, no. 1, pp. 81–96, 1981.

[145] D. Sherwood, R. A. Schmidt, and C. Walter, "Rapid movements with reversals in direction," *Experimental Brain Research*, vol. 69, no. 2, pp. 355–367, 1988.

[146] S. Balasubramanian, A. Melendez-Calderon, and E. Burdet, "A robust and sensitive metric for quantifying movement smoothness," *IEEE transactions on biomedical engineering*, vol. 59, no. 8, pp. 2126–2136, 2011.

[147] J. Liu, Y. Ren, D. Xu, S. H. Kang, and L.-Q. Zhang, "Emg-based real-time linear-nonlinear cascade regression decoding of shoulder, elbow, and wrist movements in able-bodied persons and stroke survivors," *IEEE Transactions on Biomedical Engineering*, vol. 67, no. 5, pp. 1272–1281, 2019.

[148] Y. Kim, S. Stapornchaisit, H. Kambara, N. Yoshimura, and Y. Koike, "Muscle synergy and musculoskeletal model-based continuous multi-dimensional estimation of wrist and hand motions," *Journal of Healthcare Engineering*, vol. 2020, 2020.

[149] A. Sarasola-Sanz, N. Irastorza-Landa, F. Shiman, E. Lopez-Larraz, M. Spüler, N. Birbaumer, and A. Ramos-Murguialday, "Emg-based multi-joint kinematics decoding for robot-aided rehabilitation therapies," in *2015 IEEE International Conference on Rehabilitation Robotics (ICORR)*, pp. 229–234, IEEE, 2015.

[150] A. Dwivedi, Y. Kwon, A. J. McDaid, and M. Liarokapis, "A learning scheme for emg based decoding of dexterous, in-hand manipulation motions," *IEEE Transactions on Neural Systems and Rehabilitation Engineering*, vol. 27, no. 10, pp. 2205–2215, 2019.

[151] N. F. Lepora and G. Pezzulo, "Embodied choice: how action influences perceptual decision making," *PLoS computational biology*, vol. 11, no. 4, 2015.

[152] S. Pettersson and B. Lennartson, "Stability and robustness for hybrid systems," in *Proceedings of 35th IEEE Conference on Decision and Control*, vol. 2, pp. 1202–1207, IEEE, 1996.

[153] D. Liberzon, *Switching in systems and control*. Springer Science & Business Media, 2003.

[154] S. De Jesus-Mota, M. N. Beaulieu, and R. Botez, "Identification of a mimo state space model of an f/a-18 aircraft using a subspace method," *The Aeronautical Journal*, vol. 113, no. 1141, pp. 183–190, 2009.

[155] Q. Zhang, M. Hayashibe, P. Fraisse, and D. Guiraud, "Fes-induced torque prediction with evoked emg sensing for muscle fatigue tracking," *IEEE/ASME Transactions on Mechatronics*, vol. 16, no. 5, pp. 816–826, 2011.

[156] I. Lawrence and K. Lin, "A concordance correlation coefficient to evaluate reproducibility," *Biometrics*, pp. 255–268, 1989.

[157] J. O. Rawlings, S. G. Pantula, and D. A. Dickey, *Applied regression analysis: a research tool*. Springer Science & Business Media, 2001.

[158] C. Ethier, D. Acuna, S. A. Solla, and L. E. Miller, "Adaptive neuron-to-emg decoder training for fes neuroprostheses," *Journal of neural engineering*, vol. 13, no. 4, p. 046009, 2016.

[159] M. V. Liarokapis, P. K. Artemiadis, K. J. Kyriakopoulos, and E. S. Manolakos, "A learning scheme for reach to grasp movements: On emg-based interfaces using task specific motion decoding models," *IEEE journal of biomedical and health informatics*, vol. 17, no. 5, pp. 915–921, 2013.

[160] J. Schmidhuber and S. Hochreiter, "Long short-term memory," *Neural Comput*, vol. 9, no. 8, pp. 1735–1780, 1997.

[161] D. Biswas, L. Everson, M. Liu, M. Panwar, B.-E. Verhoef, S. Patki, C. H. Kim, A. Acharyya, C. Van Hoof, M. Konijnenburg, *et al.*, "Cornet: Deep learning framework for ppg-based heart rate estimation and biometric identification in ambulant environment," *IEEE transactions on biomedical circuits and systems*, vol. 13, no. 2, pp. 282–291, 2019.

[162] C. Wang, W. Guo, H. Zhang, L. Guo, C. Huang, and C. Lin, "semg-based continuous estimation of grasp movements by long-short term memory network," *Biomedical Signal Processing and Control*, vol. 59, p. 101774, 2020.

[163] L. Rane, Z. Ding, A. H. McGregor, and A. M. Bull, "Deep learning for musculoskeletal force prediction," *Annals of biomedical engineering*, vol. 47, no. 3, pp. 778–789, 2019.

[164] C. Wang, X. Wu, Y. Ma, G. Wu, and Y. Luo, "A flexible lower extremity exoskeleton robot with deep locomotion mode identification," *Complexity*, vol. 2018, 2018.

[165] A. Ameri, M. A. Akhaee, E. Scheme, and K. Englehart, "Real-time, simultaneous myoelectric control using a convolutional neural network," *PloS one*, vol. 13, no. 9, 2018.

[166] A. Ameri, M. Akhaee, E. Scheme, and K. Englehart, "Regression convolutional neural network for improved simultaneous emg control.," *Journal of neural engineering*, vol. 16, no. 3, p. 036015, 2019.

[167] A. d'Avella, "Modularity for motor control and motor learning," in *Progress in Motor Control*, pp. 3–19, Springer, 2016.

[168] M. Tagliabue, A. L. Ciancio, T. Brochier, S. Eskiizmirliler, and M. A. Maier, "Differences between kinematic synergies and muscle synergies during two-digit grasping," *Frontiers in human neuroscience*, vol. 9, p. 165, 2015.

[169] P. Parker, K. Englehart, and B. Hudgins, "Myoelectric signal processing for control of powered limb prostheses," *Journal of electromyography and kinesiology*, vol. 16, no. 6, pp. 541–548, 2006.

[170] R. M. Singh, S. Chatterji, and A. Kumar, "A review on surface emg based control schemes of exoskeleton robot in stroke rehabilitation," in *Machine Intelligence and Research Advancement (ICMIRA), 2013 International Conference on*, pp. 310–315, IEEE, 2013.

[171] A. J. Young, L. H. Smith, E. J. Rouse, and L. J. Hargrove, "A comparison of the real-time controllability of pattern recognition to conventional myoelectric control for discrete and simultaneous movements," *Journal of neuroengineering and rehabilitation*, vol. 11, no. 1, p. 5, 2014.

[172] E. Bizzi and V. C. Cheung, "The neural origin of muscle synergies," *Frontiers in computational neuroscience*, vol. 7, p. 51, 2013.

[173] L. H. Ting and J. L. McKay, "Neuromechanics of muscle synergies for posture and movement," *Current opinion in neurobiology*, vol. 17, no. 6, pp. 622–628, 2007.

[174] F. Li, Q. Wang, S. Cao, D. Wu, Q. Wang, and X. Chen, "Lower-limb muscle synergies in children with cerebral palsy," in *2013 6th International IEEE/EMBS Conference on Neural Engineering (NER)*, pp. 1226–1229, IEEE, 2013.

[175] M. Ison and P. Artemiadis, "The role of muscle synergies in myoelectric control: trends and challenges for simultaneous multifunction control," *Journal of neural engineering*, vol. 11, no. 5, p. 051001, 2014.

[176] S. Muceli, N. Jiang, and D. Farina, "Extracting signals robust to electrode number and shift for online simultaneous and proportional myoelectric control by factorization algorithms," *IEEE Transactions on Neural Systems and Rehabilitation Engineering*, vol. 22, no. 3, pp. 623–633, 2014.

[177] F. Hug, "Can muscle coordination be precisely studied by surface electromyography?," *Journal of electromyography and kinesiology*, vol. 21, no. 1, pp. 1–12, 2011.

[178] A. Ajiboye and R. Weir, "Muscle synergies as a predictive framework for the emg patterns of new hand postures," *Journal of neural engineering*, vol. 6, no. 3, p. 036004, 2009.

[179] N. Jiang, H. Rehbaum, I. Vujaklija, B. Graimann, and D. Farina, "Intuitive, online, simultaneous, and proportional myoelectric control over two degrees-of-freedom in upper limb amputees," *IEEE transactions on neural systems and rehabilitation engineering*, vol. 22, no. 3, pp. 501–510, 2014.

[180] M. V. Liarokapis, P. K. Artemiadis, P. T. Katsiaris, and K. J. Kyriakopoulos, "Learning task-specific models for reach to grasp movements: Towards emg-based teleoperation of robotic arm-hand systems," in *Biomedical Robotics and Biomechatronics (BioRob), 2012 4th IEEE RAS & EMBS International Conference on*, pp. 1287–1292, IEEE, 2012.

[181] D. J. Berger and A. d'Avella, "Effective force control by muscle synergies," *Frontiers in computational neuroscience*, vol. 8, p. 46, 2014.

[182] K. Nishida, S. Hagio, B. Kibushi, T. Moritani, and M. Kouzaki, "Comparison of muscle synergies for running between different foot strike patterns," *PLoS One*, vol. 12, no. 2, p. e0171535, 2017.

[183] D. D. Lee and H. S. Seung, "Learning the parts of objects by non-negative matrix factorization," *Nature*, vol. 401, no. 6755, pp. 788–791, 1999.

[184] P. Paatero and U. Tapper, "Positive matrix factorization: A non-negative factor model with optimal utilization of error estimates of data values," *Environmetrics*, vol. 5, no. 2, pp. 111–126, 1994.

[185] D. J. Clark, L. H. Ting, F. E. Zajac, R. R. Neptune, and S. A. Kautz, "Merging of healthy motor modules predicts reduced locomotor performance and muscle coordination complexity post-stroke," *Journal of neurophysiology*, vol. 103, no. 2, pp. 844–857, 2009.

[186] C. Alessandro, I. Delis, F. Nori, S. Panzeri, and B. Berret, "Muscle synergies in neuroscience and robotics: from input-space to task-space perspectives," *Frontiers in computational neuroscience*, vol. 7, p. 43, 2013.

[187] G. Torres-Oviedo, J. M. Macpherson, and L. H. Ting, "Muscle synergy organization is robust across a variety of postural perturbations," *Journal of neurophysiology*, vol. 96, no. 3, pp. 1530–1546, 2006.

[188] L. Tang, X. Chen, S. Cao, D. Wu, G. Zhao, and X. Zhang, "Assessment of upper limb motor dysfunction for children with cerebral palsy based on muscle synergy analysis," *Frontiers in human neuroscience*, vol. 11, p. 130, 2017.

[189] J. Liu, S. H. Kang, D. Xu, Y. Ren, S. J. Lee, and L.-Q. Zhang, "Emg-based continuous and simultaneous estimation of arm kinematics in able-bodied individuals and stroke survivors," *Frontiers in neuroscience*, vol. 11, p. 480, 2017.

[190] J. Roh, W. Z. Rymer, E. J. Perreault, S. B. Yoo, and R. F. Beer, "Alterations in upper limb muscle synergy structure in chronic stroke survivors," *Journal of neurophysiology*, vol. 109, no. 3, pp. 768–781, 2012.

[191] K. M. Steele, M. C. Tresch, and E. J. Perreault, "The number and choice of muscles impact the results of muscle synergy analyses," *Frontiers in computational neuroscience*, vol. 7, p. 105, 2013.

[192] M. C. Tresch and A. Jarc, "The case for and against muscle synergies," *Current opinion in neurobiology*, vol. 19, no. 6, pp. 601–607, 2009.

[193] M. C. Tresch, V. C. Cheung, and A. d'Avella, "Matrix factorization algorithms for the identification of muscle synergies: evaluation on simulated and experimental data sets," *Journal of neurophysiology*, vol. 95, no. 4, pp. 2199–2212, 2006.

[194] Y. P. Ivanenko, R. E. Poppele, and F. Lacquaniti, "Five basic muscle activation patterns account for muscle activity during human locomotion," *The Journal of physiology*, vol. 556, no. 1, pp. 267–282, 2004.

[195] I. Delis, S. Panzeri, T. Pozzo, and B. Berret, "Task-discriminative space-by-time factorization of muscle activity," *Frontiers in human neuroscience*, vol. 9, p. 399, 2015.

[196] G. Martino, Y. P. Ivanenko, A. d'Avella, M. Serrao, A. Ranavolo, F. Draicchio, G. Cappellini, C. Casali, and F. Lacquaniti, "Neuromuscular adjustments of gait associated with unstable conditions," *Journal of neurophysiology*, vol. 114, no. 5, pp. 2867–2882, 2015.

[197] M. W. Berry, M. Browne, A. N. Langville, V. P. Pauca, and R. J. Plemmons, "Algorithms and applications for approximate nonnegative matrix factorization," *Computational statistics & data analysis*, vol. 52, no. 1, pp. 155–173, 2007.